OLEKSANDR BEZVIKONNYI

INVESTIGATION OF NEW ORGANIC SEMICONDUCTORS FOR ORGANIC LIGHT EMITTING DIODES

DOCTORAL DISSERTATION

Kaunas
2020

KAUNAS UNIVERSITY OF TECHNOLOGY

OLEKSANDR BEZVIKONNYI

INVESTIGATION OF NEW ORGANIC SEMICONDUCTORS FOR ORGANIC LIGHT EMITTING DIODES

Doctoral dissertation
Technological Sciences, Materials Engineering (T 008)

2020, Kaunas

This doctoral dissertation was prepared at Kaunas University of Technology, Faculty of Chemical Technology, Department of Polymer Chemistry and Technology during the period of 2015–2019. The studies were supported by the Research Council of Lithuania.

Scientific Supervisor:

Prof. Dr. Habil. Juozas Vidas GRAŽULEVIČIUS (Kaunas University of Technology, Technological sciences, Materials engineering T 008).

Scientific Advisor:

Dr. Habil. Dmytro VOLYNIUK (Kaunas University of Technology, Natural sciences, Chemistry N 003).

Doctoral dissertation has been published in:
http://ktu.edu

Editor:

Dr. Armandas Rumšas (Publishing Office “Technologija”)

KAUNO TECHNOLOGIJOS UNIVERSITETAS

OLEKSANDR BEZVIKONNYI

ORGANINIŲ PUSLAIDININKIŲ, SKIRTŲ ORGANINIAMS ŠVIESOS DIODAMS, TYRIMAI

Daktaro disertacija
Technologijos mokslai, Medžiagų inžinerija (T 008)

2020, Kaunas

Disertacija rengta 2015-2019 metais Kauno technologijos universiteto Cheminės technologijos fakultete, Polimerų chemijos ir technologijos katedroje. Mokslinius tyrimus rėmė Lietuvos mokslo taryba.

Mokslinis vadovas:

Prof. habil. dr. Juozas Vidas GRAŽULEVIČIUS (Kauno technologijos universitetas, technologijos mokslai, medžiagų inžinerija, T 008).

Mokslinis konsultantas:

Habil. dr. Dmytro VOLYNIUK (Kauno technologijos universitetas, gamtos mokslai, chemija, N 003).

Interneto svetainės, kurioje skelbiama disertacija, adresas:
http://ktu.edu

Redagavo:

dr. Armandas Rumšas (leidykla “Technologija”)

LIST OF ABBREVIATIONS

AIE	Aggregation-induced emission
ACQ	Aggregation-caused quenching
BTD	2,1,3-Benzothiadiazole
CE	Current efficiency
CELIV	Charge extraction by linearly increasing voltage technique
CIE	Commission Internationale de l'Eclairage
CT	Charge transfer
CV	Cyclic voltammetry
D-A	Donor-acceptor
D-A-D	Donor-acceptor-donor
DACT-II	9-[4-(4,6-Diphenyl-1,3,5-triazin-2-yl)phenyl]-N^3,N^3,N^6,N^6-tetraphenyl-9*H*-carbazole-3,6-diamine
DF	Delayed fluorescence
DFT	Density functional theory
DMAC-DPS	10,10′-(4,4′-Sulfonylbis(1,4-phenylene))bis(9,9-dimethyl-9,10-dihydroacridine
DPPS	Diphenyl-bis[4-(pyridin-3-yl)phenyl]silane
DSC	Differential scanning calorimetry
EA_{CV}	Electron affinity measured by CV
EA_{PE}	Electron affinity measured by photoelectron emission method
EBL	Electron blocking layer
EIL	Electron injection layer
EL	Electroluminescent
EML	Emitting layer
EQE	External quantum efficiency
E_S	Energy of singlet state
E_T	Energy of triplet state
ETL	Electron transport layer
FIrpic	Iridium(III)bis(4,6-di-fluorophenyl)-pyridinato-*N*,C^2)picolinate
FRET	Förster resonance energy transfer
HAT-CN	Dipyrazino[2,3-f:2',3'-h]quinoxaline-2,3,6,7,10,11-hexacarbonitrile
HBL	Hole blocking layer
HIL	Hole injection layer
HOMO	Highest occupied molecular orbital
HTL	Hole transport layer
IC	Internal conversion
ICT	Intramolecular charge transfer

IP^{CV}	Ionization potential measured by CV
IP^{PE}	Ionization potential measured by photoelectron emission method
$Ir(piq)_2(acac)$	Bis(1-phenylisoquinoline)(acetylacetonate)iridium(III)
$Ir(ppy)_3$	Tris[2-phenylpyridinato-C^2,*N*]iridium(III)
ISC	Intersystem crossing
IQE	Internal quantum efficiency
ITO	Indium-tin oxide
LEB	Low energy band
LUMO	Lowest unoccupied molecular orbital
mCP	1,3-Bis(*N*-carbazolyl)benzene
MLCT	Metal-to-ligand charge transfer
MS	Mass spectrometry
NPB	*N*,*N*'-Di(1-naphthyl)-*N*,*N*'-diphenyl-(1,1'-biphenyl)-4,4'-diamine
o-DiCbzBz	9,9'-(2-(1-phenyl-1*H*-benzo[d]imidazol-2-yl)-1,3-phenylene)bis(9*H*-carbazole)
OLED	Organic light emitting diode
PE	Power efficiency
PF	Prompt fluorescence
PhOLED	Phosphorescent organic light emitting diode
PL	Photoluminescence/photoluminescent
RISC	Reverse intersystem crossing
RTP	Room temperature phosphorescence
TADF	Thermally activated delayed fluorescence
TAPC	4,4′-Cyclohexylidenebis[*N*,*N*-bis(4-methylphenyl)benzenamine]
TCTA	Tris(4-carbazoyl-9-ylphenyl)amine
TCz1	3,6-bis(carbazol-9-yl)-9-(2-ethylhexyl)-9*H*-carbazole
TOF	Time-of-flight
TPBi	2,2',2''-(1,3,5-Benzinetriyl)-tris(1-phenyl-1*H*-benzimidazole)
TSPO1	Diphenyl-4-triphenylsilylphenylphosphine oxide
TTA	Triplet-triplet annihilation
UV	Ultraviolet
ZFS	Zero-field splitting
4CzIPN	2,4,5,6-Tetra(9*H*-carbazol-9-yl)isophthalonitrile
λ	Wavelength
μ	Drift mobility of charge carriers
τ	Emission lifetime
Φ	Photoluminescence quantum yield

CONTENTS

1. INTRODUCTION

Substantiation of the scientific problem

Humanity entered the digital era in the twenty-first century. All the aspects of modern life including work and recreation are affected by the rapidly accelerating integration of computers and the society. The major way of comprehension of massive data as well as every-day information for people is visual interpretation. Monitors help to simplify scientific, manufacturing or any other kind of activities. The development of the display technology helps to make complex things dramatically easier to deal with.

The ease of the visual perception of information is a driver of rapid changes in the culture, industry and the commercial sector. The technology of organic light emitting diodes (OLED) has many advantages in comparison with the competitive technologies which make it one of the most promising for further expansion. The valuable properties of OLEDs are design simplicity, low cost, low mass, low consumption of electricity, high definition and quality of picture, wide viewing angles, negligible times of response, a wide range of operational temperatures etc.[1,2] The milestone of one billion OLED displays fabricated for smartphones was achieved in July 2018.[3] The next big step is the wide use of flexible and transparent displays.

Researchers around the globe are involved in overcoming the challenges of OLED technology which are the obstacles for its undisputable dominance in the global display market. The main point of them is the decrease of the cost of energy consumption as well as the increase of the lifetime of devices, especially of those emitting blue light.[4] Blue emitters are required to have high energy levels of excited states. As a consequence, it is more complicated to direct energy to provide blue emission than green and red. Bonds of blue emitters tend to break down, and excitation is deactivated preferably by non-radiative ways.[4,5] The challenge in the field of the OLED technology is the efficiency increase of devices avoiding negative effects, such as high cost, insufficient stability of the product, and the complexity of the fabrication process.

Investigation of the most promising recent approaches to increase the efficiency of OLEDs, such as the phenomenon of thermally activated delayed fluorescence (TADF), aggregation-induced emission (AIE) or aggregation induced emission enhancement (AIEE), electrophosphorescence (phosphorescent OLED, PhOLED), ambipolarity of emitting species is relevant for developing better understanding of the ways how illuminating devices can be improved under control of the color-tunable electroluminescence.

In order to achieve the required characteristics and quality of OLEDs, specifically designed molecular structures of electroactive compounds have to be utilized in the functional layers of the devices. **The aim of the presented work** is comprehensive analysis of the structure-properties relationship of new organic electroactive compounds necessary for the improvement of OLEDs.

The tasks of the dissertation:

- Investigation of photophysical, electroluminescent, thermal properties of new carbazolyl- and 1,2,3,4-tetrahydrocarbazolyl-substituted benzothiadiazoles with donor-acceptor-donor structures;
- Photophysical and electroluminescent investigation of new symmetrical and asymmetrical donor-acceptor-donor bipolar derivatives of benzonitrile containing phenoxazine, phenothiazine, dimethyldihydroacridine, carbazole moieties as donor units;
- Photophysical and electroluminescent study of the new donor-acceptor-donor type TADF emitters with diphenylsulfone as the acceptor and 2-(trifluoromethyl)-10*H*-phenothiazine, 10,11-dihydro-5*H*-dibenz[b,f]azepine, 5*H*-dibenz[b,f]azepine, 4-methoxy-9*H*-carbazole or 1,2,3,4-tetrahydro-9*H*-carbazole as donor units;
- Study of thermal, photophysical, electrophysical and electroluminescent properties of the new derivatives of methoxytriazine containing *tert*-butylcarbazole moieties;
- Investigation of methoxycarbazolyl-disubstituted dibenzofurane derivatives as hosts for guest:host systems of TADF-based and phosphorescent OLEDs;
- Photophysical and electroluminescent investigation of the new diphenylsulfones substituted by *tert*-butylcarbazole and carbazole units in *para*- and *ortho*- positions as hosts for TADF-based OLEDs.

Novelty and relevance of the thesis:

- Red non-doped OLEDs based on new donor-acceptor-donor emitters with a benzothiadiazole acceptor and carbazolyl donors were designed, fabricated and characterized;
- The possibility of tuning the characteristics of TADF and AIEE by selection of dimtehyldihydroacridine, phenoxazine, carbazole and phenothiazine donating substituents in donor-acceptor-donor benzonitrile derivatives was demonstrated for the first time;
- Newly designed and synthesized TADF emitters based on diphenylsulfone and dibenzothiohene derivatives with two di-*tert*-butyldimethyldihydroacridine substituents were utilized in the fabrication of efficient OLEDs;
- Photophysical and electroluminescent characterization of the series of triphenyltriazine substituted by tert-butylcarbazolyl moieties as TADF emitters was performed for the first time;
- The suitability of methoxycarbazolyl-disubstituted dibenzofurans which showed acceptable charge transporting properties for the application as hosts for green TADF OLEDs and green/red PhOLEDs was demonstrated for the first time;

- For the first time, a diphenylsulfone-based donor-acceptor-donor derivative was successfully employed as an efficient host for TADF OLED.

Contribution of the author:

The presented scientific work and the analysis of its results were conducted by the author in collaboration with the colleagues/co-authors of the publications from Kaunas University of Technology, Vilnius University, National Taiwan University and other institutions. Methoxycarbazolyl-disubstituted dibenzofurans were synthesized by dr. A. Bučinskas. All other series of the studied compounds were synthesized by dr. D. Gudeika. The author analyzed the results of theoretical calculations. The author made contribution to the photophysical investigations and characterization of the series of carbazolyl- and 1,2,3,4-tetrahydrocarbazolyl-substituted benzothiadiazoles and conducted them for all other series of investigated derivatives. Device fabrication was done by the author except for OLEDs made in Taiwan for the series of TADF emitters based on diphenylsulfone or dibenzothiophene and di(*tert*-butyl)dimethyldihydroacridine. The author in collaboration with scientific consultant habil. dr. D. Volyniuk conducted measurements and analysis of the electrochemical, photoelectrical, charge-transporting properties of the investigated compounds.

2. LITERATURE REVIEW

The *Literature review* chapter contains the information from articles of the author (see *7. List of publications on the subject of the thesis*).

2.1. Organic light emitting diodes

The pioneer steps in the investigations of the contact between the electrode and the organic crystal was accomplished by Martin Pope's group in 1960.[6] Three years later, they achieved electroluminescence (EL) of anthracene crystals with and without doping into tetracene under high vacuum.[4] As the result of researches of EL in thin films and crystals of organic materials conducted in the 1960s, Williams and Schadt presented the first organic light emitting diode (OLED) working at ~400 V based on anthracene crystals and optimized electrodes.[7] In the next decade, scientists were focused on the synthesis and the doping concentration control of the conjugated polymers.[8-10]

The dawn of the era of OLEDs began with the first efficient devices fabricated by Ching Tang and Steven Van Slyke from Eastman Kodak in 1987.[11] They used a multi-layer structure with hole transporting and electron transporting layers and reduced the operating voltage, which led to the increase of efficiency. This was a fundamental discovery for the whole technology making tectonic changes in the branch of the illumination industry.

At the same time, there was a significant development in the research of conjugated polymers, oligomers and their use in optoelectronics.[12-17] The 1990s were spent on the improving polymer light emitting diodes form the first fabricated devices to efficient ones.[18,19] In the 21st century, OLED is being considered as one of the major lighting technologies.[20-23]

In general, OLED is an electroluminescent device which consists of a heterostructure of layers of semiconducting organic materials between the cathode and the anode.[3] The number of functional layers varies starting from one depending on the goal of use. The scheme of the optimized OLED structure is presented in Fig. 2.1. The hole and electron injection layers, HIL and EIL, respectively, induce charge carriers from electrodes. The hole (HTL) and electron (ETL) transport layers help to transfer them to the emitting layer (EML) via an electric field. The blocking layers for holes (HBL) and electrons (EBL) can be used for interference of charge carriers in a transmission to the opposite part of a device. The radiative recombination of the electron-hole pairs called excitons takes place in EML. This layer can be a neat film of a bipolar/ambipolar emitter or a layer of emissive species doped into a host for an efficient energy transfer. The created light is extracted from the surface of a diode through an anode and a glass substrate.

Organic semiconductors are organic polymers and small molecules with a π-electron conjugated system.[24] Their semiconducting properties originate in the hybridization of atomic orbitals. π- and σ- bonds have axial symmetry as they are covalent bonds formed along a connective line between two atomic nuclei. s- and p-atomic orbitals may be hybridized in hydrocarbons into three sp^2- orbitals situated at an angle of 120° with each other and one unchanged p_z- atomic orbital located perpendicular to them. The spatial superposition of atomic orbitals where the

electron wave function has the biggest amplitude is called the molecular orbital which is determined by π- and σ- chemical bonds. More specifically, π- bonds are formed by p_z- atomic orbitals, while σ- bonds are created by sp^2- orbitals. π-conjugation serves a key role in the determination of semiconducting properties of organic derivatives. Solids of organic semiconductors are formed as a result of intermolecular van der Waals interactions, which is the major difference from the structures of non-organic semiconductors where strong covalent bonds dominate.

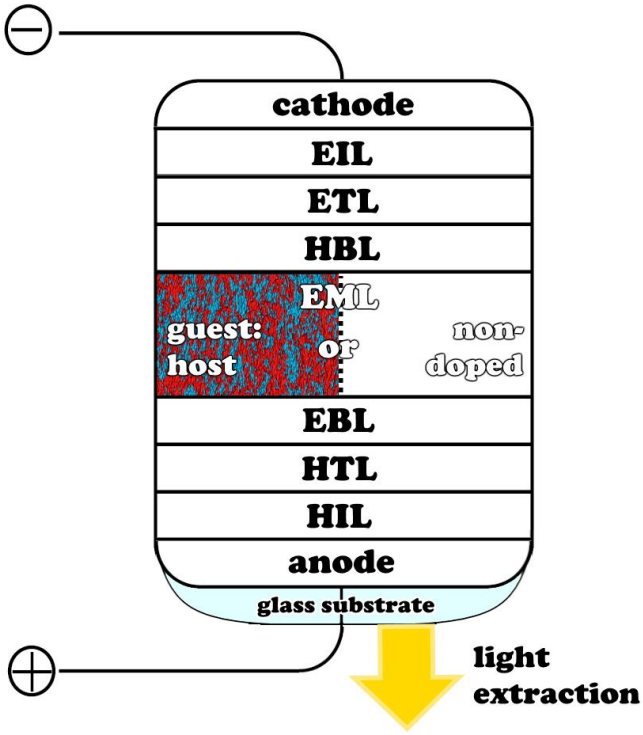

Fig. 2.1 Schematic structure of optimized OLED

Excitons utilized in OLED are the so-called Frenkel excitons, quasiparticles of a small binding radius, unlike Wannier–Mott excitons of non-organic semiconductors. Considering the unique capabilities of short-lived small-distance molecular interactions, Frenkel excitons perfectly fit the goal of EML functioning in an OLED. Under excitation in organic compounds, an electron is removed from the highest occupied molecular orbital (HOMO) to the lowest unoccupied molecular orbital (LUMO) thus leaving a hole. There is a HOMO-LUMO gap of forbidden energy levels with a value of 1.4–4 eV fitting well for the emission in the optical range. It gives a pass for unique physical and chemical characteristics suitable for optoelectronic applications. In OLED, holes and electrons migrate on the HOMO and LUMO of molecules of the respective layers to EML. The radiative deactivation of an electron-hole pair occurs on the interfaces of EML and neighbor layers. Dealing with the Frenkel excitons dictates the optimal doping concentration in a guest:host system and the appropriate thickness of EML considering the mean free

path of a few dozens of nanometers. Too little thickness may cause electrical breakdown.

Luminescence is a residual over heat spontaneous emissive radiation.[25,26] Kasha's rule postulates that luminescence arises from the lowest energy level of an excited state after nonradiative transitions from upper vibrational sublevels. Electroluminescence (EL) is a luminescence of molecules excited by electricity. The nature of electronic processes taking place in organic semiconductors performing EL in OLEDs can be analyzed from the photoluminescence (PL) investigation of corresponding materials. PL is the luminescence induced by radiation. One of the major photophysical characteristics, PL quantum yield Φ is the ratio of the emitted photons to the particles of an electromagnetic wave absorbed by the material. Φ is dependent purely on the excitation light source wavelength according to Vavilov-Kasha's rule derived from Kasha's rule. As maintained by the Franck-Condon principle, the correlation between the distribution of spectra of molecules and an integrated overlap of wavefunctions of quantum harmonic oscillators of the ground and excited states involved in a transition is quadratic. Thus, the PL spectrum is red-shifted to the corresponding absorbance spectrum. The difference in the peak position of these two spectra is called the Stokes shift. The anti-Stokes shift is considered in cases of the highest energy emission spectral peak having a smaller wavelength than the lowest energy absorption peak. It can reveal the impact of the local excited (LE) states or nonlinear phenomena into emissive processes.[25] According to Levshin's law, there is a mirror image symmetry of absorption and PL spectra described by Kennard-Stepanov relation.[27-29] Symmetry breaks under the effects of the reabsorption or excitation transfer.

Major characteristics are used for a convenient comparison of different OLEDs, such as EL spectra, CIE coordinates, current, power and external quantum (EQE) efficiency. 1931 (Commission Internationale de l'Eclairage) CIE coordinates are the color index, the quantitative link between the emission spectra and the perceived color. The current efficiency is a ratio of the luminance of light extracted from the OLED external surface to the density of the electrical current supplied to the device. Power efficiency is defined as the ratio of the radiation flux to the electrical power used to supply OLED. EQE is the ratio of the number of photons extracted from the diode emissive surface to the number of electrons injected in OLED. EQE is an electroluminescent analogue of Φ and has a linear dependence with it[1]:

$$EQE = \gamma \eta_{S/T} \Phi \eta_{out} \quad (2.1)$$

where γ stands for the charge balance factor, the ratio of decaying excitons to injected charge carriers. For an efficient radiative recombination of excitons, the amount of electrons and holes must be as close to equality as possible, which would correspond to the maximum γ of 1. It impels to optimize the structure of devices by selecting layers with the appropriate charge carrier transport characteristics and tuning their thickness. $\eta_{S/T}$ is the radiation recombination factor which reveals the portion of excitons used in emissive processes. It has the internal quantum efficiency

(IQE), the percentage of excitons employed in emission, as its limit. η_{out} is the outcoupling factor, the indicator of the fraction of light emitted from the external surface of a device. Without using advanced substrates for out-coupling treatment, it is usually around 30%.

2.2. Bipolar fluorescent emitters with benzothiadiazole acceptor

Excitation upon electricity produces 25% of singlet and 75% of triplet excitons due to the statistics of the orientation of a spin angular momentum of an electron-hole pair. Fluorescence is a radiative relaxation of the first singlet excited state S_1. Prompt fluorescence (PF) is considered if singlet excitons were originally located on S_1. Therefore, the maximum value of IQE is 25% for fluorescent emitters since only singlet excitons emit light. This determines the highest possible values of EQE up to ~7–8% for fluorescent OLEDs without advanced substrates. In order to simplify the fabrication process for industries, non-doped EML of one organic emissive material is preferred. Thus, a fluorescent emitter should have a pronounced ambipolar charge-transporting property for providing γ close to 1.

Properties of ambipolar organic compounds containing electron-donating and electron-accepting fragments can be optimized by controlling the number of the donor and acceptor units in the structures.[10] The strength of donor-acceptor interactions is influenced by accepting moieties and π-conjugated bridges.[30] Usually, strong accepting moieties and short bridges enhance donor-acceptor interactions.[31] 2,1,3-Benzothiadiazole (BTD) is a typical electron-withdrawing moiety amenable to facile ring modification. Introduction of such fragments into molecules may facilitate electron-injection or charge-transport and enable to tune band gaps.[32,33] BTD moieties are utilized in the design of π-conjugated compounds for different applications.[34] Carbazole compounds are known as classic hole transporters.[35] They have been extensively used in many materials with high charge carrier mobility. Some of them exhibit ambipolar characteristics.[36] Carbazole derivatives are utilized in various electronic and optoelectronic devices including OLEDs.[37] There are many reports on benzothiadiazole derivatives containing donor groups. For example, Lee and co-workers[38] synthesized π-conjugated organic dyes containing triphenylamino and BTD moieties (HKK-BTZ1, Fig. 2.2). Compounds with the double-bond bridged moieties showed a bathochromic shift of the ultra-violet absorption band relative to that of the compound that has a single bond between the electroactive moieties. The teams of Tao[39] and Xu[40] reported on BTD derivatives containing carbazole units which appeared to be promising organic light emitting materials (CBTD, Fig. 2.2) exhibiting high thermal stability (featuring a decomposition onset temperature of ~260–300 °C). Promarak *et al*.[41] demonstrated solution processed efficient green and red electroluminescent devices containing BTD and carbazole derivatives. Recently, Ni *et al*.[42] reported on red TADF emitters with a D-A-D structure containing BTD and diphenylamine moieties, 9,9-dimethyl-9,10-dihydroacridine or 9H-carbazole. Red OLEDs containing BTZ-DMAC (Fig. 2.2) doped into 4,4'-bis(carbazol-9-yl)biphenyl (CBP) showed a maximum EQE of 8.8%.[42] Derivatives containing carbazole and benzothiadiazole moieties intended for photovoltaic applications have also been reported.[43]

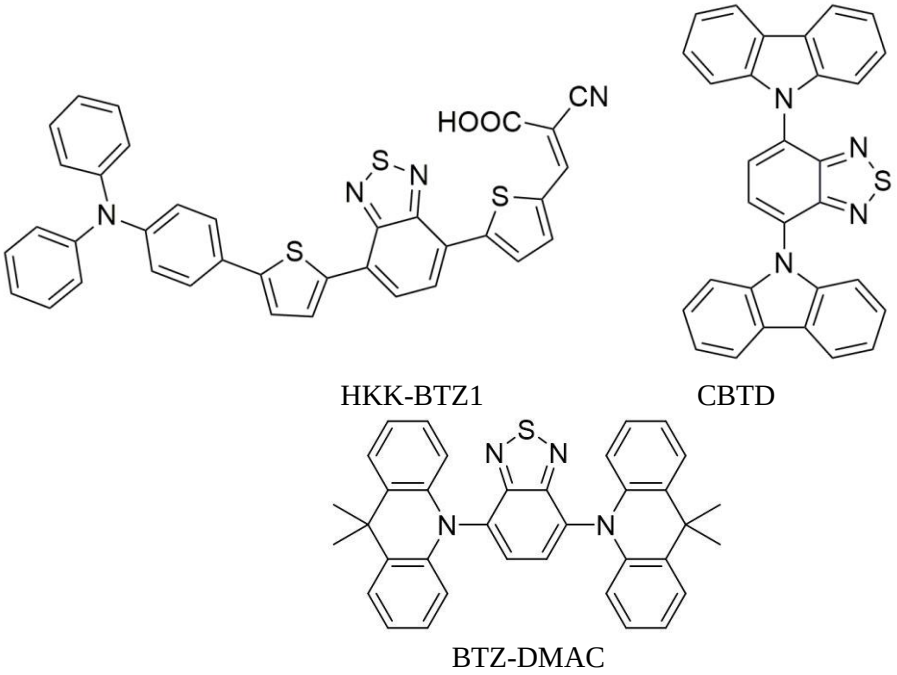

HKK-BTZ1 CBTD

BTZ-DMAC

Fig. 2.2 Chemical structures of HKK-BTZ1, CBTD and BTZ-DMAC

Development of new ambipolar derivatives of BTD which could be used as charge transporting materials or as emitters is still of great interest. Additional information on the structure-properties relationship of BTD and carbazole derivatives would also be useful for the design of new efficient organic ambipolar semiconducting emitters.

2.3. Phosphorescent emitters

Multiplicity *2S+1* is an indicator of the number of spatial orientations of the spin vectors of an electron pair. According to the Pauli exclusion principle, singlet and triplet excited states are formed when an atom is excited depending on the spin multiplicity: 1 for singlet and 3 for triplet levels. Thus, the transition from the first excited triplet T_1 state to the ground state S_0 involves a change in the electronic state making it improbable. This radiative transition called phosphorescence is forbidden, consequently, by the selection rule. As the result, phosphorescence lifetime values vary typically from 10^{-6} s up to seconds.[24-25] It strongly contradicts a PF with a lifetime of emission τ_{PF} within the range of 10^{-9}–10^{-7} s.[24-25] T_1 level has a smaller energy than S_1.[24-25]

Phosphorescence can be detected experimentally as it appears at extremely low temperatures. In such conditions, due to a lack of intermolecular interactions with oxygen molecules, electrons on T_1 deactivate more preferably through phosphorescence than via non-radiative relaxation. Electrophosphorescence was detected at liquid nitrogen temperature for ketocoumarin-based compounds for the first time in 1990.[44]

Employment of triplet excitons into luminescence can increase the efficiency of devices by four times. Efficient electrophosphorescence was achieved in 1999 for iridium phenyl-pyridine complexes with an emission decay rate of ~10^6 s^{-1}. The technology of PhOLED has become one of the first successful attempts of reaching maximum IQE since then. The problem of the stable and efficient blue emission for OLED is not solved by this technology though.[45] The EQE values of 27.3[46], 38.2[47], 36.4[47] and 14.4%[48] were achieved for red, yellow, green and deep-blue PhOLEDs, respectively. Prohibition of the selection rule was overcome by the facilitating of spin-orbit coupling induced by heavy metal particles incorporated into an organic matrix. Metal-ligand interactions determine the nature of numerous electronic transitions not only from the frontier molecular orbitals in phosphorescent dyes. If phosphorescent transitions are localized on organic ligand moieties, these emissive processes are called as ligand-centered (LC) for ππ* transitions or intraligand charger transfer (ILCT) for charger transfer (CT) transitions. Phosphorescence of the heavy metal substituents is tied with the excitation of *d*- electrons. Thus, the metal-centered (MC) state emits via dd* phosphorescence. If excitation transfer occurs from a ligand to a metal, the corresponding dπ* MLCT (metal-to-ligand charge transfer) state is involved in emission.

An important role in advancing the phosphorescent capabilities of emitters belongs to tuning triplet levels. Most of them have the so-called zero-field splitting (ZFS) of T_1 determined fully by the spin-orbit coupling of the d- orbital of a metal atom. ZFS is dramatically influenced by the molecular structure and depends on the planarity and symmetry of phosphor. Phosphorescent emitters with atoms of iridium and platinum are most common for PhOLEDs. ^{3}LC(ππ*) emitters have the smallest ZFS of up to 1 cm^{-1}. Bigger ZFS in the range of 3.8 to 38 cm^{-1} occurs in many phosphorescent dyes of a various nature of excited states. ^{3}MLCT compounds reached the largest values from 50 up to 211 cm^{-1}.[45] The high cost of such earth-rare materials is the biggest disadvantage, and it forces scholars to search for alternatives.[3]

$Ir(piq)_2(acac)$ (bis(1-phenylisoquinoline)(acetylacetonate)iridium(III))[45] is a heavy-metal-containing red phosphor with the melting point of 366–370 °C. Its energy of HOMO and LUMO are at levels of -5.2 and -3 eV, respectively. The 1-phenylisoquinoline substituent partially quenches triplet-triplet annihilation (TTA) and lowers the lifetime of the triplet excited state.[49] 23.7% of EQE for $Ir(piq)_2(acac)$-based red PhOLED was achieved in 2011.[50]

$Ir(ppy)_3$ or tris[2-phenylpyridinato-C^2,*N*]iridium(III)[45] is a well-known emitter for green PhOLEDs and the most widely used starting material for the synthesis of green phosphorescent dyes. Its high Φ makes IQE close to 100%[51-53]. The melting point of $Ir(ppy)_3$ is 451 °C. The HOMO level has an energy of -5.6 eV. The value for LUMO is -3 eV. Dilute chloroform solution has spectral peaks of absorption at 340 nm and the PF band at 512 nm. $Ir(ppy)_3$ with the C_3 symmetry has four $MLCT_1$ transitions formed by 36 levels as the sum of the impact of ZFS and specific spin-orbit interactions. This dye is sensitive to the presence of oxygens. $Ir(ppy)_3$ is also fully soluble in common solvents which make it inappropriate for the fabrication of

solution-possessed EML. The EQE of 21.6% was reached for green PhOLED containing $Ir(ppy)_3$ as emissive species.[54]

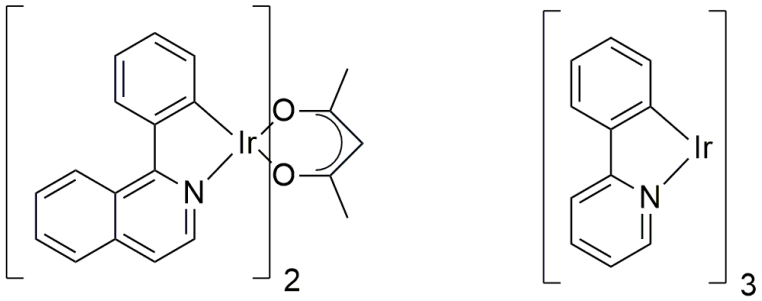

$Ir(piq)_2(acac)$ $Ir(ppy)_3$

Fig. 2.3 Chemical structure of $Ir(piq)_2(acac)$ and $Ir(ppy)_3$

A promising area of research is the design of purely organic dyes which would exhibit RTP efficiently in OLEDs in the near future.[55-64] An intermolecular CT and/or an introduction of aromatic carbonyls into the molecular structure can lead to enhancement of spin-orbit interactions necessary for minimizing the RTP lifetime in order to avoid the interception of energy by air interactions.[65-68] Non-radiative intersystem crossing from the vibrational levels of S_1 to those of T_1 (ISC) is spin-forbidden. Therefore, its constant rate k_{ISC} is small and is in the range of 10^6-10^{11} s^{-1}. It may be intensified for compounds without a heavy metal content by *d*-electrons of sulfur[69-72], bromine, phosphorus, iodine, tellurium, etc.[55] Stimulated ISC harvests triplet states for RTP as it is quicker than the interception of electronic excitation energy by oxygen molecules.

It was reported that an important factor of micelle-stabilized RTP appearance in phosphorescent aromatic hydrocarbons substituted by strong electron-withdrawing moieties is the fluorescence quenching.[73] The heavy atom induced ISC state was in that case responsible for PF yield Φ_{PF} quenching (2.2) and simultaneous RTP facilitating via ISC.

$$k_{PF} = \frac{\Phi_{PF}}{\tau_{PF}} = \Phi_{PF}(k_r^S + k_{IC}^S + k_{ISC}) \quad (2.2)$$

k_{PF}, k_r^S, k_{IC}^S stand for the rate constants of PF, radiative and non-radiative (internal conversion) relaxation of the S_1 state, respectively.

The Zeonex®, polystyrene polymer or specific rigid solid matrix is usually used for investigations in the field for its unique capabilities of suppressing any intermolecular interactions.[72-76] Elimination of excimer/exciplex formation, and quenching of non-radiative thermal decays gives a way for the observation of the RTP phenomenon. This is due to the suppressing molecular vibrations under the condition of no interactions with oxygen molecules in the guest:matrix doping system.

2.4. Thermally activated delayed fluorescent emitters

TADF phenomenon[77-80] is proposed as one of the novel approaches towards solving the problem of the 25% IQE limit (Fig. 2.4) and the high cost of phosphorescent dyes containing heavy metal atoms considering that TADF emitters are generally purely organic. In 2016, 36.7% of EQE for sky-blue OLEDs based on this approach with CIE coordinates (0.18, 0.43) was reported.[81] The emissive species in these devices were derivatives of spiro-acridine and tirazine. TADF is the emission of excitons transferred from the first triplet T_1 to the first singlet S_1 excited state via the mechanism of reverse intersystem crossing (RISC). Thermal motion of atoms makes RISC possible.[82,83]

Description of the physical processes happening in TADF dyes is shown in the Jablonski diagram (Fig. 2.4).

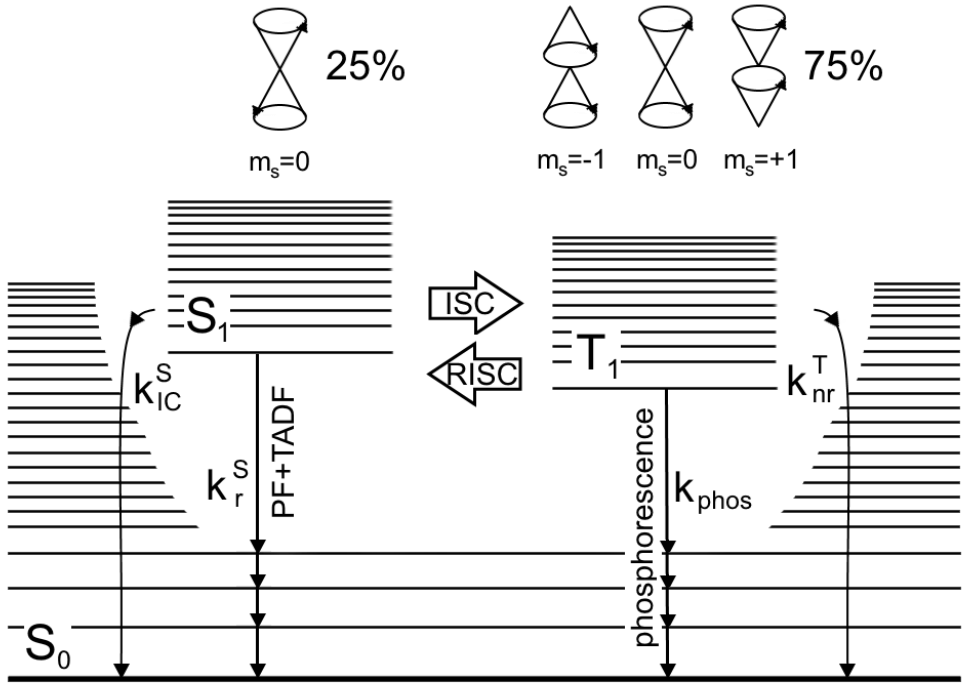

Fig. 2.4 Vector model of spin angular momentum and its statistical distribution when molecules are excited by electrical current and the simplified Jablonski diagram for TADF compounds

RISC transition of exciton requires the appropriate values of the difference between the energy levels ΔE_{ST} of the first excited states.[84] The values of T_1, S_1 level energy can be evaluated from the high energy onsets of the phosphorescence and fluorescence spectra, respectively. The dependence of the RISC constant rate k_{RISC} and the temperature can be ascribed to the Boltzmann distribution[85] (2.3) which may be applied in most of the cases of LE absence giving the thermal energy needed for RISC to be nearly 26 meV at 300 K:

$$k_{RISC} \sim e^{-\frac{\Delta E_{ST}}{k_B T}} \quad (2.3)$$

Kinetic equations (2.2) and (2.4) determine the radiative decay rate constants for PF and DF types of emission in the case of the TADF phenomenon[85-87]:

$$k_{DF} = k_{nr}^{T} + k_{RISC}\left(1 - \frac{k_{ISC}}{k_r^S + k_{IC}^S + k_{ISC}}\right) \quad (2.4)$$

k_{nr}^{T} is attributed to the non-radiative relaxation of the T_1 state. RISC usually has a constant rate of 10^3–10^6 s^{-1}. The fluorescence quantum yield is the sum of PF and DF yields:[85-87]

$$\Phi_F = \Phi_{PF} + \Phi_{DF} = \sum_{k=0}^{n} \Phi_{PF}(\Phi_{ISC}\Phi_{RISC})^k = \Phi_{PF}\frac{1}{1-\Phi_{ISC}\Phi_{RISC}} \quad (2.5)$$

where Φ_{ISC}, Φ_{RISC} correspond to the yields of T_1 states formed by ISC and S_1 states formed by RISC, respectively. The maximum value of Φ_{ISC} is 1-Φ_{PF}.

$$\Phi_{RISC} = \frac{k_{RISC}}{k_{phos} + k_{nr}^{T} + k_{RISC}} \quad (2.6)$$

$$\Phi_{ISC} = k_{ISC}\tau_{PF} \quad (2.7)$$

For efficient TADF emitters, ΔE_{ST} should be small enough for the fast RISC, usually less than 0.1eV. The energy levels of S_1 and T_1 states can be given by the following equations:[85-87]

$$E_{S_1} = E_{HOMO} - E_{LUMO} + J \quad (2.8)$$

$$E_{T_1} = E_{HOMO} - E_{LUMO} - J \quad (2.9)$$

where $E_{HOMO} - E_{LUMO}$ is the so-called 'optical band gap', the difference in the energy values of the highest occupied (HOMO) and the lowest unoccupied (LUMO) molecular orbitals, and J stands for the spin-exchange energy which is the same for both excited states. In the first-order approximation, ΔE_{ST} would be equal to $2J$. J is defined as the overlap integral of wave functions of frontier orbitals Φ_{HOMO} and Φ_{LUMO}[85-87]:

$$J = \iint \Phi_{LUMO}(r_1)\Phi_{HOMO}(r_2)\left(\frac{e^2}{r_1 - r_2}\right)\Phi_{LUMO}(r_2)\Phi_{HOMO}(r_1)dr_1 dr_2 \quad (2.10)$$

Reduction of the spin exchange energy results in minimizing ΔE_{ST}.[88] Accomplishment of these conditions requires the localization of well separated

frontier molecular orbitals on different substituents. Such a distribution of the frontier molecular orbitals leads to the difference in dipole moments μ_e (in the excited state) and μ_g (in the ground state).

The optimal design strategy for a TADF emitter is to construct linear donor-acceptor (D-A) and donor-acceptor-donor (D-A-D) molecules where HOMO and LUMO would be strongly set apart on the electron donating and accepting moieties of the excited molecule, respectively.[65,89,90] The excited state is characterized generally by the intramolecular CT state in this case.[91,92]

In D-A-D molecules, near-orthogonal geometry minimizes ΔE_{ST} thus making TADF possible.[93,94] Various heterocycles, such as acridane, phenoxazine, phenothiazine and carbazole, were used as donor moieties, and cyano, sulfone, triazine, xanthone, benzophenone and carbonyl moieties were employed as acceptor units to develop TADF emitters with different emission profiles.[79,85,95-104] Rational molecular design of derivatives containing electron-accepting cyano-substituted moieties and electron-donating fragments results in TADF emitters.[105]

A cyanobenzene moiety containing a single cyano group in the conjugated phenyl ring shows a reduced electron withdrawing strength and a weaker intermolecular CT interaction in D-A type derivatives.[105] Compared to dicyano-substituted moieties, monocyano-substituted moieties were less commonly employed for the design of TADF emitters. TADF materials with electron accepting cyanobenzene and electron donating phenoxazine moieties were recently reported.[106] OLEDs containing layers of these emitters showed an EQE of up to 19.9%. The tuning of the emission of TADF emitters based on phenoxazine and triphenyltriazine was achieved by changing the number of donor substituents.[107] A study of derivatives of acridan and various CN-containing donors including cyanobenzene revealed that the TADF emission wavelengths were tunable from deep blue to yellow not only by the acceptor strength but also by the control of the acceptor conformation (twist angles).[108]

The selection of the appropriate acceptor is evidently a crucial point in the search for highly efficient TADF emitters.

4CzIPN is a highly thermally stable TADF exhibiting material of carbazolyldicyanobenzene reported by Adachi *et al.* in 2012. The EQE maximum of 19.3% was achieved for the corresponding OLED.[79] It has intramolecular CT occurring between four carbazolyl electron donors and a dicyanobenzene acceptor. The large dihedral angle of 60° between the moieties due to steric hindrance causes experimental ΔE_{ST} to be 0.08 eV. Quenching of non-radiative ways of relaxations was ascribed to the limited torsion flexibility promoted by the introduction of cyano groups. As a result of the high quantum yield, 4CzIPN performed as an excellent green TADF among dozens of reported[109] doped EML of OLEDs reaching an EQE value up to 31.2%[110] in the absence of advanced light extraction. This derivative features HOMO and LUMO levels at -5.8 and -3.4 eV, respectively.[111] Its melting point is over 300 °C.

The more fitting parameters for green TADF OLED as ~9 meV value of ΔE_{ST} smaller than the thermal energy and Φ of 100% were achieved by the substitution of the diphenylaminocarbazole donor moiety by electron accepting triphenyltriazine

for DACT-II (9-[4-(4,6-diphenyl-1,3,5-triazin-2-yl)phenyl]-N^3,N^3,N^6,N^6-tetraphenyl-9*H*-carbazole-3,6-diamine) reported by Adachi *et al.* in 2015. These characteristics, due to matching HOMO/LUMO distributions, resulted in an EQE of 29.6% for green OLEDs with losses of efficiency related to out-coupling only. The energy values of HOMO and LUMO are -5.5 and -3.2 eV, respectively. Excellent TADF features were provided by strong k_{RISC} reaching $6.88 \cdot 10^4$ s^{-1} at 300 K massively overcoming k_{ISC} of ~$9.2 \cdot 10^6$ s^{-1} consistent after heating. Interestingly enough, TADF was found to be efficient even at 200 K ($6.88 \cdot 10^4$ s^{-1} of k_{RISC}), which dramatically widens the temperature range for device operation.[112]

It has been shown that the modification of hosts by *tert*-butyl groups can lead to the blocking of energy-loss pathways of TADF emitters distributed in the host leading to the enhancement of OLED efficiency.[113] 'Full-exciton radiation' was achieved in TADF OLEDs using diphenylphosphine oxide as the acceptor linked to *tert*-butylcarbazoles.[114] Direct attachment of *tert*-butyl groups to donating carbazole of D-A-D-type TADF emitters made it possible to increase the device performance.[115] While *tert*-butylcarbazole moieties are widely utilized in TADF emitters,[116] there are no examples of the usage of the *tert*-butyl substituted acridan moiety in the design of TADF dyes yet. Modification of carbazole with *tert*-butyl substituents in the structure of 4CzIPN facilitated solution processing OLED fabrication to a great extent.[117]

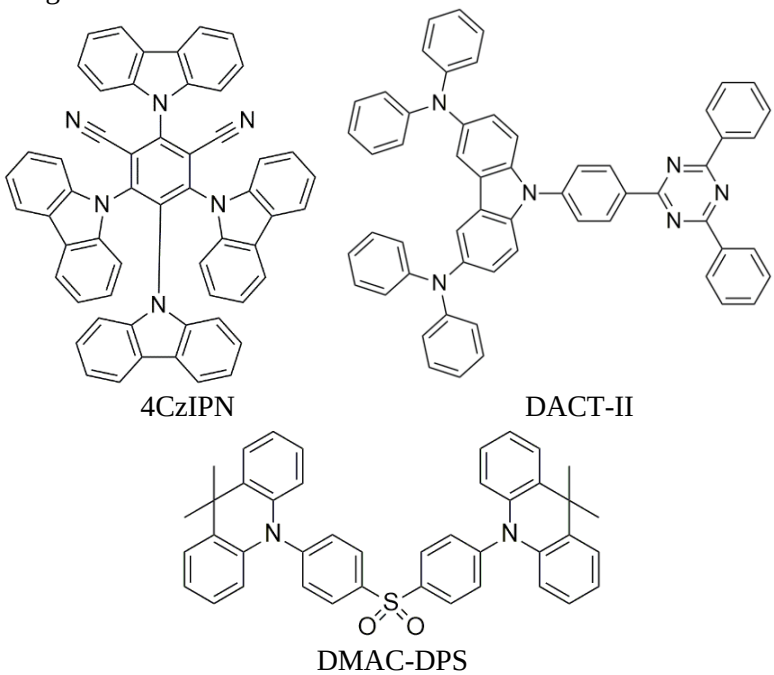

Fig. 2.5 Chemical structure of 4CzIPN, DACT-II and DMAC-DPS

Methods of spectroscopy are used for CT detection accompanying TADF. Molecules with a dipole moment interact differently with the environment of different polarity. Usually, in non-polar solvents, a TADF derivative emits $^1\pi\pi^*$

fluorescence and ^{1}CT emission in a polar medium. The intermolecular CT character of emission of the investigated compounds in polar solutions is evident by the monotonical bathochromic shift of the PL spectral peak with a change of solvents to a more polar one. The Onsager description[118] of non-specific electrostatic interactions between the solvent and the solute gives a pass to the theories of the solvatochromic effect in the absorption and emission spectra. The Lippert-Mataga[119-121] plots based on the relation of the Stokes' shift $\Delta\tilde{\nu}$ and the orientation polarizability Δf are defined by the equation:

$$\Delta\tilde{\nu} = \frac{2\Delta f}{4\pi\varepsilon_0\hbar c a^3}(\mu_e - \mu_g)^2 + \Delta\tilde{\nu}^0 \quad (2.11)$$

Superscript ^{0} is an indication of the absence of a solvent. a stands for the Onsager cavity radius. The approximated slopes with great linear relationships correspond to the $(\mu_e - \mu_g)^2$, revealing the change of dipole moments after excitation. It is worth mentioning that the assumptions of the Lippert-Mataga approach require linearity and a positive value of the slope. If not, it cannot be applied for the description of the luminophore.[122]

Highest Φ_{RISC} yields happen for the compounds whose ratio between DF and PF yields is more than four. Φ_{PF} and Φ_{DF} can be estimated from calculating the integral sum of the respective PL decay components. Another exhibition of these yields can be manifested from the increase of the intensity of the solution after degasation[93] by more than four freeze/thaw operations or deoxygenation by nitrogen or argon. The difference in intensity would be attributed to DF. Interaction between the studied molecules and the molecules of air quench phosphorescence, which is a quantum mechanically forbidden transition and significantly promotes the non-radiative relaxation of the T_1 state. The condition for suppressing vibrational decays having an impact on the triplet states is the absence of air. Otherwise, the DF yield is dramatically reduced. In the case of TADF, the position peak should be very close after degassing/deoxygenation thus indicating the same radiative way of relaxation from S_1 for excitons originated on this state and formed on T_1. An increase of intensity bigger than by four times may be a good indication of strong TADF occurring in a sample. Equivalent experiments can be conducted with solid-state samples, doped Zeonex® or polystyrene films.

Formulas (2.12), (2.13) describe the population of S_1 and T_1 states over time:[123]

$$\frac{dS_1}{dt} = -\left(k_r^S + k_{IC}^S + k_{ISC}\right)S_1 + k_{RISC}T_1 \quad (2.12)$$

$$\frac{dT_1}{dt} = -\left(k_{phos} + k_{nr}^T + k_{RISC}\right)T_1 \quad (2.13)$$

Their solutions are:

$$T_1(t) = T_0 e^{-(k_{phos}+k_{nr}^T+k_{RISC})t} \quad (2.14)$$

$$S_1(t) = \frac{k_{RISC}}{k_r^S+k_{IC}^S+k_{ISC}-(k_{phos}+k_{nr}^T+k_{RISC})} T_0 e^{-(k_{RISC}+k_{phos})t} \quad (2.15)$$

As it can be seen from the formulae, the involvement of triplet states determines longer lifetimes for TADF than τ_{PF}, 10^{-9}-10^{-7} s. The easiest instrument to exclude the TADF phenomenon as a cause of emission is the detection of the absence of DF with lifetimes in the μs range. It can be easily concluded from the analysis of PL spectra recorded with a delay or PL decay curves recorded at room temperature. Besides, TADF shows smaller lifetimes than phosphorescence ordinarily has. TADF and PF should have close spectral behavior revealing radiative deactivation of triplet excitons through the $S_1 \rightarrow S_0$ transition. The polarity of the host may cause bathochromic shifts of the TADF spectral peak promoted by local dipolar interactions between the host and the guest molecules.[86]

Persistent steady-state TADF intensity I_{TADF}^{SS} is determined by the initial population T_0 of triplet excitons, which directly corresponds to the intensity of excitation:[123]

$$I_{TADF}^{SS} = f_{inst} k_{f0} \int_0^\infty S_1(t)dt = f_{inst} k_{f0} \frac{T_0 k_{RISC}}{(k_{phos}+k_{nr}^T+k_{RISC})(k_r^S+k_{IC}^S+k_{ISC}-(k_{phos}+k_{nr}^T+k_{RISC}))} \quad (2.16)$$

f_{inst} represents an instrumental factor, k_{f0} stands for the constant rate of the natural decay. Considering

$$k_r^S + k_{IC}^S + k_{ISC} \gg k_{phos} + k_{nr}^T + k_{RISC} \quad (2.17)$$

Equation (2.17) is simplified to yield:

$$I_{TADF}^{SS} = f_{inst} k_{f0} \frac{T_0 k_{RISC}}{(k_{phos}+k_{nr}^T+k_{RISC})(k_r^S+k_{IC}^S+k_{ISC})} \quad (2.18)$$

At a low temperature, the thermal motion of atoms is not sufficient for RISC ($k_{RISC} \ll k_{phos} + k_{nr}^T$) to make triplet excitons overcome ΔE_{ST} energy barrier[123]:

$$I_{TADF}^{SS} = f_{inst} k_{f0} \frac{T_0 k_{RISC}}{(k_{phos}+k_{nr}^T)(k_r^S+k_{IC}^S+k_{ISC})} \quad (2.19)$$

As RISC intensifies at a higher temperature, TADF can be experimentally detected by an increase of DF intensity to the value:[123]

$$I_{TADF}^{SS} = f_{inst} k_{f0} \frac{T_0}{k_r^S + k_{IC}^S + k_{ISC}}$$

(2.20)

There is an experimental solution to distinguish TADF and other possible delayed processes taking place in the sample at room temperature.[123] For example, sometimes, DF accompanies TTA, the phenomenon of the extermination of two triplet excitons with the creation of one singlet exciton with two-times higher energy which recombines radiatively. Usually, it can be easily differentiated by evaluating singlet and triplet energy levels from the onset of the respective PL and phosphorescence spectra. However, sometimes, higher triplet states than T_1 contribute in TTA, which is harder to confirm. For compounds with this type of emission, a constant rate of phosphorescence k_{phos} is opposed to the quenching constant rate of the diffusion collision of triplet excitons k_{TTA}.

Initially, $k_{TTA} \ll k_{phos} + k_{nr}^T + k_{RISC}$ showed quadratic dependence of intensity induced by TTA upon the excitation dose represented by T_0 population:[123]

$$I_{TTA}^{SS} = \frac{f_{inst} k_{TTA}}{2(k_{phos} + k_{nr}^T)} T_0^2$$

(2.21)

Higher triplet population with an increase of intensity of excitation leads to larger rates of TTA. Equation (2.21) can be rewritten as:[123]

$$I_{TTA}^{SS} = \frac{f_{inst}}{2} T_0$$

(2.22)

TADF differs from TTA by its continuous linear dependence of the emission intensity on the excitation dose. It corresponds to the slope of 1 of the graphical fit on the corresponded log-log scale. For derivatives with TTA, initial quadratic correlation (the slope of 2) transforms into linear at a higher excitation intensity. If the slope is prominently in the middle between 1 and 2, the occurrence of competitive delayed emissive processes of a different origin can be postulated.

2.5. Aggregation induced emission enhancement

Most luminophores exhibit the so-called aggregation-caused quenching (ACQ).[124] ACQ is the phenomenon of a negligible PL in the solid or aggregate state due to the strong intermolecular π-π stacking. This results in the efficiency drop of emitting dyes employed in OLEDs or other optoelectronic applications based on thin films of organic semiconducting materials. A planar aromatic core is very common for organic dyes. As a result of the presence of π-π stacking caused by this, ACQ appearance was considered as a sort of general rule for fluorophores. However, cases of a more prominent Φ upon aggregation in contrast with diluted solutions for luminogens have been known for a long time, at least since Sir George Gabriel Stokes's investigations in 1853.[125] Significant attention to the opposite to ACQ phenomenon was not paid prior to the 21st century, when the concept of aggregation-induced emission (AIE) was introduced by Tang *et al.* (compound 1, Fig. 2.6).[124]

AIE provides an opportunity of utilization of organic dyes in EML of OLEDs for efficient electroluminescence without the obstacle of emission suppression caused by π-π stacking. The importance of such an achievement forced to conduct massive researches in order to systemize the knowledge and highlight the main principles of the AIE mechanism.

Since 2001, many derivatives exhibiting AIE have been explored, which led to the consensus that the restriction of intramolecular rotations and vibrations should be considered as the major cause of the phenomenon. The structural rigidification leads to Φ increase in the solid state for the corresponding type of dyes. It can be provided by low temperature, doping into rigid host matrices including polymers or high viscosity environment. Unlike the conventional ACQ materials, the structure of dyes exhibiting AIE is highly twisted, which reduces π-π stacking and intramolecular motions in dependence of the vibrational amplitude and/or conformational flexibility. Massive suppressing of the non-radiative path for the deactivation of singlet excited states of a luminophore takes place in solids and aggregates for AIE luminogens. For example, if such compounds contain aromatic rings, these substituents operate as rotors when fully solvated and consume excitation energy with the following rapid non-radiative decay.[125]

However, new types of derivatives exhibiting AIE were discovered recently which do not contain rotors. In this case, utilization of the restriction of intramolecular motion cannot be applied as usual for the explanation of a high Φ when a compound is aggregated. It is very important to mention that the restriction of both intramolecular rotations and vibrations should be considered at great length. Some of the alternative rotor-free mechanisms of AIE include E/Z isomerization and photo-cyclization.[125] Phenomena related to AIE are of great interest in the field of the OLED technology as well. The main one is aggregation induced emission enhancement which is characterized by the non-zero quantum efficiency of compounds when solvated and significant enhancement of Φ in solids. The AIE-like effect, crystallization induced emission, can occur for materials in the crystal phase. Due to the specific kinetics of physical processes, phosphorescence specifically can be originated due to the aggregation or crystallization of compounds.

It has also been discovered that some TADF luminophores are characterized additionally by AIE (DPS-PXZ, DAcIPN, Fig. 2.6).[126,127] Novel electroluminescent materials exhibiting aggregation-induced delayed fluorescence are considered to be the best candidates for doping-free electroluminescent devices up to now (TPE-TPAPBI, Fig. 2.6).[116,128] The further development of TADF/AIE electroluminescent materials may result in the fabrication of non-doped OLEDs with better performance than that of the doped ones.

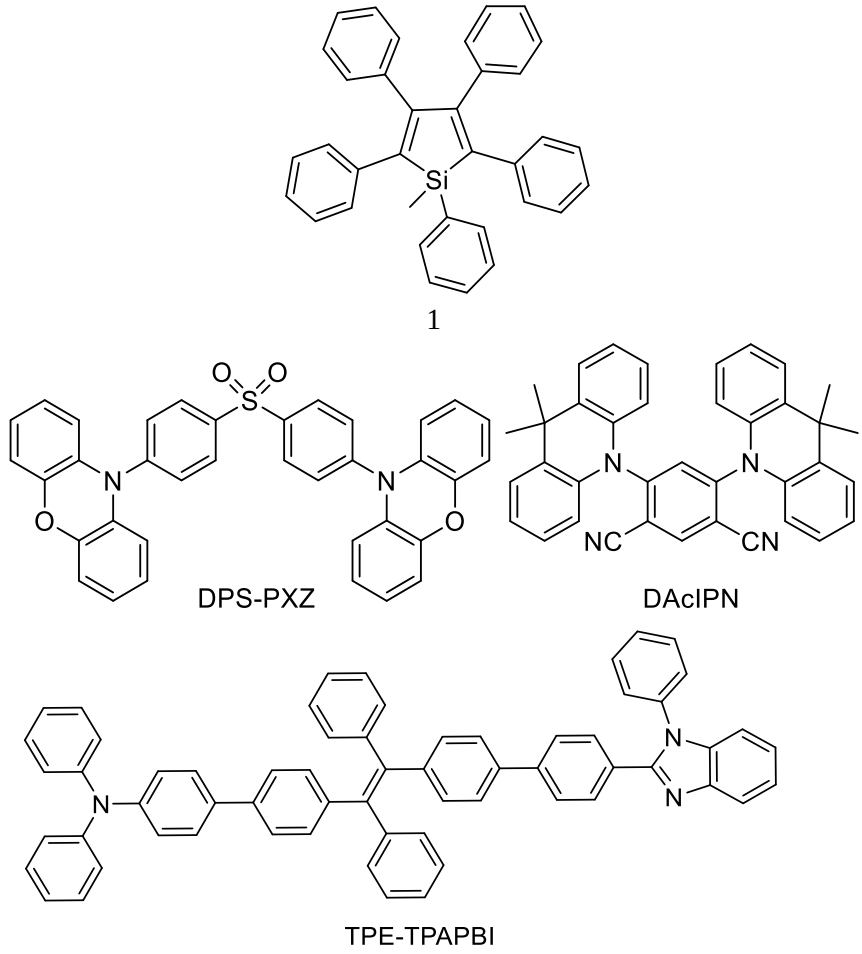

Fig. 2.6 Chemical structure of compounds exhibiting AIE/AIEE

2.6. Hosts for guest:host emitting systems

As it was mentioned above, a major step in developing the OLED technology was the research of the doping concentration control of the conjugated polymers in 1970s.[8-10] In 2000, Shirakawa, MacDiarmid, Chiang, and Heeger received the Nobel Prize in chemistry for the investigation in the field.[129] It started in 1977 with the observation that electron conductivity is enhanced by doping polyacetylene.[8]

Electronic excitation energy transfer via non-radiative transitions of energy from the molecules of the host to the guest became a very important tool for the cost reduction of a device and an increase of its efficiency. Förster resonance energy transfer (FRET)[130,131] is a mechanism of dipole-dipole resonance energy transfer. FRET takes place only if transitions between excited and ground states of chromophores are allowed in the dipole-dipole approximation. Spectral overlap of the donor emission and acceptor absorption would indicate the possibility of

efficient transfer of energy. Another major approach is the Dexter mechanism[132] for exchange energy transfers caused by dipole-dipole, dipole-quadrupole and magnetic interactions.

Electronic excitation energy is transferred from the host to the guest via FRET and the Dexter mechanism as it is dipole-allowed for triplet excitons. That is dissimilar to fluorophores in host:guest systems in which the energy of singlet excitons is transferred via FRET only. One of the obvious requirements for the host materials for PhOLED is to have a higher T_1 energy level than that of the phosphorescent molecule for harvesting triplet excitons.

In order to get effective light generation, the employment of triplet excitons is important, but it is not less important to avoid or diminish the quenching pathways. Therefore, one of the fundamental factors in the design of effective OLEDs is the selection of a host for a host-guest system. In principle, host materials should conform to the following requirements: a high triplet energy, appropriate HOMO and LUMO levels, bipolar charge transporting properties, etc.[133] Many host materials were reported for either phosphorescent or TADF OLEDs.[134-136] However, incomparably less research was done in the search for versatile host materials which can be applied both for PhOLEDs and TADF OLEDs. Many effective OLEDs were designed by using hole-transporting and host materials containing a carbazole moiety as the electron-donating unit.[136,137] In most cases, carbazole is selected due to its high triplet energy, good thermal stability and useful optical and charge-transporting properties of carbazole derivatives.[138] Carbazole-substituted derivatives of dibenzofuran have been reported previously.[139] It was suggested to use them as host materials for PHOLEDs.

TCz1 or 3,6-di(9-carbazolyl)-9-(2-ethylhexyl)carbazole[140] having a high mobility of electrons of up $3 \cdot 10^{-4}$ $cm^2V^{-1}s^{-1}$ at an electric field of $5 \cdot 10^5$ Vcm^{-1} is used very often as an ambipolar matrix for guest:host EML for OLEDs. It has -5.8 and -2.6 eV of HOMO and LUMO energies, respectively. TCz1 is denoted by a signature double emissive band of PL and EL with two peaks at around 390 and 410 nm, which makes it easy to spot its emissive contribution into spectra when it is present.

o-DiCbzBz (9,9'-(2-(1-phenyl-1H-benzo[d]imidazol-2-yl)-1,3-phenylene)bis(9*H*-carbazole))[141] is a universal host material for highly efficient TADF OLEDs and red, green, blue PhOLEDs. The HOMO/LUMO energies of o-DiCbzBz are -5.8 and -2.3 eV, respectively. TADF OLED with an EML of 4CzIPN doped into this matrix exhibited EQE up to 26.3%. For blue PhOLEDs, the maximum EQE of 31.8% was achieved with this host.[141] o-DiCbzBz has ambipolar characteristics due to the inclusion of two carbazole moieties and a benzimidazole acceptor.

mCP or 1,3-bis(N-carbazolyl)benzene[142] is used not just as matrix material for guest:host systems but also often as HIL, HTL, EBL. For example, it is used as a host for blue PhOLEDs due to high E_{T1} of 2.91 eV for triplet harvesting and a high HOMO energy of -6.1 eV. Its LUMO features energy of -2.4 eV. The absorption spectral bands of dilute THF solutions of mCP are located at 292 and 338 nm while the peaks of PL have wavelengths of 345 and 360 nm.

A pale yellow powder of TAPC (4,4′-cyclohexylidenebis[N,N-bis(4-methylphenyl)benzenamine][143]) is widely employed in OLED fabrication due to its high quality hole transport properties. The HOMO/LUMO energy values are -5.5 and -2 eV, respectively. The E_{T1} of TAPC of 2.87 eV is higher than for common phosphorescent dyes. As the result, this compound can operate as a host material for blue phosphors in PhOLEDs.

TCTA (tris(4-carbazoyl-9-ylphenyl)amine)[54] is a light-yellow solid used for the fabrication of HIL, HTL and as a host for doped EML in various optoelectronic devices including OLEDs and perovskite solar cells. It owes its great hole transporting characteristics to the electron-rich moieties of the carbazole and triarylamine core. TCTA can also be used as EBL or for the blocking of excitons due to its low electron mobility and a high LUMO energy of -2.4 eV. Its HOMO energy level is -5.7 eV. TCTA can be employed as a host for phosphors in green, red and white PhOLEDs because of suitability for the guest HOMO-LUMO gap of 3.3 eV.

Introduction of methoxy groups to the structure of host materials may increase their electrochemical stability.[144] Enhancement of hydrogen bonding between oxygen atoms of methoxy groups and hydrogen atoms results in the achievement of efficient packing in films resulting in high thermal stability, high glass transition and effective charge transport.[137,145-149] Also, it is known that, upon methoxy substitution, the HOMO energies of the compounds are increased, and the ionization potential values are decreased, which results in more effective hole injection.[150-152] However, it is common knowledge that no derivatives of methoxy-substituted carbazole capable of effectively transporting both holes and electrons have been reported so far. Therefore, it is of interest to further study the structure-properties relationship of methoxy-substituted carbazoles.

Despite the well-known excellent TADF properties, diphenylsulfone-based materials as hosts remain rare to this day. In 2019, Chin *et al*. reported a series of asymmetric D-A-D' compounds with diphenylsulfone as the acceptor unit, carbazole as one donor moiety, and 3,6-di-*tert*-butyl-carbazole, or 7,7-dimethyl-5,7-dihydroindeno[2,1-b]carbazole as the other one.[153] By using them as sensitizers in DPEPO composed with 5,9-diphenyl-5*H*,9*H*-[1,4]benzazaborino[2,3,4-k,l]phenazaborine (DABNA-1) as TADF emitting species in OLEDs resulted in an EQE of 12–14%. The establishment of structural relationships in order to achieve effective energy transfer is crucial for a rational design of diphenylsulfone derivatives capable of complete operating as host materials for TADF emitters.

Benefiting from color purity and stability, highly efficient devices, representing the so-called 3.5 generation of OLEDs were developed by using light-emitting layers based on a combination of TADF hosts and simple fluorescent emitters.[154]

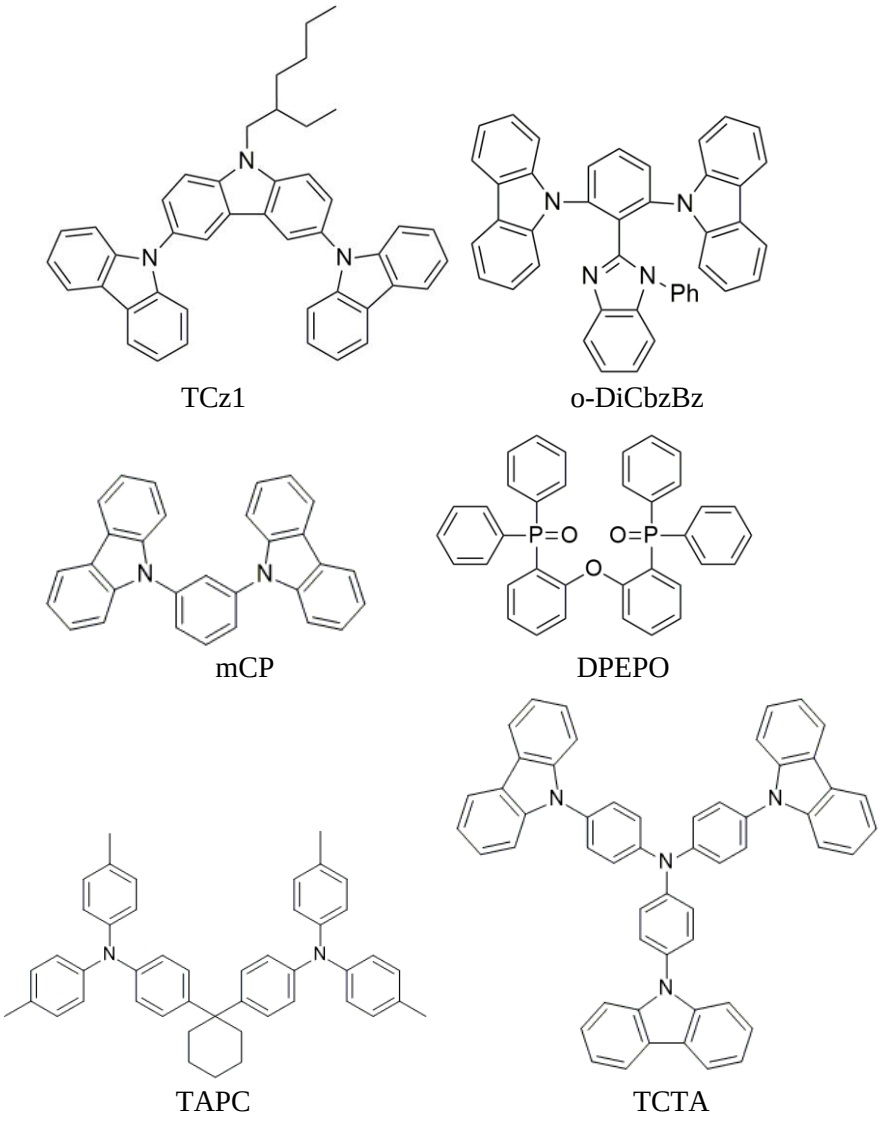

Fig. 2.7 Chemical structure of TCz1, o-DiCbzBz, mCP, DPEPO, TAPC and TCTA

2.7. Conclusions from the literature review

Application of the variety of novel approaches in the field of OLED technology which led to an improvement of the efficiency of devices was discussed. Intermolecular and intramolecular interactions of organic compounds determine the characteristics of materials. π- and σ- bonds are responsible for the semiconducting properties of organic materials. Consequently, organic semiconductors are characterized by π- conjugation, which makes them different from inorganic ones, in

which, the structure is determined by strong covalent bonds without conjugation. This is the most important advantage of OLED materials. π-Conjugation provides a way to manage electroluminescence by tuning the optical band gap which fits Frenkel excitons of a small binding radius perfectly.

A necessary condition for achieving the desired characteristics of OLED is the rational optimization of the device structure. Experimental signs of the optimal design of devices are evident quantitatively. The choice of the appropriate thicknesses of the layers results in a drop of the value of turn-on voltage pointing to the efficient charge carrier transfer from electrodes to the recombination sites and inside the EML. As it was shown,[25-29] methods of photonics allow predicting electroluminescent properties of emissive species from the photophysical investigation. In order to achieve the maximum value of EQE, there should be a balance of holes and electrons on recombination sites. It can be achieved by the careful selection of the appropriate hole and electron transport layers.

Upon electrical excitation, due to the statistics of the orientation of the spin angular momentum of an exciton, one quarter of the electron-hole pairs are singlets and the rest are triplets. This means that, without advanced substrates, fluorescent OLEDs would have a maximum EQE of ~7–8%. For the simplification of the structure of fluorescent OLEDs, their EML is preferred to be non-doped, which requires high and balanced charge carrier mobilities. The bipolar properties of donor-acceptor compounds can be tuned by the selection of donor and acceptor moieties and by the tuning of π-conjugation. BTD is a well-known electron-withdrawing moiety while carbazole is used as a typical donor.[32,33] BTD derivatives are expected to be successfully employed as bipolar fluorescent emitters for fluorescent OLEDs.

For the harvesting of triplet excitons by up-conversion to singlet states, which would dramatically enhance the device efficiency, different methods were introduced, such as TTA (maximum EQE of ~19%), TADF and electrophosphorescence (~30% for both).[47,81] Further investigation of donor-acceptor-donor benzonitrile derivatives exhibiting both TADF and AIEE is very promising for the employment of the compounds for host-free EML in TADF-based OLEDs.

Electrophosphorescence is achieved by the facilitation of spin-orbit coupling induced by heavy metals, usually platinum or iridium. The biggest obstacle for electrophosphorescence is an interception of the excitation energy by air, which deactivates excitons in the non-radiative way. Minimizing the lifetime of triplet excitation by using aromatic carbonyl compounds may lead to RTP, which overcomes the 25% limit of IQE. However, the RTP method needs to be improved to a great extent as it cannot be used practically in OLEDs currently. Nevertheless, the investigation of the probable RTP in a series of methylphenylsulfone derivatives is the matter of great interest. Study of differently substituted derivatives with carbazole or *tert*-butyl carbazole units doped into the polymer matrix to suppress intermolecular motions can give more information about the requirements for RTP to successfully compete with PF, DF and non-radiative deactivation of excited states.

The discovery of the increase of the conductivity of the organic layer by doping was one of the first most important steps in the history of OLED technology.[8-10] Guest:host systems give an opportunity to secure the amount of emissive species in EML by using a host material for energy transfer. The small binding radius of Frenkel excitons determines the optimal concentration of doping. Host material should feature high energy levels of excited states for the transfer of excitation from the host to the guest, match of the energies of the frontier molecular orbitals of the guest and host molecules, high charge carrier mobilities. The use of the doped EML may enhance the Φ of the emitter or facilitate TADF because the guest:host system is a unique physical medium in which the polarity of the host can change the kinetics of the emissive processes. Dibenzofuran-based compounds substituted by methoxycarbazolyl moieties are expected to correspond to the requirements for efficient hosts for TADF OLEDs and PhOLEDs. Donor-acceptor-donor compounds with the diphenylsulfone moiety as the central core are well-known TADF emitters. However, they have not been used as the hosts for TADF emitters yet. At the same time, the design of donor-diphenylsulfone-donor derivatives can be considered for the purpose of the charge carrier transport, which is an interesting direction of the investigation.

3. EXPERIMENTAL PART

3.1. Instrumentation and methods

Luminescence measurements were done by using *Edinburgh Instruments FLS980* and *Aventes AvaSpec-2048XL* spectrometers. The integrating sphere of the *FLS980* (a xenon lamp as the source of excitation; wavelength: 330 nm) was used for recording the Φ of samples at 300 K by the absolute method. A *FLS980* spectrometer and a *PicoQuant LDH-D-C-375* laser with the excitation at 374 nm were used to obtain the data of PL decay curves.[90] The weighted sum of the squares of deviations of the calculated points χ^2 is in the diapason from 1 to 1.3. At least 5 freeze/thaw cycles and vacuum pumping were used for degassing dilute tetrahydrofuran solutions. An *Aventes AvaSpec-2048XL* spectrometer was used for measuring electroluminescence and absorbance spectra. The first singlet E_{S1} and triplet E_{T1} excited states were calculated from the onsets of fluorescent and phosphorescent peaks, respectively, recorded at the liquid nitrogen temperature.

Ionization potentials (*IP*) and electron affinities (*EA*) were estimated from cyclic voltammetry according to Equations (3.1) and (3.2):

$$IP_{CV} = (E_{onset}^{ox} + 4.8)\ [\text{eV}] \quad (3.1)$$

$$EA_{CV} = -\left(E_{onset}^{red} + 4.8\right)\ [\text{eV}] \quad (3.2)$$

where E_{onset}^{red} and E_{onset}^{ox} are the onset reduction and oxidation potentials versus Fc/Fc^{+}.

The alternative calculation may be as follows:

$$IP_{CV} = |-(1.4 \cdot 1e \cdot E_{onset}^{ox}) - 4.6\,|\ [\text{eV}].^{155} \quad (3.3)$$

HOMO and LUMO energies were calculated by the B3LYP/6-31G(d) method.

IP^{PE} is the ionization potential of thin solid layers estimated by photoelectron emission spectrometry. E_A^{PE} is electron affinity of thin solid layers estimated by Formula (3.4):

$$EA^{PE} = IP^{PE} - E_g \quad (3.4)$$

Optical E_g were taken from the absorption spectra of the layers.

The *IP* of vacuum-deposited films were obtained from photoelectron emission spectra recorded by electron photoemission spectrometry in air as published elsewhere.[156] The setup of the *IP* measurements consisted of a monochromator (*CM110* 1/8m), a deep ultra-violet deuterium lamp *ASBN-D130-CM*) and a *6517B Keithley* electrometer. The values of *IP* from photoelectron spectroscopy I_P^{PE} were taken at crossing the points of the abscissa axis with the fitting lines which extrapolated the linear parts of low-energy edges of the corresponding photoelectron emission spectra.

Hole and electron mobilities were calculated by using Formula (3.5):

$$\mu = \frac{d^2}{Ut_{tr}} \tag{3.5}$$

where d is the thickness of the vacuum-deposited films, U is the voltages applied to the samples by using a *6517B* electrometer (*Keithley*) at the moment of excitation by a 355 nm wavelength laser (*EKSPLA NL300*); t_{tr} is the transit time. To obtain t_{tr} for the holes and electrons, the time-of-flight (TOF) method was conducted by applying positive or negative voltages to the samples with structure ITO (15 Ω/sq)/film of the studied compound/Al, respectively. Photocurrent transients were recorded by a *TDS 3032C* oscilloscope (*Tektronix*). As it is widely accepted, charge drift mobility versus electric fields (E) is presented according to the Poole–Frenkel relationship (3.6):

$$\mu = \alpha_0 e^{\alpha E^{1/2}} \tag{3.6}$$

where α is the field dependence parameter.[157]

OLEDs were fabricated by the step-by-step vacuum thermal evaporation method under the pressure of $2 \cdot 10^{-6}$ mBar. OLEDs fabrication was done by using vacuum equipment from *Kurt J. Lesker* in-built in an *MB EcoVap4G* glove box. The thermal deposition rates of organic layers were in the range of a few tenths of nanometres per second. Simultaneous density-voltage and luminanace-voltage dependences were recorded by using a calibrated *PH100-Si-HA-D0* photodiode, a *6517B* electrometer and a *2400C* sourcemeter from *Keithley* and a Power and Energy Monitor *11S-LINK*. All the electrophysical characterization was done at room temperature without passivation.

Luminous flux Φ is the light power as perceived by the human eye. Thus, *PE* of OLED is defined as the ratio of the Φ produced by the device and the electrical input power P. Φ can be defined as

$$\Phi = K_m \int_{380}^{770} \Phi_E V d\lambda \tag{3.7}$$

If Φ_e is the measured spectral radiant flux radiated by the device in the visible region, V denotes the normalized spectral luminosity distribution function in the optical range, K_m is the maximum photometric radiant equivalent which is equal to 683 lm/W.

The brightness of OLED is defined as the ratio of the luminous intensity of the emitting surface of the device within a cone enclosing a solid angle to the area of its projection in a plane perpendicular to the direction of tracking. For the evaluation of brightness, Formula (3.8) is used:

$$L_{V,O} = K_r U \frac{S}{FF} \frac{d^2}{\tau S_{OLED} S_{pd}} \quad (3.8)$$

U is the voltage, S denotes photosensitivity of the *PH100-Si-HA-D0* photodiode, d is the distance between the photodiode and OLED, τ stands for the transparency coefficient. S_{OLED}, S_{pd} are areas of the radiating surface of OLED and the detecting surface of photodiode, respectively. *FF* is a fill factor of the spectral sensitivity of the photodiode. K_r is responsible for the transition of radiometric values into photometric ones:

$$K_r = \frac{\Phi}{\int_{380}^{770} \Phi_E d\lambda} \quad (3.9)$$

CE is estimated as the ratio of the brightness to the current density. EQE is strongly linked to the radiant efficiency of OLED:

$$EQE = \frac{\int_{380}^{770} \Phi_E d\lambda}{P} \quad (3.10)$$

The Theoretical Density Functional Theory (DFT, B3LYP 6–31(d,p) basis set calculations were performed by using the *Gaussian 09* program for the theoretical calculation of the HOMO/LUMO levels.[158]

3.2. Materials

Aluminum is usually used as a metal cathode for device fabrication because of small energy required to eject an electron from the electrode. Its photoelectric work function is around 4.2 eV. The thickness of aluminum was at least 100 nm in order to avoid the electrical breakdown of an OLED. Indium-tin oxide (ITO) is a traditional material for the transparent anode located on a glass substrate. The work function of ITO is 4.7 eV.

Despite being excellent and widely used materials for electrodes, they are employed in an OLED structure together with injection layers. Energetic barriers of ITO and aluminum with molecular orbitals of the respective internal organic layers are too significant for charge carriers to overcome without HIL and EIL, respectively. Layers of molybdenum trioxide (MoO_3) or HAT-CN were used as HIL in the work. Lithium fluoride (LiF) was taken as the EIL. It lowers the energy level for electron injection from 4.2 to 2.9 eV suitable for most ETLs. The thickness of the injection layers bigger than a few nanometers is harmful for the device structure as they would function as an insulator.

HAT-CN or dipyrazino[2,3-f:2',3'-h]quinoxaline-2,3,6,7,10,11-hexacarbonitrile

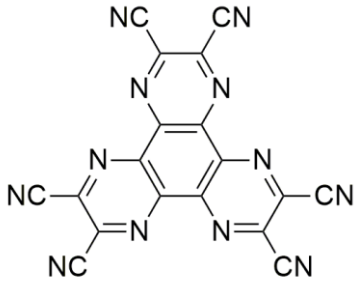

Fig. 3.1 Chemical structure of HAT-CN

The LUMO energy level lying around -5.6 eV makes HAT-CN an excellent material for the hole injection as electrons are smoothly transferred to ITO.[159,160] This electron-deficient compound as a member of the family of 1,4,5,8,9,12-hexaazatriphenylenes is denoted by high rigidity of the planar, aromatic discotic structure and great capabilities of π-π stacking. The efficiency of OLEDs including solution-processed devices with employment of HAT-CN is bigger than for diodes with other prominent HILs like the conventional poly(3,4-ethylenedioxythiophene) polystyrene sulfonate (PEDOT:PSS).[161,162]

NPB or N,N'-di(1-naphthyl)-N,N'-diphenyl-(1,1'-biphenyl)-4,4'-diamine

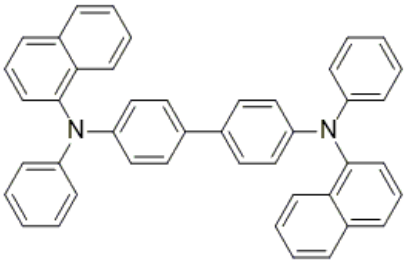

Fig. 3.2 Chemical structure of NPB

NPB is a straw-colored powder. It is well known as one of the most used materials in optoelectronics for the hole injection and transport. Its HOMO level is -5.5 eV, and -2.4 eV for LUMO.

TSPO1 or diphenyl[4-(triphenylsilyl)phenyl]phosphine oxide[163,164]

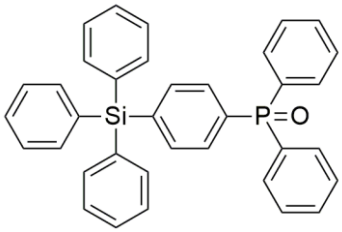

Fig. 3.3 Chemical structure of TSPO1

The powder of TSPO1 has a HOMO level of -6.8 eV, which makes an enormous energetic barrier for holes to penetrate into ETL. At the same time, -2.5 eV of LUMO is sufficient for the transfers of electrons to EML. Such conditions make it perfect for the employment as HBL. It also features a high E_{T1} of 3.36 eV.

DPPS or diphenyl-bis[4-(pyridin-3-yl)phenyl]silane[165]

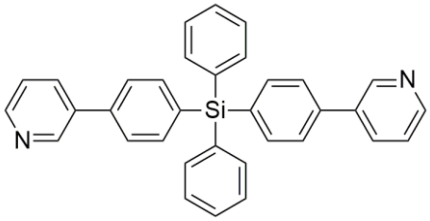

Fig. 3.4 Chemical structure of DPPS

DPPS is an electron-deficient tetra-phyenylsilane derivative substituted by two pyridyl groups used for hole blocking and electron transport. Its E_{T1} is 2.7 eV. The HOMO level has an energy level of -6.5 eV, whereas for LUMO it is -2.5 eV.

TPBi or 2,2',2''-(1,3,5-Benzinetriyl)-tris(1-phenyl-1-H-benzimidazole)[166,167]

TPBi is a white powder which is widely used for the fabrication of ETL in OLEDs.[168] The energy levels of HOMO and LUMO are -6.2 and 2.7 eV, respectively. It emits at 302 nm in the dilute chloroform solution.

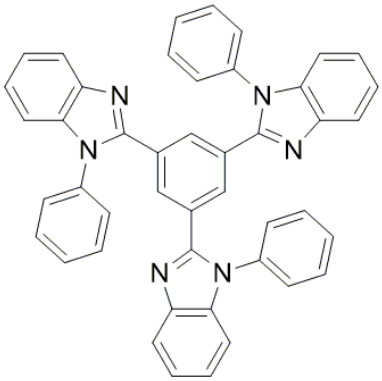

Fig. 3.5 Chemical structure of TPBi

The first series of the studied compounds are emitters with D-A-D and D-π-A-π-D structures, of three 2,1,3-benzothiadiazole derivatives of electron-accepting benzothiadiazole and donating 3,6-di-*tert*-butyl-carbazolyl, 9-ethyl-3-vinyl-carbazolyl and 1,2,3,4-tetrahydro-9-carbazolyl moieties: 4,7-bis(1,2,3,4-tetrahydro-9*H*-carbazol-9-yl)benzo[c][1,2,5]thiadiazole (**1.1**), 4,7-bis(3,6-di-*tert*-butyl-9*H*-carbazol-9-yl)benzo[c][1,2,5]thiadiazole (**1.2**) and 4,7-bis((E)-2-(9-ethyl-9*H*-carbazol-3-yl)vinyl)benzo[c][1,2,5]thiadiazole (**1.3**).[169]

The second series of compounds are TADF donor-acceptor-donor emitters **2.1**–**2.5** having cyano substituted phenyl moiety as acceptor and carbazole, phenothiazine, phenoxazine, 9,9-dimethyl-9,10-dihydroacridine moieties as donors: 2,5-bis(9,9-dimethyl-9,10-dihydroacridin-10(9*H*)-yl)benzonitrile (**2.1**), 5-(9,9-Dimethyl-9,10-dihydroacridin-10(9*H*)-yl)-2-(10*H*-phenoxazin-10-ylbenzonitrile (**2.2**), 5-(9*H*-Carbazol-9-yl)-2-(10*H*-phenothiazin-10-yl)benzonitrile (**2.3**), 5-(9*H*-Carbazol-9-yl)-2-(9,9-dimethyl-9,10-dihydroacridin-10(9*H*)-yl)benzonitrile (**2.4**) and 2,5-bis(10*H*-phenoxazin-10-yl)benzonitrile (**2.5**).[170]

The third series of the investigated dyes are symmetrical donor-acceptor-donor TADF emitters **3.1**–**3.3**: bis(4-(2,7-di-*tert*-butyl-9,9-dimethyl-9,10-dihydroacridine-10-yl)phenyl) sulfone (**3.1**), bis(3-(2,7-di-*tert*-butyl-9,9-dimethyl-9,10-dihydroacridine-10-yl)phenyl) sulfone (**3.2**) and 3,6-bis[9,9-dimethyl-2,7-bis(*tert*-butyl)-9,10-dihydroacridin-10-yl]-9-thia-9,9-fluorenedione (**3.3**).[171]

The fourth series of the investigated compounds (**4.1**–**4.3**) were designed as TADF emitters.

3,6-di-tert-butyl-9-(2-(4,6-diphenyl-1,3,5-triazin-2-yl)phenyl)-9H-carbazole (4.3)

A mixture of 2-(3,6-di-*tert*-butyl-9*H*-carbazol-9-yl)benzaldehyde (1a) (0.5 g, 1.30 mmol), benzamidine hydrochloride hydrate (0.34 g, 2.19 mmol), Na_2CO_3 (0.23 g, 2.19 mmol) and $Cu(OAc)_2$ (10 mol%) was stirred in toluene and heated at 110 °C in air overnight. After cooling to room temperature, the reaction mixture was poured into water and extracted with chloroform. The crude product was purified by column chromatography on silica gel by using EtOAc/hexane (1:7) as an eluent and

crystallized from the eluent mixture of solvents to give **4.3** as yellowish crystals. FW = 586.78 g/mol, m.p. 258–259 °C. Yield: 0.52 g, 68%. 1H NMR (300 MHz, CDCl3): δ = 8.57 (dd, J = 7.8, 1.6 Hz, 1H), 8.12–8.07 (m, 4H), 8.04 (d, J = 1.6 Hz, 2H), 7.84–7.66 (m, 3H), 7.50 (t, J = 7.8 Hz, 2H), 7.35 (t, J = 7.8 Hz, 6H), 7.13 (d, J = 7.8 Hz, 2H), 1.44 (s, 18H). 13C NMR (75 MHz, CDCl3): δ = 172.3, 171.2, 142.2, 140.1, 137.4, 135.9, 135.7, 132.6, 132.4, 132.2, 130.5, 128.7, 128.4, 128.3, 123.4, 116.1, 108.9, 34.6, 32.1. MS (APCI+, 20 V), m/z (%): 588 ([M+H]+). Elemental analysis calcd. (%) for $C_{41}H_{38}N_4$: C 83.92; H 6.53; N 9.55; found: C 83.96; H 6.57; N 9.59.

9-(2-(4,6-bis(3-methoxyphenyl)-1,3,5-triazin-2-yl)phenyl)-3,6-di-tert-butyl-9H-carbazole (4.2)

The procedure was similar to that used for the synthesis of **4.3** but 3-methoxybenzamidine hydrochloride hydrate (0.28 g, 1.51 mmol) was used instead of benzamidine hydrochloride hydrate. After cooling to room temperature, the reaction mixture was poured into water and extracted with chloroform. The crude product was purified by column chromatography on silica gel by using EtOAc/hexane (1:9) as an eluent, and crystallized from the eluent mixture of solvents to give **4.2** as yellowish crystals. FW = 646.84 g/mol, m.p. 171–172 °C. Yield: 0.44 g, 52%. 1H NMR (300 MHz, CDCl3): δ= 8.53 (dd, J = 7.7, 1.6 Hz, 1H), 8.03 (d, J = 1.6 Hz, 2H), 7.90 – 7.84 (m, 2H), 7.82 – 7.59 (m, 5H), 7.34 (dd, J = 8.6, 1.6 Hz, 2H), 7.25 (t, J = 7.6 Hz, 2H), 7.15 (d, J = 8.6 Hz, 2H), 7.05 (dd, J = 8.6, 1.3 Hz, 2H), 3.79 (s, 6H), 1.43 (s, 18H). 13C NMR (75 MHz, CDCl3): δ = 172.6, 171.1, 159.6, 142.3, 139.8, 137.4, 137.1, 135.5, 132.7, 132.3, 129.9, 129.3, 128.0, 123.6, 123.5, 121.4, 118.5, 116.1, 113.2, 109.0, 55.3, 34.6, 32.0. MS (APCI+, 20 V), m/z (%): 648 ([M+H]+). Elemental analysis calcd. (%) for $C_{43}H_{42}N_4O_2$: C 79.85; H 6.55; N 8.66; O 4.95; found: C 79.89; H 6.57; N 8.71.

9,9'-(2-(4,6-diphenyl-1,3,5-triazin-2-yl)-1,3-phenylene)bis(3,6-di-tert-butyl-9H-carbazole) (4.1)

To a flask containing sodium hydride (0.14 g, 5.79 mmol), 3,6-di-*tert*-butyl-9*H*-carbazole (0.89 g, 3.18 mmol) was added in anhydrous DMF under nitrogen atmosphere and stirred for 5 minutes at room temperature. To this solution, 2-(2,6-difluorophenyl)-4,6-diphenyl-1,3,5-triazine (1b) (0.5 g, 1.45 mmol) in DMF (10 ml) was added dropwise. After addition, the reaction mixture was stirred for 12 h at 120 °C. Then, the reaction solution was poured into cold water, and the precipitate was filtered and dried under vacuum. The crude product was purified by column chromatography on silica gel by using EtOAc/hexane (1:9) as an eluent and crystallized from the eluent mixture of solvents to give **4.1** as yellowish crystals. FW = 864.19 g/mol, m.p. 295–296 °C. Yield: 0.45 g, 36%. 1H NMR (300 MHz, CDCl3): δ = 7.96 (dd, J = 8.5, 7.3 Hz, 1H), 7.91 (d, J = 1.6 Hz, 4H), 7.84 (d, J = 7.7 Hz, 2H), 7.42 (dd, J = 7.3, 6.2 Hz, 4H), 7.40–7.32 (m, 6H), 7.25 (d, J = 8.5 Hz, 4H), 7.12 (t, J = 7.7 Hz, 4H), 1.41 (s, 36H). 13C NMR (75 MHz, CDCl3): δ = 170.5,

142.4, 140.3, 138.8, 135.4, 131.8, 131.62, 130.0, 128.5, 127.8, 123.4, 123.3, 116.0, 109.3, 34.6, 32.0. MS (APCI+, 20 V), m/z (%): 865 ([M+H]+). Elemental analysis calcd. (%) for $C_{61}H_{61}N_5$: C 84.78; H 7.12; N 8.10; found: C 84.81; H 7.15; N 8.14.

The fifth series consists of 2,8-bis(3,6-dimethoxy-9*H*-carbazol-9-yl)dibenzo[b,d]furan (**5.1**), 2,8-bis(2,7-dimethoxy-9*H*-carbazol-9-yl)dibenzo[b,d]furan (**5.2**) and 2,8-bis(2,3,6,7-dimethoxy-9*H*-carbazol-9-yl)dibenzo[b,d]furan (**5.3**).[172]

The sixth series of the investigated compounds are diphenylsulfone derivatives: bis(4-(2-(trifluoromethyl)-phenothiazine-10-yl)phenyl)sulfone (**6.1**), bis(4-(10,11-dihydro-5*H*-dibenz[b,f]azepine-5-yl)phenyl)sulfone (**6.2**), bis(4-(5*H*-dibenz[b,f]azepine-5-yl)phenyl)sulfone (**6.3**), bis(4-(4-methoxy-9*H*-carbazole-9-yl)phenyl)sulfone (**6.4**) and bis(4-(1,2,3,4-tetrahydrocarbazole-5-yl)phenyl)sulfone (**6.5**).[173]

4. RESULTS AND DISCUSSION

The *Results and Discussion* chapter contains the information from articles of the author (see *7. List of publications on the subject of the thesis*).[169-173]

4.1. Carbazolyl- and 1,2,3,4-tetrahydrocarbazolyl-substituted benzothiadiazoles as emitters for fluorescent organic light emitting diodes

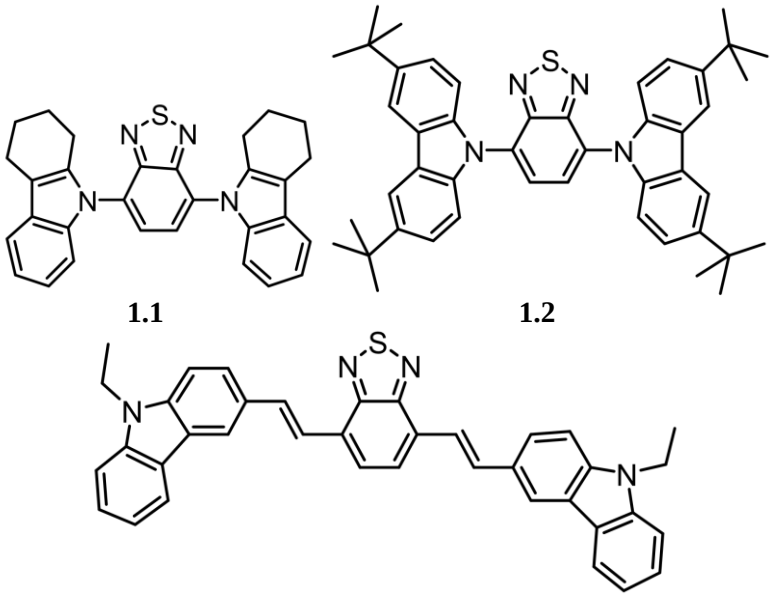

1.1 **1.2**

1.3

Fig. 4.1 Chemical structures of differently substituted benzothiadiazole derivatives[169]

Ground-state geometries of benzothiadiazole derivatives in the toluene solvent were optimized at the B3LYP/6-31G(d, p) level by using the density functional theory (DFT) and the *Gaussian 09* software.[158] Our calculation revealed that molecules in the ground state can have several conformers. The HOMOs and LUMOs of **1.1**–**1.3** are illustrated in Fig. 4.2.

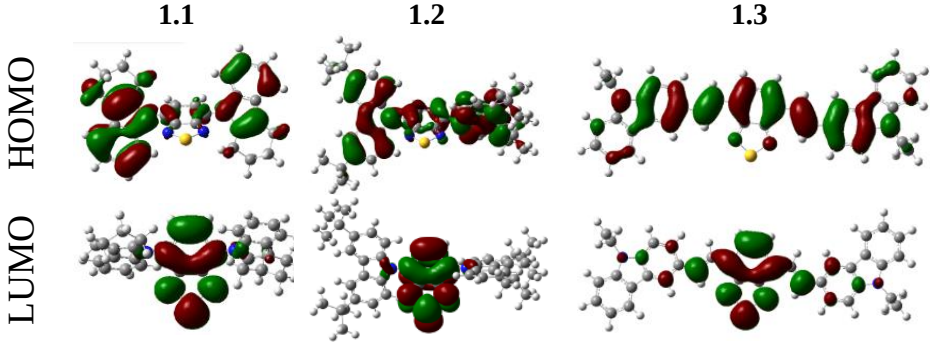

Fig. 4.2 HOMO and LUMO orbitals of benzothiadiazole derivatives

Electron densities in HOMO are extended almost throughout the entire molecules of **1.1–1.3**, while most of the electron densities in LUMO concentrate on the benzothiadiazole unit. The dihedral angles and oscillator strengths of the transitions of the derivatives were calculated by using the time-dependent DFT approach. The calculations revealed twisted geometries of derivatives **1.1** and **1.2** with dihedral angles between the acceptor and the donors varying in the range of 61–71°. Compound **1.3** shows an almost flat structure. The reduction of the dihedral angle from the twisted molecule to the flat one (**1.1** > **1.2** > **1.3**) causes an increase of the HOMO–LUMO overlap and oscillator strength.

4.1.1. Photophysical properties

The absorption spectra of the dilute solutions of derivatives **1.1–1.3** in toluene and of the films are presented in Fig. 4.3. Normalized fluorescence spectra of the dilute solutions in toluene, of molecular dispersions in polystyrene, and of the solid samples of the derivatives are depicted in Fig. 4.4. The broad and structureless band with peak positions at 434, 476 and 497 nm for **1.1–1.3**, respectively, illustrates the presence of intramolecular CT. The lowest energy absorption bands of the solutions of **1.2** and **1.3** are shifted by 42 and 63 nm towards longer wavelengths with a 2-fold and 10-fold increase of the oscillator strength in comparison with that of compound **1.1** due to the increased π-conjugation system and the increased overlapping between HOMO and LUMO.

Similarly to toluene solutions, solid films of compounds **1.1–1.3** were characterized by both high-energy absorption bands (300–350 nm) caused by π–π* and n–π* transitions of the conjugated benzothiadiazole and carbazole moieties; whereas low-energy absorption bands (452–514 nm) originated from the HOMO–LUMO intramolecular CT transition. Slight red-shifts of the intramolecular CT absorption bands and different distribution of their intensities were observed for the films of compounds **1.1–1.3** in comparison to those recorded for toluene solutions. This observation can be attributed to either aggregation or polarity effects in the solid state.

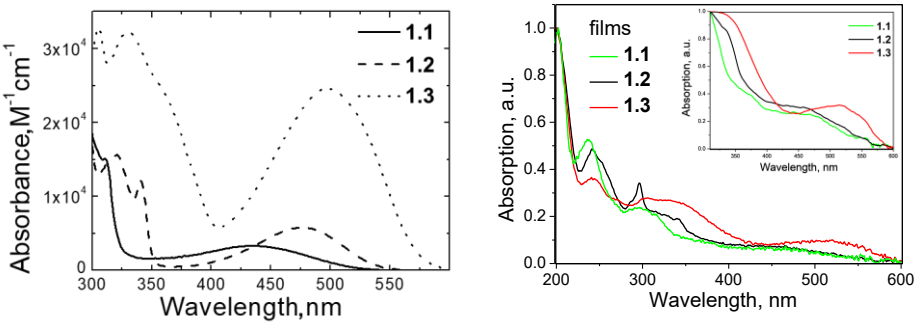

Fig. 4.3 Absorption spectra of the solutions in toluene (a) and spin-coated films (b) of compounds **1.1** (solid line), **1.2** (dashed line), **1.3** (dotted line)

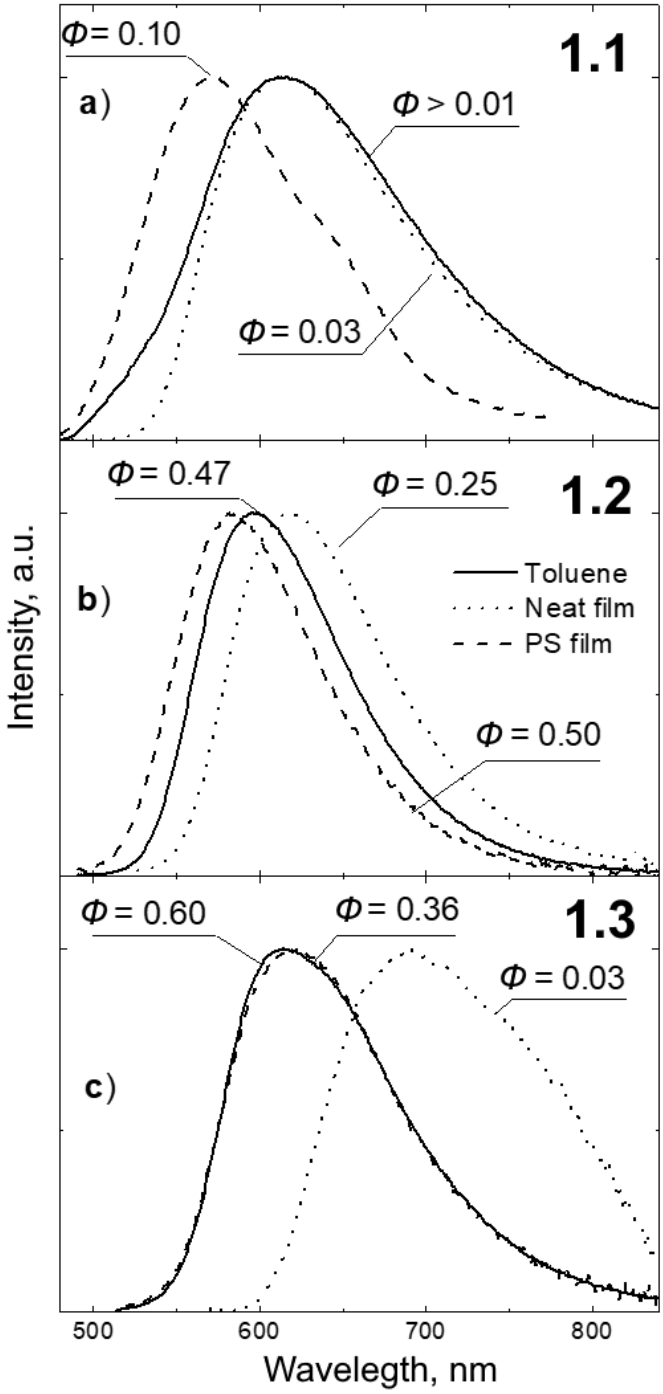

Fig. 4.4 Normalized fluorescence spectra of molecular dispersions of benzothiadiazole derivatives in PS (1 wt%, dashed line), of 1 μM solutions in toluene (solid line) and of the solid samples (dotted line) of (a) **1.1**, (b) **1.2** and (c) **1.3**

Derivative **1.3** dissolved in toluene exhibited broad and weak PL emission with a peak at 613 nm (Fig. 4.5a). A neat film of **1.3** exhibited PL emission similar to that of the solution with a higher intensity (Φ = 0.03) and a narrower spectrum (Fig. 4.4c). 1,2,3,4-tetrahydrocarbazolyl-substituted benzothiadiazole embedded in the polystyrene matrix demonstrated a spectrum with a peak blue-shifted by 40 nm and an increased emission intensity (Φ = 0.1). The weak emission of **1.3** in the solution may be explained by the twisted molecular structure and oscillations of the side groups.

The suppression of these oscillations in the polymer matrix or neat film leads to the rise of the emission intensity. Dispersed in polystyrene, derivative **1.2** demonstrated 5-fold higher Φ relative to compound **1.3** without *tert*-butyl moieties. PL quantum yields of 0.47 and 0.25 were estimated for the solution and neat film of **4**, respectively. A relatively high Φ of the solid film can be explained by molecular planarization.[174] The photoluminescence spectrum of the liquid solution of **1.3** in toluene exhibited a similar spectrum to that of the solid solution in the polystyrene film, only the estimated Φ of the molecular dispersion in PS was lower (Φ = 0.36, comparing to Φ = 0.6 for the solution in toluene).

The emission of the neat film of derivative **1.3** was broad and red shifted, which indicates the formation of excimers. A decrease of the fluorescence efficiency in the solid state was observed for many compounds. It is explained by excitation migration-related quenching. The coplanarity of molecule **1.3** apparently enhances exciton coupling, which promotes the nonradiative decay due to excitation migration to intrinsic defects.[42,175]

The charge transfer phenomena of compounds **1.1–1.3** were studied by recording the fluorescence spectra of the solutions in the solvents of different polarities. The photophysical data of the solutions of **1.1–1.3** in different solvents are presented in Table 4.1. Derivative **1.3** dissolved in the solvents of different polarity demonstrated an extremely low emission.

A similar compound possessing carbazole instead of 1,2,3,4-tetrahydracarbazolyl substituents demonstrated very efficient luminescence in a non-polar solvent.[176]

Increasing the solvent polarity for the solutions of compounds **1.2** and **1.3** resulted in considerable broadening and bathochromic shifts of the fluorescence bands as well as in a considerable decrease of emission quantum yields from *ca.* 0.47 and 0.6 (for the solutions in nonpolar solvents) to 0.05 and 0.35 (for the solutions in a polar solvent), and a decrease of the emission lifetime from 15.7 and 4.9 ns (for the solutions in nonpolar solvents) to 4.3 and 4.4 ns (in a polar solvent), respectively. The estimated τ_R decay time values are 4–9 times longer for the twisted molecule (**1.2**) in comparison to the flat one (**1.3**). A similar dependence was observed for τ_{NR} decay times.

The absorption spectra of compounds **1.1–1.3** demonstrate two broad well-resolved bands. Absorption maxima at 300–350 nm can be attributed to benzothiadiazole[177] and carbazole[178] moieties.

Table 4.1 Photophysical properties of the dilute solutions, solid films and 1 wt% solid solutions in polystyrene matrixes of benzothiadiazole derivatives

1.1	λ_{abs}(nm)[a] (ε[b], L mol^{-1}cm^{-1})	λ_F^{max} (nm)[c]	Φ	τ (ns)		
Toluene	434 (3352)	613	<0.01	0.93[82%] 3.38[10%] 14.57[8%]		
THF	426 (3357)	575	<0.01	14.69[46%] 4.49[40%] 0.32[14%]		
Acetone	419 (3459)	577	<0.01	13.48[62%] 4.57[24%] 0.37[14%]		
DMF	419 (3224)	580	<0.01	-		
Neat film	-	612	0.03	0.02[59%] 2.81[41%]		
PS film	-	572	0.10	9.58[65%] 0.27[35%]		
1.2	λ_{abs}(nm)[a] (ε[b], L mol^{-1}cm^{-1})	λ_F^{max} (nm)[c]	Φ	τ (ns)	τ_R (ns)[d]	τ_{NR} (ns)[d]
Toluene	476 (5806)	596	0.47	15.7	33.4	29.6
THF	467 (5903)	607	0.28	13.7	48.9	19
Acetone	458 (5480)	631	0.07	6.7	95.7	7.2
DMF	460 (4913)	655	0.05	4.3	86	4.5
Neat film	-	618	0.25	11.14[93%] 2.75[7%]	44.6	14.9
PS film	-	581	0.50	18.4 [93%], 0.2 [7%]	36.8	36.8
1.3	λ_{abs}(nm)[a] (ε[b], L mol^{-1}cm^{-1})	λ_F^{max} (nm)[c]	Φ	τ (ns)	τ_{avg} (ns)	τ_R (ns)[d]	τ_{NR} (ns)[d]
Toluene	497 (24642)	614	0.60	4.9 [87%] 1.2 [13%]	4.5	7.4	11.2
THF	497 (30362)	638	0.45	5.4 [91%] 1.5[9%]	5	11.2	9.2
Acetone	491 (26433)	664	0.44	5.2[94%] 1.2[6%]	5	11.3	8.9
DMF	499 (25397)	681	0.35	4.42[92%] 1.2[8%]	4.2	11.9	6.4
Neat film	-	692	0.03	0.30[41%] 0.77[39%] 2.29[21%]	0.9	30.1	0.9
PS film	-	623	0.36	4.4[81%] 1.6 [19%]	3.9	10.7	6

[a] Absorption maximum. [b] Molar extinction coefficient. [c] Fluorescence maximum. [d] Radiative, non-radiative decay time constants calculated as τ/Φ and $\tau/(1-\Phi)$, respectively

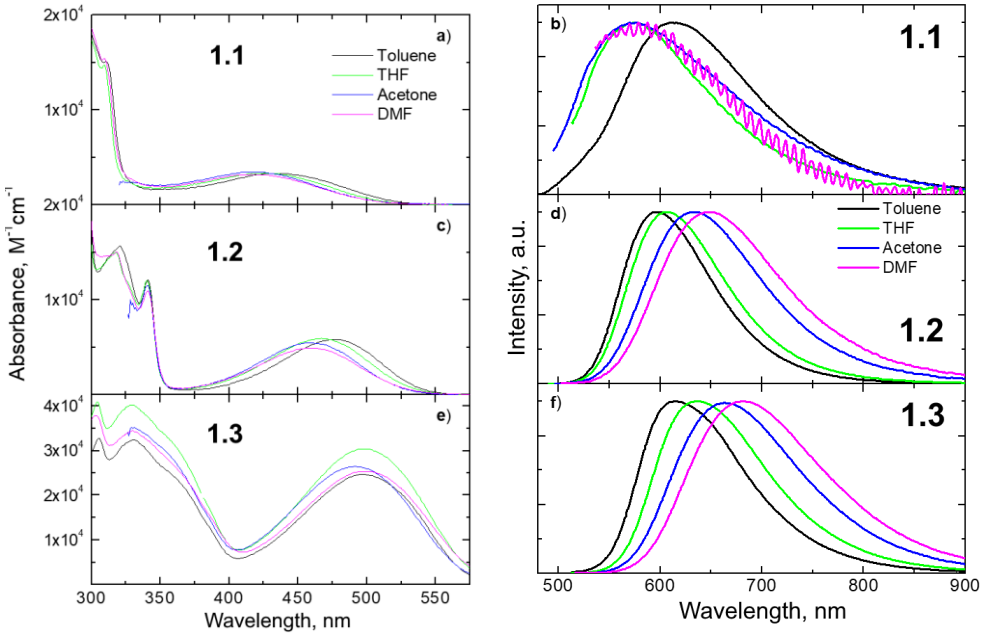

Fig. 4.5 (a), (c), (e) absorption and (b), (d), (f) fluorescence spectra of benzothiadiazole derivatives in solvents of different polarity

PL transients and the spectra of **1.1–1.3** embedded into the Zeonex® matrix were recorded at ambient conditions and at 20 K. All the compounds demonstrated single exponential prompt fluorescence decays.

Derivatives **1.2** and **1.3** did not show any luminescence after prompt fluorescence. The absence of long-lived states in a similar compound with the carbazole side groups has been observed previously.[179]

Compound **1.1** demonstrated very weak phosphorescence (E_T = 2.15 eV) at 20 K (Fig. 4.6) and delayed fluorescence at room temperature.

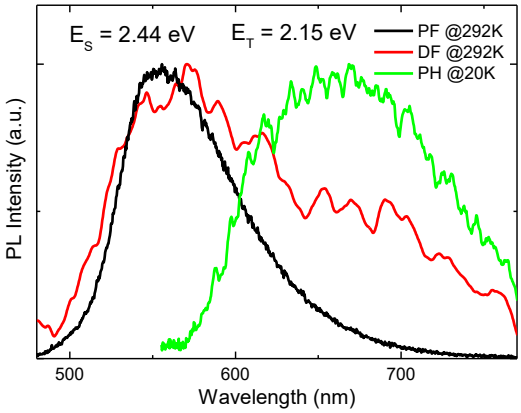

Fig. 4.6 PF and DF spectra recorded at ambient temperature and phosphorescence spectrum recorded at 20 K of 1 wt% solid solution of **1.1** in Zeonex®

4.1.2. Photoelectrical properties

Since compounds were designed for optoelectronic applications, the ionization potentials of their thin solid layers were estimated by electron photoemission spectrometry. The electron photoemission spectra and ionization potentials of **1.1–1.3** are depicted in Fig. 4.7. The I_P^{PE} values of the films of **1.1–1.3** ranged from 5.64 to 5.82 eV. Derivatives **1.1** and **1.2** were characterized by similar I_P^{PE} values, while **1.2** demonstrated the lowest IP_{EP} due to the presence of stronger donating di-*tert*-butyl carbazole units.

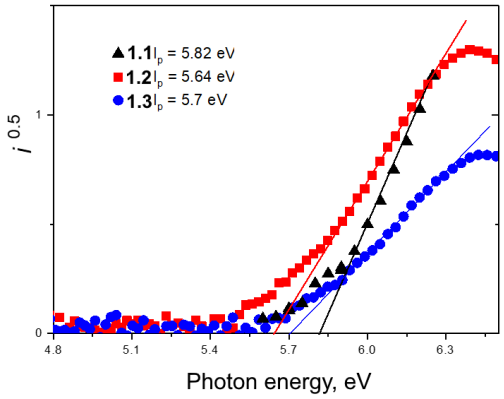

Fig. 4.7 Electron photoemission spectra of solid samples of benzothiadiazole derivatives

The charge transporting properties of the layers of **1.1–1.3** were explored by the TOF technique. The results are summarized in Table 4.2. Fig. 4.8 shows the plots of hole and electron drift mobilities (μ_h, μ_e) of the layers of **1.2, 1.3** and of the layers of the molecular dispersions in bisphenol-Z polycarbonate (PC-Z) versus the electric field.

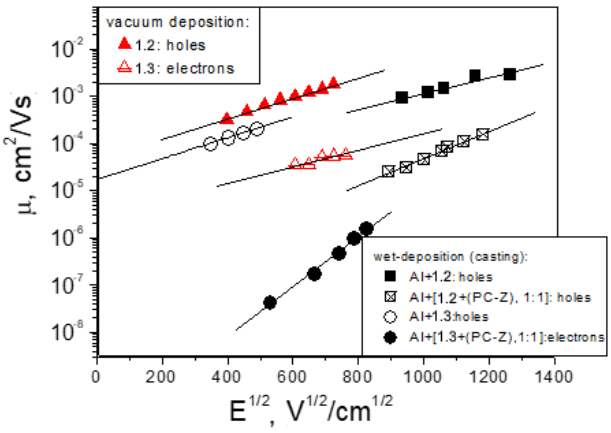

Fig. 4.8 Hole and electron drift mobilities *versus* electric field for layers of compounds **1.2** and **1.3** doped in PC-Z

In the wet-deposition processes of fabrication of TOF samples, PC-Z was used for getting films with uniform thicknesses.

Similar charge-transporting properties were observed for compounds **1.2** and **1.3**. Thus, μ_h of **1.2** and **1.3** ranged from *ca.* $1 \cdot 10^{-4}$ cm^2/Vs to $3 \cdot 10^{-4}$ cm^2/Vs at an electric field of $2.4 \cdot 10^5$–$1.6 \cdot 10^5$ Vcm^{-1}, while the μ_e of **1.2** and **1.3** were found to be more than one magnitude lower in comparison to hole mobilities. In addition, the charge-transporting properties of **1.2** were investigated by using vacuum-deposited samples. The obtained hole mobilities for these samples were in good agreement with the hole mobilities of the wet-casted layer of **1.2** (Fig. 4.8). It was impossible to estimate the hole and electron mobilities either for the neat layer or for the solid solution of **1.1** since the transit times were not obtained from the corresponding current transients. Apparently, compound **1.1** exhibited weak charge-transporting properties due to the presence of weaker donating units of 1,2,3,4-tetrahydrocarbazole in comparison to those of compound **1.2** having stronger donating di-*tert*-butyl carbazole units. Another explanation of this observation can be the strongly dispersive charge-transport, due to which, transit times were not observed for compound **1.1**. Therefore, the charge-drift mobility of **1.1** was not estimated. Indeed, compounds **1.2** and **1.3** were also characterized by strongly dispersive charge-transport. Bipolar charge-transporting properties of compounds **1.2**, **1.3** with rather high charge mobilities show that they have a potential for the application as non-doped functional (light-emitting) layers in OLEDs.

Table 4.2 Charge mobilities in the layers of compounds **1.2** and **1.3**

Material, host polymer	$\mu_e/cm^2V^{-1}s^{-1}$	$\mu_h/cm^2V^{-1}s^{-1}$	*d*, μm
Samples made by drop casting			
Al+**1.2**	-	$2.9 \cdot 10^{-3}$ (at $1.6 \cdot 10^6$ V/cm)	1.4
Al+[**1.2**+(PC-Z), 1:1]	-	$1.8 \cdot 10^{-4}$ (at $1.4 \cdot 10^6$ V/cm)	3.3
Al+**1.3**	-	$2.1 \cdot 10^{-4}$ (at $2.4 \cdot 10^5$ V/cm)	6.0
Al+[**1.3**+(PC-Z), 1:1]	$1.5 \cdot 10^{-6}$ (at $6.7 \cdot 10^5$ V/cm)	-	0.5
Vacuum-deposited samples			
1.2	$5.7 \cdot 10^{-5}$ (at $5.8 \cdot 10^5$ V/cm)	$1.7 \cdot 10^{-3}$ (at $5.3 \cdot 10^5$ V/cm)	1.9

μ_e – electron drift mobility value; μ_h – hole drift mobility value; *d* – layer thickness (μm).

4.1.3. Device fabrication and characterization

Compounds **1.2** and **1.3** were selected for the study of their electroluminescent properties. To estimate their applicability in fluorescent OLEDs, thermally-deposited devices with the following structures were fabricated: ITO/ MoO_3 (1 nm)/ NPB (40 nm)/non-doped EML **1.2** or **1.3** (25 nm)/ TSPO1 (5 nm)/ TPBi (40 nm) / LiF (0.5 nm)/ Al (80 nm) (Fig. 4.9a). To ensure charge balance in the devices, MoO_3 (HIL) and NPB (HTL) were used, while TSPO1 and TPBi served as the electron-transporting materials. They possess the appropriate HOMO, LUMO energies (Fig.

4.9a). The devices with light-emitting layers of **1.2** and **1.3** were named as devices *A* and *B*, respectively. In order to plot the equilibrium energy diagram for these devices, electron affinities (E_A^{PE}) of 2.5 and 2.85 eV for **1.2** and **1.3** in the solid-state were obtained by using the optical band-gap energies (E_g) of 2.29 and 2.08 eV estimated from the absorption spectra of the layers (Fig. 4.7 and 4.9a, Tbl.4.1).[180] Stable at different applied voltages, EL spectra of devices *A*, *B* were observed (Fig. 4.9b). Devices *A* and *B* exhibited red emission with the CIE coordinates of (0.55, 0.43) and (0.55, 0.41, respectively. Compounds **1.2** and **1.3** demonstrated EL spectra with the closely situated main peaks at 598 and 604 nm, respectively, which were extremely similar to their PL spectral peaks. Emission related to the other functional layers of OLEDs *A* and *B* was not observed. This observation confirms a good design of the device structure.

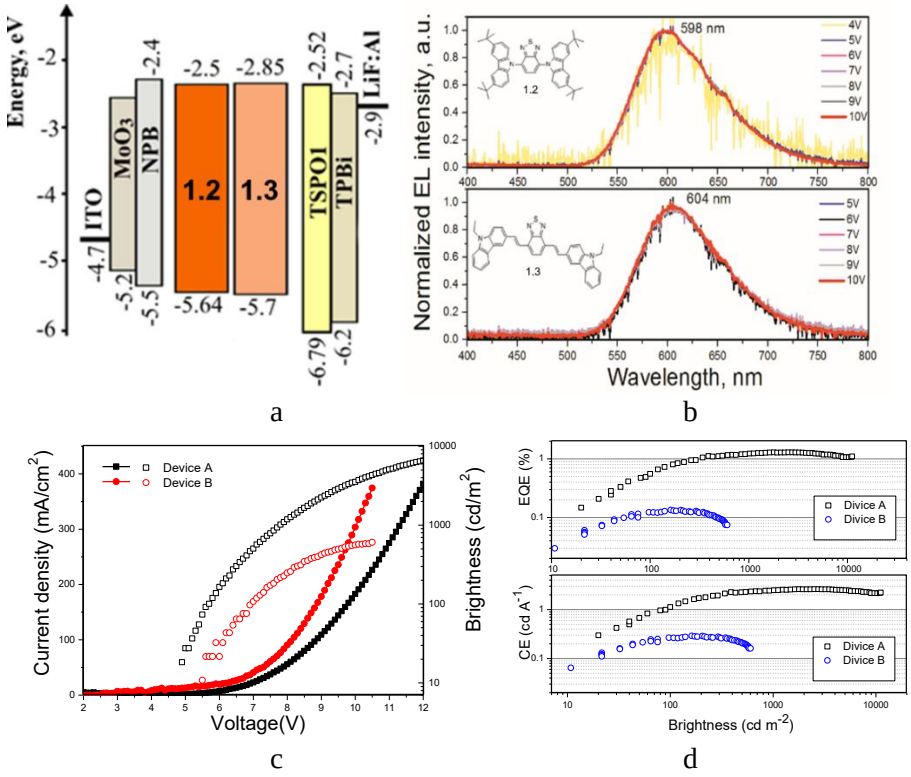

Fig. 4.9 Equilibrium energy diagram and chemical structures of functional materials (a), EL spectra taken at different voltages (b), brightness–voltage–current density curves (c) and external quantum efficiency–brightness–current efficiency curves (d) of devices *A* and *B*

Device *A* displayed the turn-on voltage of 4.9 V, which was lower than 5.5 V observed for device *B*, which, apparently, benefited from the higher charge-drift mobilities according to the brightness–voltage–current density curves (Fig. 4.9c). Moreover, both higher current efficiency of 2.65 cd/A and EQE of 1.3% were obtained for device *A* based on compound **1.2** in comparison to the current efficiency of 0.29 cd/A and EQE of 0.13% recorded for device *B* based on

compound **1.3**. These results are consistent with EQEs of 1.25–1.5% and 0.15–0.23% as theoretically predicted for fluorescent devices *A* and *B*, respectively. The theoretical EQEs were estimated according to Formula (2.1), where $\Phi = 0.25$ for **1.2** and $\Phi = 0.03$ for **1.3** in solid films, η_{out} is around 0.2–0.3.[181] A much better performance of device *A* was obtained by using compound **1.2** relatively to that of device B based on compound **1.3** can be mainly explained by a higher Φ, higher charge-drift mobilities of 4, and effective utilization of the excitation energy from intercrossed-excited-states.[182] A small efficiency roll-off observed in Fig. 4.9 for devices *A* and *B* can be interpreted in terms of the bipolar charge-transporting properties of both compounds (**1.2** and **1.3**). The performances of non-doped devices *A* and *B* are still low especially when comparing them with the EQEs of the doped OLEDs based on phosphorescent emitters or those exhibiting TADF.[65,183]

4.2. Donor-acceptor-donor benzonitrile-based emitters with different substitution pattern

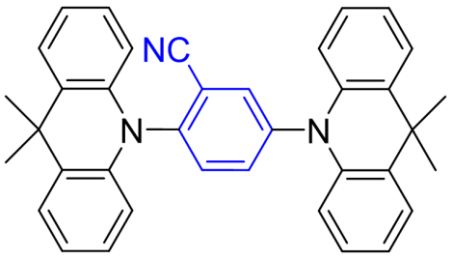

2.1

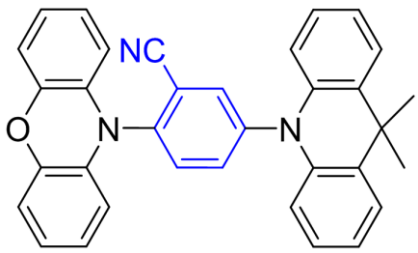

2.2

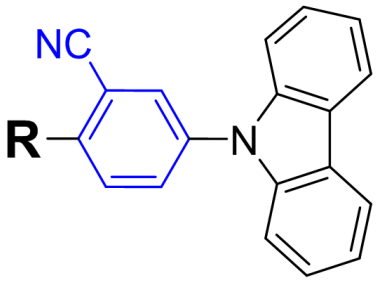

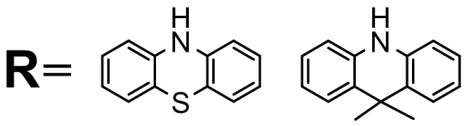

2.3 **2.4**

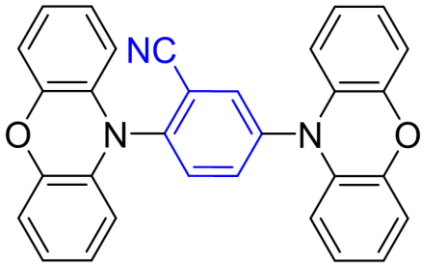

2.5

Fig. 4.10 Chemical structures of differently substituted derivatives of benzonitrile[170]

4.2.1. Photophysical properties

In order to understand the impact of substitutions of benzonitrile-based emitters on their photophysical properties, the electronic absorption and PL spectra of the solid films and dilute solutions were recorded (Fig. 4.11). Key photophysical data is collected in Table 4.3. The solutions of compounds **2.1**–**2.5** in toluene displayed quite different absorption profiles because of different donor substituents. A similarity was observed between the vibronic-structured low-energy bands in the range of 290–355 nm of the absorption spectra of the solutions of compounds **2.3** and **2.4** containing carbazole moieties. The effect of the other donor moieties, i.e., phenothiazine or 9,9-dimethyl-9,10-dihydroacridine was practically not detectable in the low-energy bands of the solutions of asymmetric compounds **2.3** and **2.4**.

Similar absorption spectra were also observed for the solutions in THF and for the films of compounds **2.3** and **2.4** (Fig. 4.11a). For the toluene solutions of compounds **2.1** and **2.2**, only absorption tails of the compounds were observed. This is due to the effects of the solvent which are observed for toluene in the range of up to 300 nm. The absorption spectra of the THF solutions of **2.1** and **2.2** showed a well-observed band peaking at 281 nm. This band is mainly related to the 9,9-dimethyl-9,10-dihydroacridine moiety. The shoulder at 316 nm related to the absorption of the phenoxazine moiety can be recognized in the absorption spectrum of the solution of compound **2.2**. The absorption spectra of the solution of compound **2.5** were characterized by a well-observed band peaking at 316 nm, which is apparently also related to the phenoxazine moiety. In the absorption spectra of toluene solutions and of the films of all the synthesized compounds, weak absorption tails extending to near 430–460 nm can be recognized. These tails are apparently related to the CT between the donors and the accepting benzonitrile unit. The solvatochromic effect for the absorption spectra of the solutions of compounds **2.1**–**2.5** was not detected. Virtually no differences in the absorption spectra of toluene solutions, THF solutions and solid films of the same compounds were detected.

Showing effect of various substitution of benzonitrile-based emitters on their emission properties, the single emission peaks in the relatively wide range of *ca*. 470-560 nm were observed in the PL spectra of the toluene solutions of compounds **2.1**–**2.5** at room temperature. Different donating abilities of the attached donors resulted in different intramolecular interactions between the donor and the accepting units, thus determining the fluorescent characteristics (Fig. 4.11b, Table 4.3). The PL spectra in the blue/sky-blue region were observed for the solutions of compounds **2.1** and **2.4**. These derivatives have a similar structure except for the substitution of the carbazole moiety for **2.4** instead of one of 9,9-dimethyl-9,10-dihydroacridine donor units of **2.1**. It can be concluded that the spectral characteristics of these compounds and their Φ values are completely determined by the dimethylacridine and the weaker carbazole donor does not have a substantial impact on the emissive properties in the case.

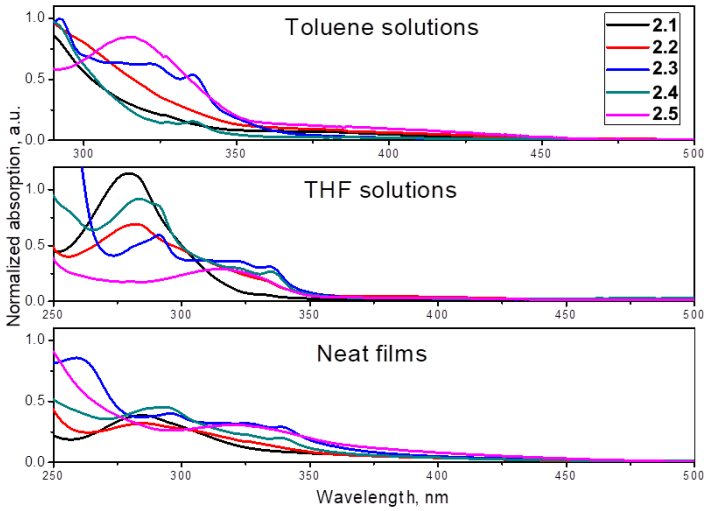

a

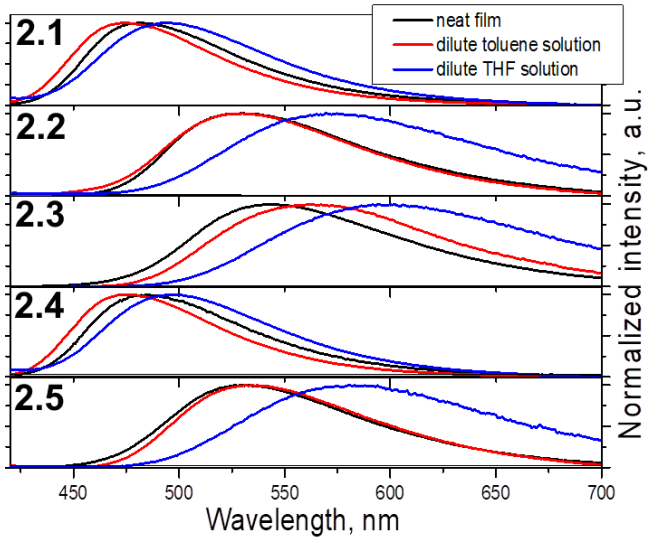

b

Fig. 4.11 Absorption (a) and PL (b) spectra of neat films, dilute toluene and THF solutions of compounds **2.1–2.5**

Similarly to **2.1** and **2.4**, the photophysical characteristics of **2.2** and **2.5** with the phenoxazine units are almost identical regardless of the 9,9-dimethyl-9,10-dihydroacridine introduction into the structure of **2.2**. However, dimethylacridine is responsible for a slight increase of Φ for films. The difference in the structures of **2.1** and **2.2** is that the phenoxazine moiety is substituted instead of one of the two donors of **2.1**. Due to being stronger than the 9,9-dimethyl-9,10-dihydroacridine electron donating substituent, phenoxazine determines the characteristics of shifting PL peaks into the green spectral range and lowering the Φ of the samples in a non-

polar medium. The film of yellow emitter **2.3** is the least emissive (Table 4.3) and the most spectrally red-shifted compound of the series, which is obviously not caused by carbazole. Phenoxazine, the strongest donor used in the investigation, exerts decisive influence on the emissive properties when it competes with carbazole in **2.3** or 9,9-dimethyl-9,10-dihydroacridine when comparing **2.3** and **2.4**. Any of two donor units of the compound which has a stronger electron donating ability than others is crucial for the determination of the photophysical properties of the donor-acceptor-donor molecule in our investigation. The PL spectra of the corresponding THF solutions were red-shifted with respect to the spectra of the solutions of the corresponding substituents. This observation indicates intramolecular CT which was widely observed for emitters containing donor and acceptor moieties.[79,184] The PL intensities of THF solutions of the compounds were found to be very sensitive to oxygen (Fig. 4.12a). This observation can be related to the triplet harvesting and converting into light via TADF. The nature of the triplet harvesting will be discussed below.

Deoxygenated toluene solutions were characterized by relatively weak emission. Their absolute *Φs* did not exceed 14%. The *Φs* of the films of the studied compounds measured in air were found to be much higher than those of the dilute solutions and reached 42%. A comparison of the *Φ* values of the solid films and of dilute solutions allows concluding that AIEE is characteristic of compounds **2.1**–**2.5** (Table 4.3).[185] Interestingly, the PL spectra of the films of the studied compounds were found in the similar range or were even blue-shifted in comparison to the PL spectra of the corresponding toluene solutions (Fig. 4.11b). This aggregation can induce not only emission intensity enhancement but also blue-shifts of the PL spectra as it was reported elsewhere.[127]

Table 4.3 Photophysical parameters of benzonitrile derivatives

Compound	λ, nmˆ	Φ_{PL} $_{THF}$*	Φ_{PL} $_{tol}$‖	Φ_{PL} $_{film}$‡	E_{S1}§, eV	E_{T1}§, eV	ΔE_{ST}§, eV	Ratio $_{dg/air}$¶	Ratio, $_{DF/PF}$†	slope‡
2.1	482	0.11	0.13	0.42	2.91 (2.72)	2.8 (2.68)	0.11 (0.04)	1.6	0.65	1
2.2	529	0.03	0.13	0.26	2.74 (2.29)	2.62 (2.27)	0.12 (0.02)	3.5	0.96	1
2.3	543	0.01	0.04	0.11	2.71 (2.63)	2.52 (2.62)	0.19 (0.01)	2.4	0.88	0.92
2.4	483	0.12	0.14	0.39	2.89 (2.56)	2.84 (2.54)	0.05 (0.02)	3	3.8	0.92
2.5	530	0.03	0.12	0.18	2.9* (2.26)	2.79* (2.24)	0.11* (0.02)	2.8	-	-

ˆWavelength of the PL peak of the neat films of compounds. *Φ of deoxygenated THF solutions. ‖ Φ of deoxygenated toluene solutions. ‡Φ of the neat films. §Estimated from the emission spectra of the neat films at 77 K. *Estimated from the emission spectra of dilute THF solutions recorded at 77 K. ¶Ratio of PL intensities of degassed and air equilibrated toluene solutions recorded at 293 K. †Ratio of DF and PF yields of the neat films estimated from the time resolved spectroscopic measurements at 293 K. ‡ Slopes of the linear fit of log-log DF integral intensity dependence on the excitation power across the entire range of applied power at 293 K. Theoretical values of E_{S1}, E_{T1} and ΔE_{ST} are presented in parentheses

DF was detected for the solid films at room temperature under inert atmosphere. DF quantum yields were found to be relatively high in comparison with those of PF. The ratios of intensities of PF and DF of the films correlate well with the ratios of emission intensities of air equilibrated and degassed toluene solutions (Table 4.3, Fig. 4.12). Both of these ratios reflect the contribution of triplet excitons in the radiative process.

In the donor-acceptor-donor molecules, near-orthogonal geometry minimizes the singlet-triplet energy splitting of the first singlet and triplet excited state energy levels making TADF possible.[93,94]

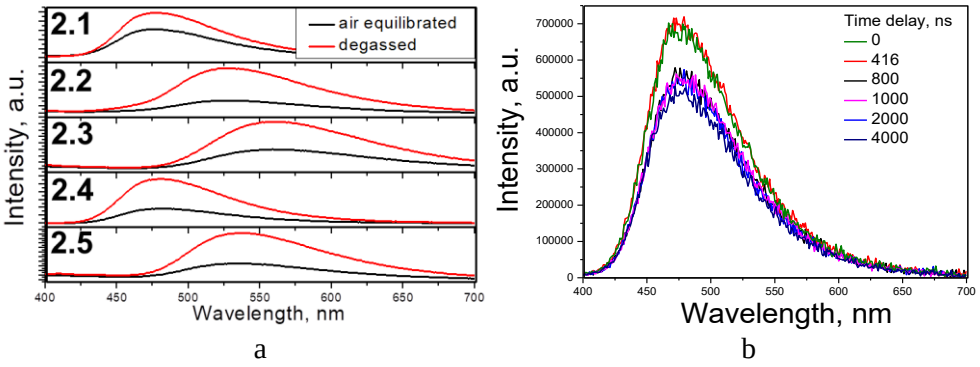

a b

Fig. 4.12 PL spectra of degassed and air equilibrated dilute toluene solutions of benzonitrile derivatives recorded at room temperature (a). Time resolved PL spectra of the film of **2.4** recorded at room temperature (b)

Energy splitting lower than 0.2 eV enables to predict TADF as the probable cause of DF. Energy levels of the singlet and triplet excited states were estimated from the onsets of the emission spectra of the neat films recorded at 77 K under inert atmosphere. (Table 4.3, Fig. 4.13b). The triplet levels of compounds depend on the triplet levels of its donors.

As it can be analyzed from the levels of E_{T1} evaluated both theoretically and experimentally, the phenoxazine donor significantly lowers the energy values of compounds **2.2** and **2.5** to ~2.6 eV because of having a strong donating ability. Correspondingly, **2.1** and **2.4** with dimethylacridine have an E_{T1} higher than 2.8 eV. The energy increase caused by this moiety is especially well pronounced when **2.3** and **2.4** are compared. The lowest E_{T1} of 2.52 eV was achieved for the neat film of **2.3** with phenothiazine, the strongest donor of all the donors used in this research. The thermal activation of DF was detected from the analysis of PL decay curves after heating up solid samples to temperatures higher than 180 K (Fig. 4.13c). This observation confirms that the origin of DF is TADF. The slopes of 0.92–1 of the linear fits of the log-log DF integral intensity dependences on the excitation power across the entire range of the applied power measured at room temperature is additional evidence of TADF (Table 4.3, Fig. 4.13d).

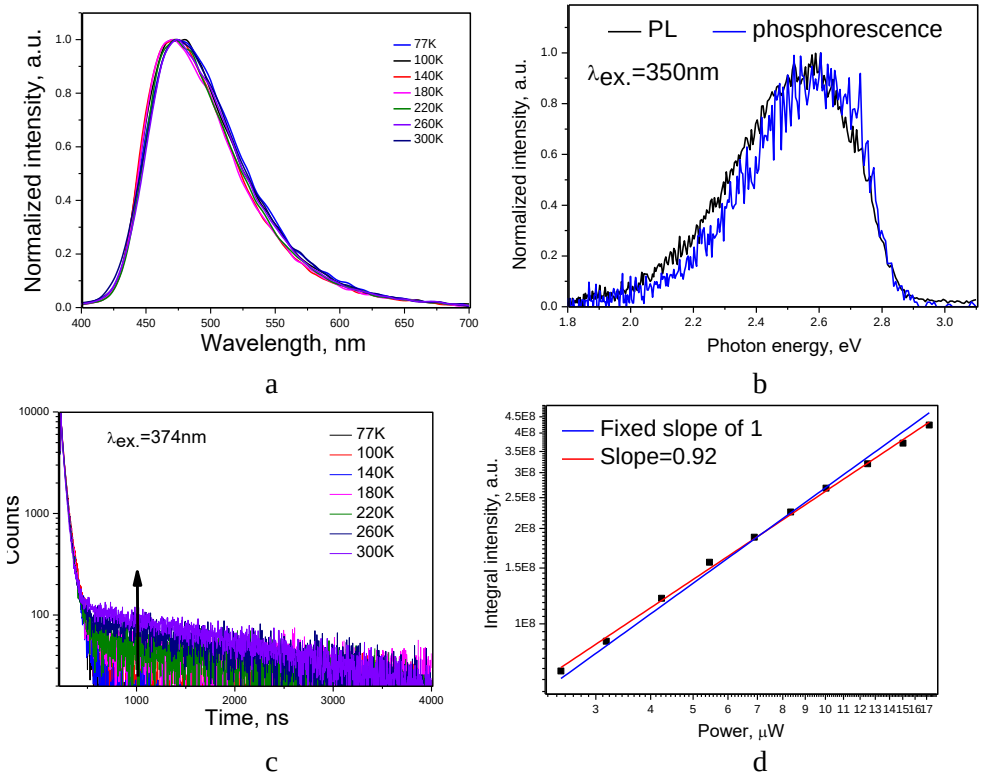

Fig. 4.13 Photophysical characteristics of the film of **2.4:** (a) PL spectra recorded at various temperatures; (b) time resolved PL spectra recorded at liquid nitrogen temperature (0 and 0.1ms delays); (c) PL decay curves recorded at various temperatures; and (d) correlation between DF integral and excitation dose recorded at room temperature

The unchanged shape of the PL spectra as well as the absence of additional emission peaks after the deoxygenation of solutions proves that fluorescence is the only radiative process available for excitons to deactivate to the ground state (Fig. 4.12). The PL spectra of the films of the studied compounds except that of **2.2** did not show any substantial changes with an increase of the temperature. A slight additional spectral shoulder for the neat film of **2.2** is attributed to phosphorescence. The strong DF shows that triplet excitons are involved in the CT emission. Slight hypsochromic (for **2.1**) and bathochromic (for **2.3**) shifts of the emission peak position in the PL spectra of films after heating, or both consecutively (a blue shift initially, and a red shift at temperatures higher than 140 K in the case of **2.4**) can be attributed to competitive processes. The intramolecular charge transfer state undergoes stronger vibrational relaxations at higher temperatures, which causes a substantive usual red shift. The slowing TADF decay requires a shift of the ^{1}CT away from the local triplet excited ^{3}LE state. A constant hypsochromic shift can be explained by the electronic coupling between ^{3}LE and ^{1}CT.

The presence of conformers with a slightly different dihedral angle between the electron donor and the acceptor units can be considered as an alternative

explanation for the blue shift. With this kind of heterogeneity, some molecules are able to feature a less relaxing CT state that emits light toward the blue region.[86] This condition can be crucial for the small singlet-triplet energy splitting. The blue shift or an additional peak at 77–100K can also be explained by the phosphorescence attributed to the higher excited triplet state which can have its own role in the determination of the TADF efficiency.[94,186]

4.2.2. Electrochemical and photoelectrical properties

Solid samples of compounds **2.1–2.5** were tested by photoelectron emission spectroscopy in air. The I_P^{PE} values of the films were found to be in the range from 5.83 to 6.0 eV (Fig. 4.14b). **2.5** with two phenoxazine moieties denoted by the lowest HOMO level representing IP. Either carbazole or trimethylacridine units as the weaker electron donors are responsible for the HOMO level increase for **2.1–2.4** with a consequent reduction of the HOMO-LUMO gap.

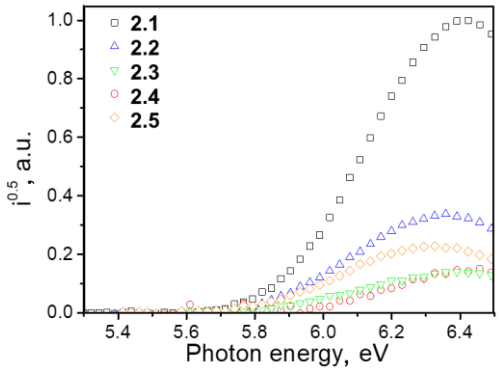

Fig. 4.14 Photoelectron emission spectra of the solid samples of compounds **2.1–2.5**

Table 4.4 Results derived from electrochemical measurements of compounds **2.1–2.5**

Compound	E_{onset}^{ox} [a] *vs* Fc, [V]	E_{onset}^{red} [a] *vs* Fc, [V]	IP^{CV}[b] / HOMO[c] [eV]	EA^{CV}[b] / LUMO[c] [eV]
2.1	0.59	-2.38	5.39/-5.21	2.39/-1.83
2.2	0.30	-2.40	5.10/-4.92	2.39/-1.92
2.3	0.31	-2.36	5.11/-5.12	2.44/-1.82
2.4	0.57	-2.47	5.37/-5.16	2.49/-1.84
2.5	0.66	-2.34	5.46/-4.96	2.28/-1.99

[a] E_{onset}^{ox} and E_{onset}^{red} were measured *vs.* ferrocene/ferrocenium. [b] Calculated with reference to ferrocene (4.8 eV). Ionization potentials and electron affinities. [c] Estimated HOMO/LUMO levels

4.2.3. Charge transporting properties

Owing to the donor-acceptor structure of the synthesized compounds, bipolar charge carrier transport was expected. In order to study the impact of donor

substituents on the charge-transporting properties of vacuum-deposited films, TOF measurements were performed regarding the generation of holes or electrons on the ITO/film interface by optical excitation through the ITO electrode by using a pulsed laser (λ = 355 nm) and different polarity of the applied voltages (positive for holes and negative for electrons). Thus, the photogenerated holes and electrons were transported through the layer from the ITO electrode to the opposite Al electrode under various external electric fields. Because of the highly dispersive charge transport, the transit times (t_{tr}) for the holes and electrons at different applied electric fields were taken from the corresponding photocurrent transients in log-log scales (Fig. 4.15). The plot of the charge drift mobility versus electric fields (E) is presented in Fig. 4.15c.

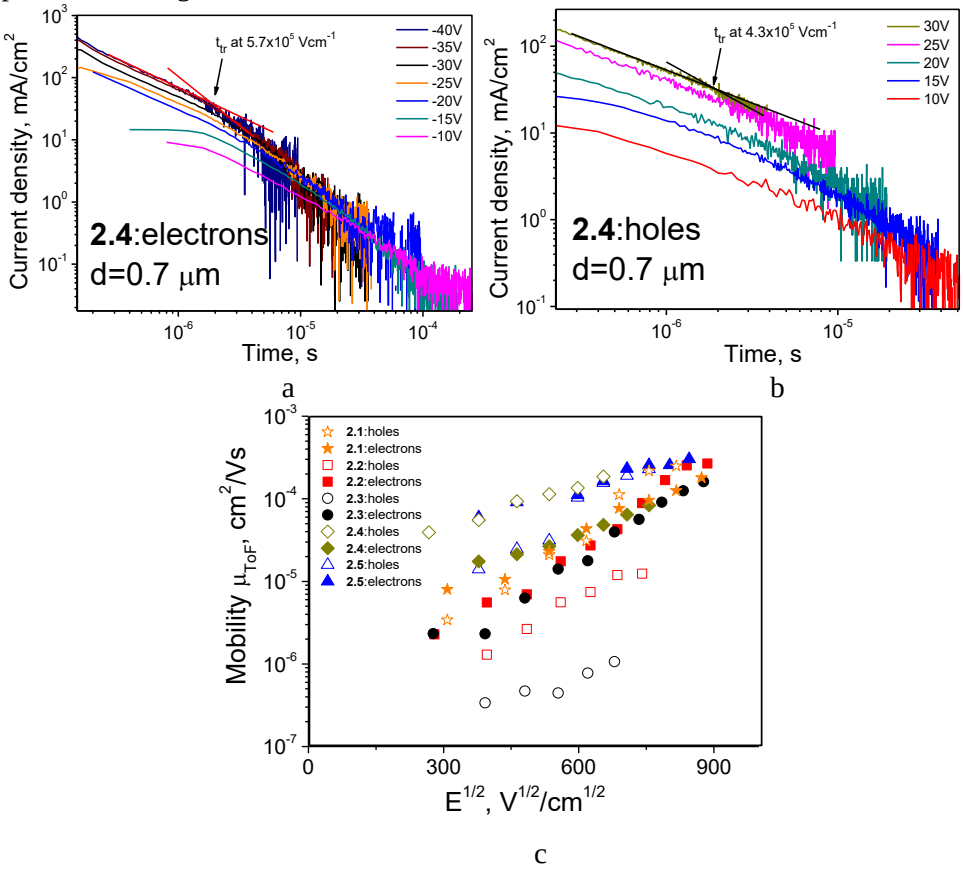

Fig. 4.15 Electron (a) and hole (b) time-of-flight current transients; charge mobility *versus* electric field dependencies (c) of the layers of compounds **2.1–2.5**

The hole mobilities of the layers of the studied compounds ranged from $3\cdot10^{-7}$ $cm^2V^{-1}s^{-1}$ to $1\cdot10^{-4}$ $cm^2V^{-1}s^{-1}$ and increased in the order **2.4**>**2.5**>**2.1**>**2.2**>**2.3**. The highest hole mobilities were observed for compounds **2.4** and **2.5** containing carbazole/acridan and phenoxazine units, respectively. The lowest hole mobility was observed for compound **2.3** containing carbazole and phenothiazine donor moieties. Since the same accepting unit was used, comparable electron mobility values were

recorded for compounds **2.1–2.5**. The values ranged from *ca.* $1.5 \cdot 10^{-4}$ $cm^2V^{-1}s^{-1}$ to $3 \cdot 10^{-4}$ $cm^2V^{-1}s^{-1}$ at an electric field of $6.9 \cdot 10^5$ Vcm^{-1}. Slight differences were apparently determined by different molecular packing of the molecules in the solid-state.

4.2.4. Device fabrication and characterization

Taking into account relatively high Φ values of up to 42% for the neat films, the bipolar charge transport, and relatively good charge-transporting properties of compounds **2.1–2.5**, they can be regarded as promising candidates for doping-free OLEDs. In order to gain insight into the electroluminescent characteristics of the studied compounds, they were used as TADF emitters in non-doped OLEDs with structures ITO / MoO_3 / NPB / non-doped EML / TSPO1 /TPBi / LiF / Al (Fig. 4.16). Non-doped light-emitting layers of these devices (named as 1A–5A) were prepared from compounds **2.1–2.5**, respectively. MoO_3 as the HIL, NPB as the HTL, TSPO1 as the hole/exciton blocking layer, TPBi as the ETL, and LiF as the EIL were employed. Fig. 4.16 shows the structure and energy diagrams of devices 1A–5A.

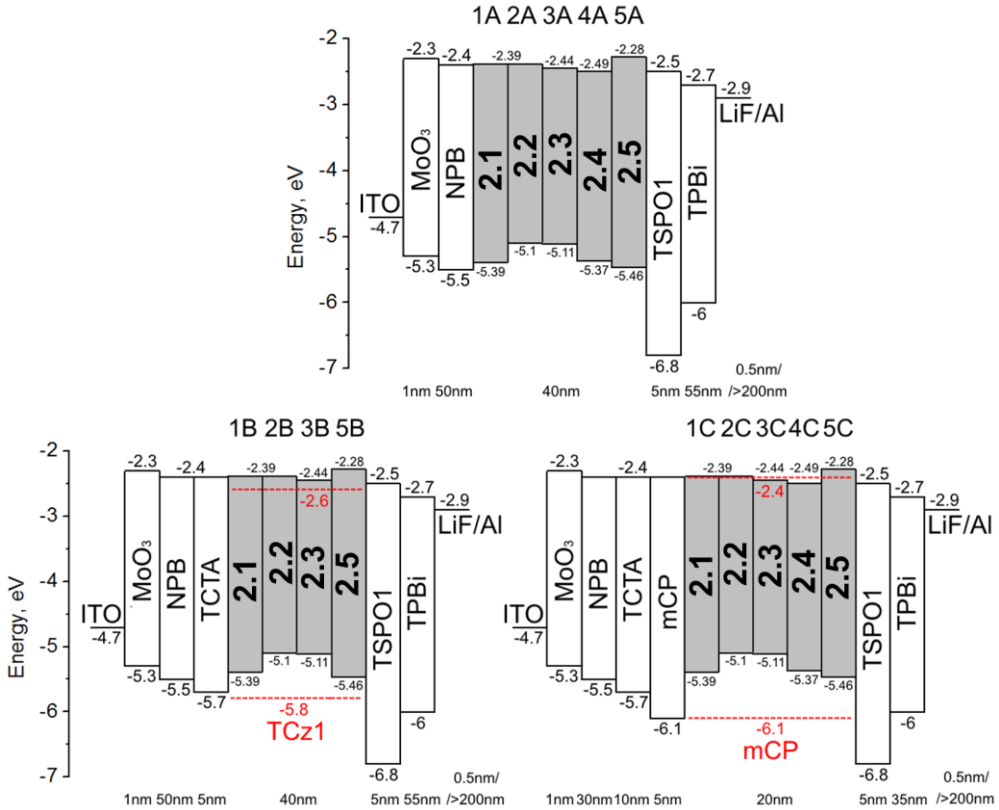

Fig. 4.16 Energy diagram of OLEDs employing compounds **2.1–2.5** as emitters

The key electroluminescent parameters of the fabricated OLEDs are listed in Table 4.5. The current density-voltage-luminance characteristics, current efficiency, power efficiency and EQE versus current density curves as well as the EL spectra are presented in Fig. 4.22. Similar EL spectra were obtained at different applied voltages thus proving that the recombination of hole-electron pairs occurred within the light-emitting layers.

In addition, the EL spectra of devices 1A–5A were in good agreement with the PL spectra of the films for the studied emitters. The EL spectra of devices 1A and 4A containing emitters with 9,9-dimethyl-9,10-dihydroacridine or carbazole moieties were blue-shifted in comparison to those of the devices based on emitters **2.2, 2.3** and **2.5** (Fig. 4.22c). CIE 1931 UCS coordinates represent the color (the blue-yellow range) of electroluminescence of the developed doping-free devices (Table 4.5). Blue OLEDs were obtained by using emitters **2.1** and **2.4** based on 9,9-dimethyl-9,10-dihydroacridine or carbazole moieties.

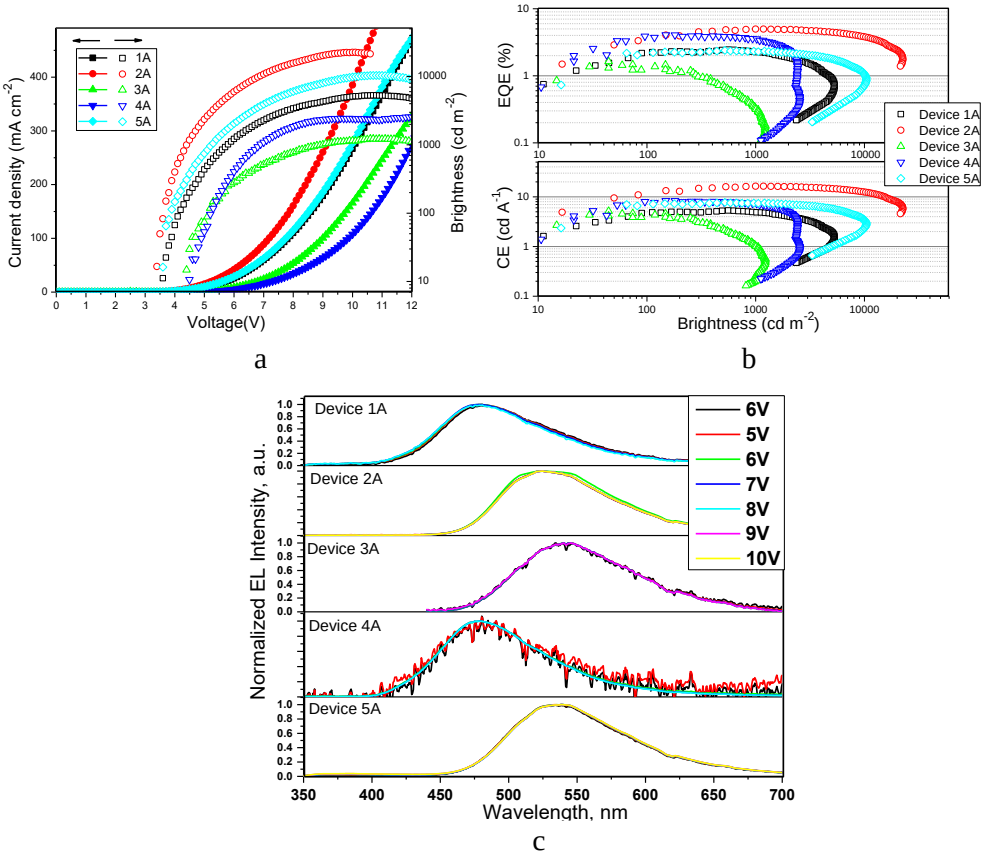

Fig. 4.17 Electroluminescent properties of non-doped OLEDs 1A–5A: voltage-current density and voltage-luminance (a), EQE, current efficiency-current density (b) characteristics and EL spectra (c)

The efficient injection of the charge carriers from the electrodes and the following transport to the emitting layer is evident by the low turn-on voltages for

all the fabricated OLEDs (3.3–4.5 V). The IQE and EQE of OLEDs, consequently, correlate to the Φ of EML and its singlet and triplet exciton employment into emission.[77] This finding is a direct indication of the TADF efficiency.

The highest values of the maximum EQEs among devices 1A–5A were obtained for devices based on TADF emitters **2.2** and **2.4** having asymmetrical structures with 9,9-dimethyl-9,10-dihydroacridine and either phenoxazine or carbazole moieties (5.0% and 4.1%, respectively). Despite the highest Φ value observed for the film of **2.1**, OLEDs based on compound **2.1** showed the maximum EQE of only 2.5%, apparently because of the smaller contribution of TADF in its emission (DF/PF intensity ratio of 0.65) (Table 4.5). The lowest maximum EQE value of 1.6% was obtained for device 3A based on compound **2.3** containing carbazole and phenothiazine donors. Most probably, it was due to both the lowest Φ value and the lowest hole mobilities of the films of the compound.

The best device 2A showed the maximum current efficiency of 16.3 cd/A, the maximum power efficiency of 12.2 lm/W, and the maximum EQE of 5% (Table 4.5). The bigger ratio of PL intensities of degassed and air equilibrated toluene solutions for green **2.2** than for blue **2.4** accounts for more efficient TADF resulting in 2A featuring bigger values of EQE than 4A. The maximum brightness of 22,600 cd/m^2 was also obtained for device 2A. The highest brightness of this device can partially be explained by the position of its electroluminescence spectrum which was in the range of the maximum sensitivity of human eyes.

Doping did not lead to any impressive improvement of the characteristics of OLEDs. For example, the doping of emitter **2.2** into the host resulted in a luminance drop from 22,600 to 14,900 cd/m^2 and a slight increase of the turn-on voltage. In addition, it also resulted in the increase of the OLED efficiency to 21.2 cd/A, 15.7 lm/W and EQE of 7.3% apparently because of the improvement of the charge-transporting properties. In addition to the previous investigation, TADF emitters **2.1–2.5** were tested in doped devices 1B–5B and 1C–5C by using TCz1 and mCP hosts, respectively. To confine the exciton recombination zone within the light-emitting layer, a relatively high concentration of the emitter (15%) was taken. The radiative charge recombination in the emitting layer with relatively small concentrations of the TADF emitter takes place mostly on the interfaces between the emitting layer and the blocking layers (transport layers in the absence of blocking layers) due to charge density distributions.[187]

In order to improve the hole-transfer, additional layers of either TCTA or mCP were used (Fig. 4.16). As well as for 1A–5A, the turn-on voltages of the doped devices are similarly low thus proving excellent injection of holes and electrons and their transport to the recombination zones. The energy mismatch of the host/guest HOMO/LUMO levels and the energy barriers with the charge transport layers led to inefficient electronic excitation energy transfer from the host to the guest with the resulting weak emission from TCz1. The electron blocking layer of mCP effectively blocked electron penetration into NPB thus enhancing electron transition from the host to the dopant. As a result, the emission of these devices with the guest:host layers related to the host became negligible. Doped devices 1B–5B exhibited higher maximum EQEs in comparison to the non-doped ones (Table 4.5).

Table 4.5 Electroluminescence parameters of benzonitrile derivatives-based OLEDs

Device	EML[a]	L_{max}, 10^3 cd/m^2 [b]	V_{on}, V [c]	η_c, cd/A [d]	η_p, lm/W [e]	EQE, % [f]	CIE [g]
ITO / MoO_3 /NPB / non-doped EML / TSPO1 / TPBi / LiF / Al							
1A	**2.1**	5.3	3.6	5.3 (4.8)	3.6 (3.6)	2.5 (2.2)	(0.187, 0.285)
2A	**2.2**	22.6	3.4	16.3 (11.5)	12.2 (10)	5 (3.5)	(0.309, 0.565)
3A	**2.3**	1.2	4.4	5.2 (4)	3.5 (2.4)	1.6 (1.3)	(0.347, 0.522)
4A	**2.4**	2.6	4.5	8.4 (7.7)	4.9 (4.6)	4.1 (3.7)	(0.181, 0.271)
5A	**2.5**	10.4	3.6	7.7 (6.9)	6 (5.6)	2.4 (2.1)	(0.337, 0.555)
ITO / MoO_3 / NPB / TCTA / emitter:TCz1 / TSPO1 / TPBi / LiF / Al							
1B	**2.1**:TCz1	3.2	3.5	5 (4.7)	3.8 (3.1)	3.1 (2.9)	(0.189, 0.214)
2B	**2.2**:TCz1	14.9	3.5	21.2 (13.8)	15.7 (10.8)	7.3 (4.7)	(0.268, 0.478)
3B	**2.3**:TCz1	8.7	4.2	11.4 (9.3)	7.5 (6.7)	3.6 (3)	(0.311, 0.546)
5B	**2.5**:TCz1	14.9	3.6	15.1 (8.2)	9.5 (6.1)	4.9 (2.7)	(0.261, 0.519)
ITO / MoO_3 / NPB / TCTA / mCP / emitter:mCP / TSPO1 / TPBi / LiF / Al							
1C	**2.1**:mCP	6.5	3.6	4.5 (2.4)	3 (1.9)	2.2 (1.2)	(0.157, 0.249)
2C	**2.2**:mCP	24.1	3.6	20.7 (8.5)	12.2 (6.7)	7 (2.9)	(0.217, 0.487)
3C	**2.3**:mCP	13.7	3.3	12 (7.7)	7.2 (6.1)	3.8 (2.4)	(0.262, 0.522)
4C	**2.4**:mCP	5	3.7	3.4 (2.3)	2.2 (1.7)	1.7 (1.2)	(0.158, 0.224)
5C	**2.5**:mCP	21.3	3.5	16.1 (9.9)	10.9 (8.3)	5.3 (3.2)	(0.234, 0.512)

[a] Type of host/guest system in EML. [b] Maximum brightness. [c] Turn-on voltage. [d] Maximum current efficiency. [e] Maximum power efficiency. [f] Maximum external quantum efficiency. [g] CIE 1931 UCS coordinates at 8V. The values in parentheses are presented at 100 cd/m^2

The highest values of maximum EQEs among devices 1B–5B were obtained for devices based on TADF emitters **2.3** and **2.5** having carbazole/phenothiazine and phenoxazine donor moieties (3.8 and 5.3%, respectively). These results are in good agreement with the Φ values of thin films and with the contribution of TADF in the degassed environment (Tables 4.3, 4.5, Figs. 4.12, 4.17b).

The effect of doping into TCz1 is clearly evident when the operational characteristics of devices 3A and 3B are compared. At a low luminance of 100 cd/A, the parameters of device 3A were found to be 4 cd/A, 2.4 lm/W, EQE of 1.3% while those of device 3B were 9.3 cd/A, 6.7 lm/W and 3%, respectively. Devices 5B and 5C also exhibited relatively high maximum EQE of 4.9 and 5.3%, respectively.

No major peak of the EL spectra of the 2B, 2C, 3B, 3C, 5B and 5C is pronounced. The emission spectra feature a secondary blue-shifted emissive peak. Such a behavior is evident for both OLEDs based on compounds **2.2** and **2.3** with different donor moieties and 5B, 5C based on symmetrical **2.5**. There is no doubt that the cause is the host/guest interaction.

It is explained by a different contribution of PF and DF into emission. RISC immediately initiates TADF thus causing the triplet excited state to be involved in the nuclear configuration of the singlet excited state. The peak splitting, previously explained by the exciplex forming abilities of a host, can occur due to the enhancement of DF by electrical excitation.[188] Two peaks most likely correspond to PF and TADF from the singlet excited state on different energy levels. The singlet excited state formed via RISC is denoted by a lower energy. The singlet excited state which causes PF differs due to the polarization of the host. The polarization of the host changes when applying more electricity to the OLED. Consequently, at high voltages, this division becomes more negligible. Considering that the PL spectra of emitters doped into TCz1 are featureless, double peaks in the EL spectra can also be attributed to electroplexes.[189] As an alternative explanation that was mentioned above, conformational heterogeneity or the impact of the higher excited triplet state can lead to a blue-shifted emission peak.

4.3. TADF emitters based on diphenylsulfone and dibenzothiophene dioxide as acceptor units and di-*tert*-butyldimethyldihydroacridine as donor moiety

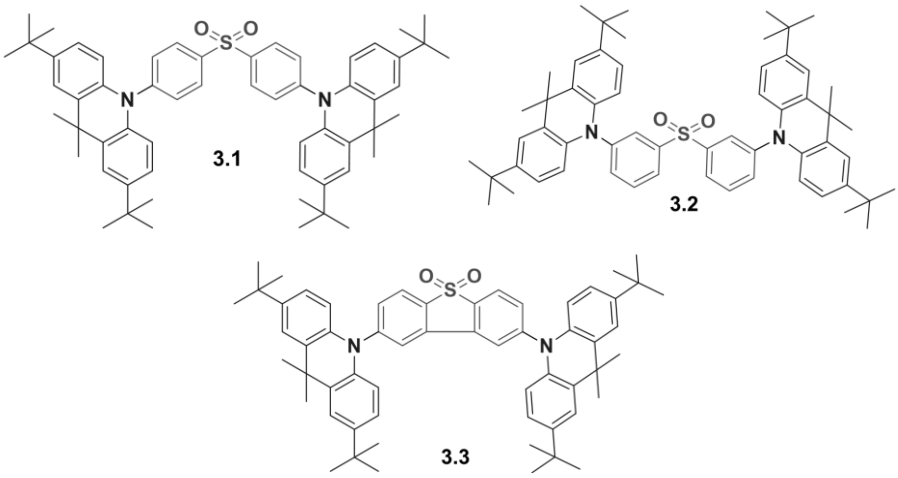

Fig. 4.18 Chemical structures of derivatives of diphenylsufone and dibenzothiophene *S*,*S*-dioxide substituted with di(*tert*-butyl)acridan[171]

4.3.1. Electrochemical and photoelectrical properties

IP_{CV} values were found to be comparable (5.19–5.23 eV). EA^{CV} was estimated by using optical E_g, and IP^{CV} values were found to range from 3.46 to 3.73 eV.

Taking into account that the energies of the molecular levels are different in solutions and in the solid state,[180] the I_P^{PE} of the solid layers of **3.1–3.3** were

additionally estimated by photoelectron emission spectrometry (Fig. 4.19a). I_P^{PE} values of 5.38 eV were obtained for all the compounds. This observation is thus in good agreement with the cyclic voltammetry data (Table 4.6). The I_P^{PE} and E_A^{PE} values of solids **3.1–3.3** are appropriate for hole and electron injections. Different acceptor moieties of compounds **3.1–3.3** virtually did not affect their energy levels.

Table 4.6 Ionization energies of diphenylsulfone and dibenzothiophene *S*,*S*-dioxide derivatives

Compound	$E_{onsetox}$ *vs* Fc, [V]	IP^{CV}, HOMO [eV]	EA^{CV}, LUMO[c] [eV]	I_P^{PE}, [eV][d]	E_A^{PE}, [eV][e]
3.1	0.42	5.19/-5.21	3.46/-1.75	5.38	2.22
3.2	0.44	5.22/-5.08	3.73/-1.63	5.38	2.21
3.3	0.45	5.23/-5.25	3.69/-2.15	5.38	2.84

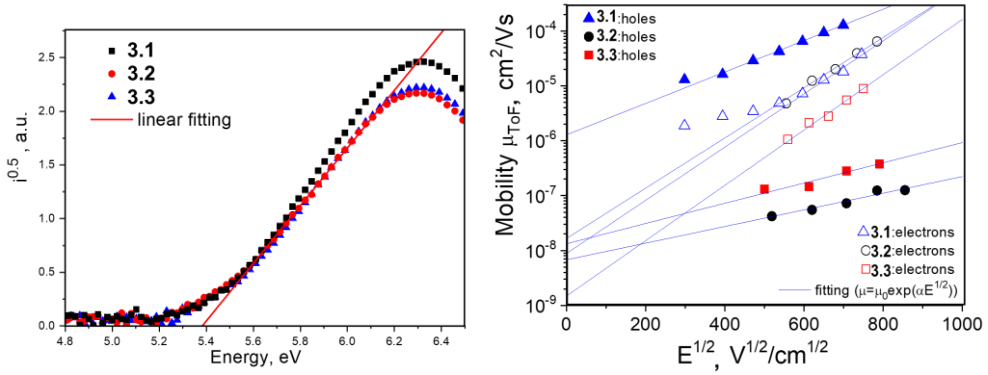

Fig. 4.19 Photoelectron emission spectra (a) and electric field dependencies of hole (filled symbols) and electron (empty symbols) drift mobilities (b) for the vacuum-deposited layers of derivatives **3.1–3.3**

The anticipated abilities to transport both holes and electrons were proved for the solid layers of donor-acceptor-donor compounds **3.1–3.3** by TOF measurements. Despite the highly dispersive charge transport, t_{tr} was estimated from the intersection points at which the tangents to the log-log plot crossed. Charge mobility-electric field dependences of the layers of **3.1–3.3** well fitted to the Poole–Frenkel relationship (Fig. 4.19b).[157] Such square-root field dependences are usually observed for organic semiconductors.[190,191] Close electron mobility values exceeding $3 \cdot 10^{-5}$ $cm^2V^{-1}s^{-1}$ at an electric field higher than $5 \cdot 10^5$ Vcm^{-1} were observed for compounds **3.1** and **3.2** with the same accepting unit diphenyl sulfone (Fig. 4.19b). Considerably lower electron mobilities were recorded for compound **3.3** with a rigid dibenzothiophene dioxide unit. Although compounds **3.1–3.3** were designed by using the same donating units (*tert*-butyl-substituted acridine moiety), very different hole mobilities were observed for their vacuum deposited layers. A hole mobility of $1.3 \cdot 10^{-4}$ $cm^2V^{-1}s^{-1}$ at an electric field of $5 \cdot 10^5$ Vcm^{-1} was observed for the layer of

compound **3.1**, while hole mobilities lower by several orders of magnitude (of $8.1 \cdot 10^{-8}$ and $2.6 \cdot 10^{-7}$ $cm^2V^{-1}s^{-1}$) were obtained for the layers of compounds **3.2** and **3.3**, respectively, at the same electric field. This result displays a strong effect of the substitution pattern and of the nature of the acceptor on the hole-transporting properties of the studied compounds. This effect is partly related to different molecular geometry and rigidity of compounds **3.1–3.3** which might result in different molecular packing in solid films. Relatively low hole mobilities of compounds **3.2** and **3.3** can be apparently explained by weak HOMO-HOMO overlapping of the neighboring molecules in solid films. High and relatively balanced hole and electron mobilities of the layers of compound **3.1** makes it the most promising candidate for OLED applications.

4.3.2. Photophysical properties

The photophysical properties of the solutions in the solvents of various polarity as well as of their neat and doped films were studied. The low-energy absorption maxima of the solutions of the compounds of their solid films are attributed to the $\pi \rightarrow \pi^*$ transition of the conjugated molecular backbone (Fig. 4.20a). The absorption band with the maximum at 286 nm of the solutions of compounds is apparently related to the absorption of acridine. An additional low-energy band at 314 nm was observed for the solutions of compound **3.3**. This band is mainly related to the absorption of dibenzothiophene dioxide. Absorption bands which could be attributed to CT states were practically not observed for dilute solutions of compounds **3.1–3.3**. However, absorption tails which can be explained by CT were recorded for the non-doped films of **3.1–3.3** (Fig. 4.20a). The solutions of diphenylsulfone-based *para*- and *meta*-substiduted compounds **3.1** and **3.2** in low-polarity toluene emitted, respectively, blue light with the intensity maximum at 487 nm and sky-blue light with the maximum at 503 nm.

Meanwhile, the dilute toluene solution of dibenzothiophene dioxide-based compound **3.3** was characterized by green emission with the maximum at 521 nm. The PL spectra of the solutions of compounds **3.1–3.3** in more polar THF were red-shifted with respect to those of toluene solutions. Such a behavior is common for donor-acceptor molecules which are characterized by the emission with intramolecular CT character.[116]

Table 4.7 Photophysical parameters of diphenylsulfone and dibenzothiophene *S*,*S*-dioxide derivatives

Compounds	λ^{abs}, nm	λ^{PL}, nm	Φ, %	τ_1, τ_2,[b] ns (χ^2)
	THF	Toluene/THF/film/doped film[a]		
3.1	282	487/522/475/475	16(20[c])/9/12/55	24, 1782 (1.118)
3.2	286	503/542/502/497	5(16[c])/3/3/46	63, 3964 (1.255)
3.3	285,315	521/577/542/521	7(15[c])/4/23/46	32, 4642 (1.096)

[a] mCP was used as the host; [b] PL life times of doped films; [c] Φs are given for deoxygenated toluene solutions in parentheses

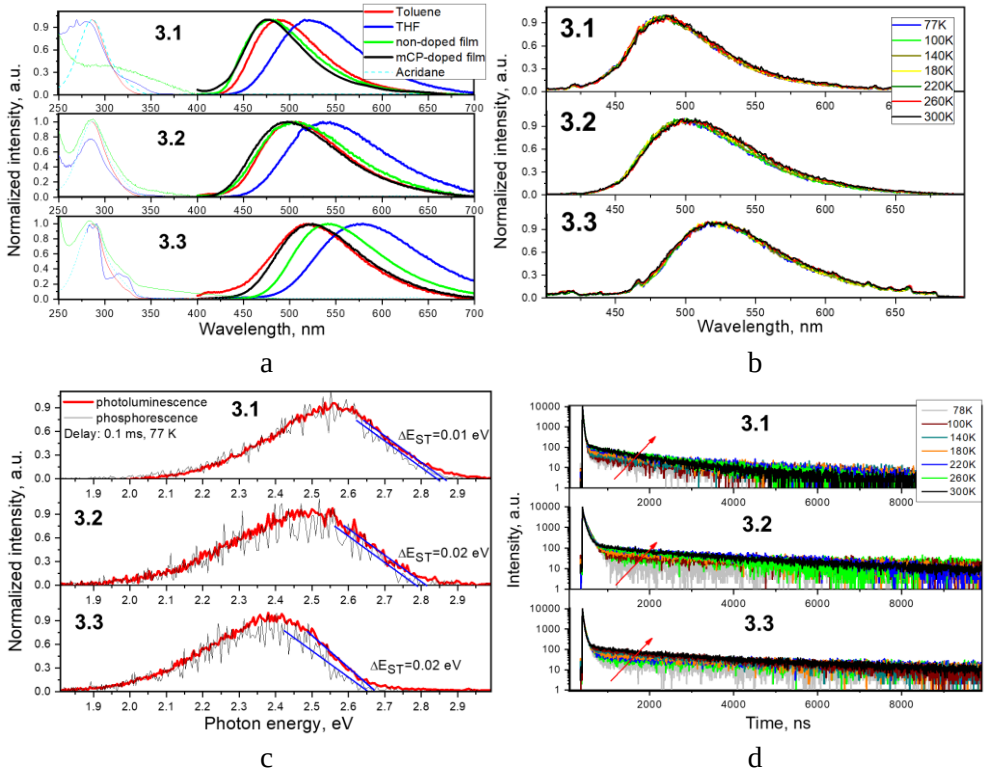

Fig. 4.20 Absorption and PL spectra of dilute toluene/THF solutions (10^{-5} M) and of non-doped and doped in mCP films for **3.1–3.3** (a); PL spectra of the doped films at various temperatures (b); PL and phosphorescence spectra of doped films (c); PL decay of doped films recorded at different temperatures

In addition to the red-shifts of the PL spectra of the THF solutions of **3.1–3.3**, the emission intensity of THF solutions is lower in comparison to those of the

corresponding toluene solutions due to higher polarity of THF. Higher Φ values ranging from 5% to 16% (Tbl. 4.7) were recorded for toluene solutions in comparison to those of the corresponding THF solutions. These Φ values of air-equilibrated toluene solutions were further increased after deoxygenation.

Relatively low Φ values were recorded for neat films of **3.1–3.3** exhibiting ACQ (Table 4.7). However, Φ values of 55, 46, and 46% were obtained for the doped films, i.e., for 10 wt% solid solutions of compounds **3.1–3.3** in mCP. Even these values do not completely display the contributions of triplet levels in the emission of solid samples since they were tested under air conditions. Because of the polarity effect, the blue-shifted PL spectrum of the film of **3.3** doped in mCP was recorded in comparison to that of the film of net **3.3**. Unexpectedly, very similar PL spectra were recorded for doped and non-doped films **3.1**:mCP and **3.2**:mCP.

In addition, the PL spectra of non-doped films of compounds **3.1** and **3.2** were blue-shifted in comparison to the PL spectra of the corresponding toluene solutions. A similar extraordinary behavior of the emission of TADF emitters in the solid-state was observed for the derivatives of adamantyl-substituted phenyltriazine and 10-spiro[acridine-9,9′-fluorene].[192] These adamantyl-substituted TADF molecules were designed by taking into account the following requirements: 1) a deep HOMO energy level for the donating moiety, 2) a shallow LUMO energy level for the accepting unit, 3) a shallower HOMO level of the donor than that of the acceptor and a deeper LUMO level of the acceptor than that of the donor for realizing CT, and 4) locally excited triplet levels (^{3}LE) of both donor and acceptor units higher than CT triplet levels. Being in good agreement with the mentioned requirements,[190] compounds **3.1** and **3.2** demonstrated a non-red-shifted emission for their neat films.

Similar PL spectra of the films of 1–3 doped in mCP were observed in the large range of temperatures from 77 to 300 K (Fig. 4.20b). Such a character of emission at different temperatures is possible when compounds are characterized by essentially identical fluorescence and phosphorescence spectra, which is usually observed at low temperatures (77 K). Indeed, similar fluorescence and phosphorescence spectra were observed by time-resolved PL measurements (Fig. 4.20c). The phosphorescence spectra were recorded by using a delay of more than 0.1 ms after excitation. The S_1 and T_1 energy levels (marked by straight lines) were taken from the onsets of the fluorescence and phosphorescence spectra.

In order to clearly provide evidence of TADF for compounds **3.1–3.3**, the fluorescence decay of the films of **3.1–3.3** doped in mCP was recorded at different temperatures (Fig. 4.20d). The fluorescence decay curves could be well fitted by double exponentials with short-lived (τ_1) and long-lived (τ_2) components (Table 4.7) which correspond to prompt and delayed fluorescence. The delayed fluorescence of compounds **3.1–3.3** is attributed to TADF because the intensity of the fluorescence of the samples rises with the temperature increase from 77 to 300 K (Fig. 4.20d, shown by arrows).

4.3.3. Device fabrication and characterization

In order to explore the effects of both rigidity of the accepting units and the *tert*-butyl modification of the donating units on the efficiencies of devices, various

compounds were tested as TADF emitters in OLEDs. The structures of TADF OLEDs 1–3 prepared by using compounds **3.1–3.3**, respectively, are shown in Fig. 4.21a. ITO, 50-nm TAPC, 10-nm mCP, 30-nm *o*-DiCbzBz doped with compounds **3.1–3.3**, 55-nm DPPS, 1-nm LiF and 100-nm Al were used for the preparation of the 1st HTL, 2nd HTL and exciton-blocking layer, EML, ETL, EIL and cathode, respectively.[193,194]

As it is visualized in Fig. 4.21b, the chosen functional layers provided good charge injection into EML.

Table 4.8 EL data of devices 1–3

EML	Driving voltage (V)[a]	CE_{max} (cd A^{-1})[b]	PE_{max} (lm W^{-1})[b]	EQE_{max} (%)[b]	Peak Wavelength (nm)[c]	CIE (x, y)[d]
3.1	6.28	61.1	64.0	24.1	495	(0.18,0.41)
3.2	7.17	58.4	52.4	19.4	518	(0.26,0.51)
3.3	7.77	54.5	55.7	15.9	525	(0.31,0.58)

[a]Operation voltage was recorded under current density is 10 mA cm^2. [b]Maximum current efficiency, maximum power efficiency and maximum quantum efficiency. [c]Peak wavelength at 3.5 V driving voltage. [d]CIE coordinates recorded at a luminance of 1000 cd·m^{-2}

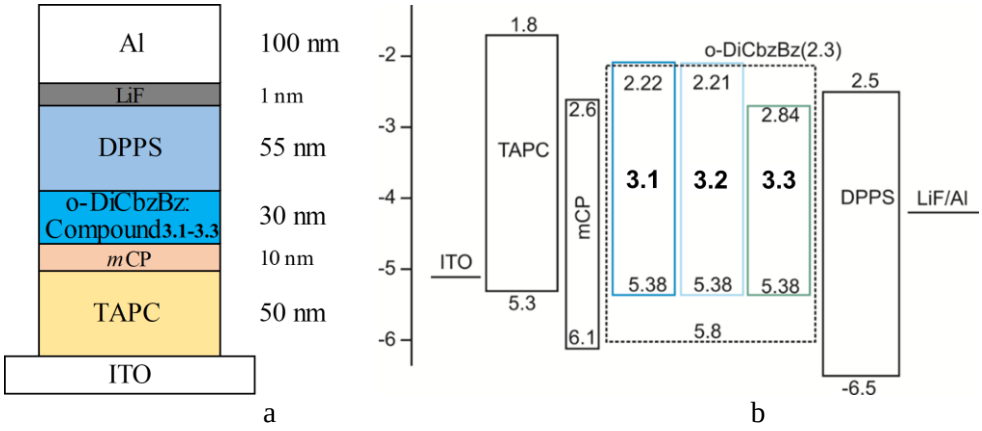

Fig. 4.21 (a) Configuration of TADF OLEDs 1–3, (b) equilibrium energy diagram

After optimizing the device structure by varying the doping ratio of the compounds and the layer thickness of ETL, the electroluminescent characteristics of three high-efficiency devices with compounds **3.1–3.3** were obtained as shown in Fig. 4.22. Except for the doping compound in the EML, the main configuration of these three devices is the same. The dopant concentration is of 24%, and the ETL layer's thickness equals to 55 nm. The high dopant concentration of 24% affects the carrier transport and determines the device performance. The device characteristics are summarized in Table 4.8. Fig. 4.22a shows their current density-voltage curves. The device with compound 1 exhibits a distinguished current density-voltage behavior because compound **3.1** possesses a higher charge carrier mobility than compounds **3.2** and **3.3** (Fig. 4.19b). In addition, this device also achieves stronger illuminance because of the better carrier balance in the EML. The device with

compound **3.2** exhibits a better performance than the device with compound **3.3**. This is because compound **3.3** exhibits a higher electron mobility and a smaller LUMO gap between the o-DiCbzBz host and itself to benefit the electron transportation and carrier recombination. The device with compound **3.1** also shows a distinguished efficiency performance with a CE_{max}, PE_{max}, and EQE_{max} of 61.1 $cd \cdot A^{-1}$, 64.0 $lm \cdot W^{-1}$, and 24.1%, respectively (Fig. 4.22b). The devices with compounds **3.2** and **3.3** show a somewhat inferior efficiency.

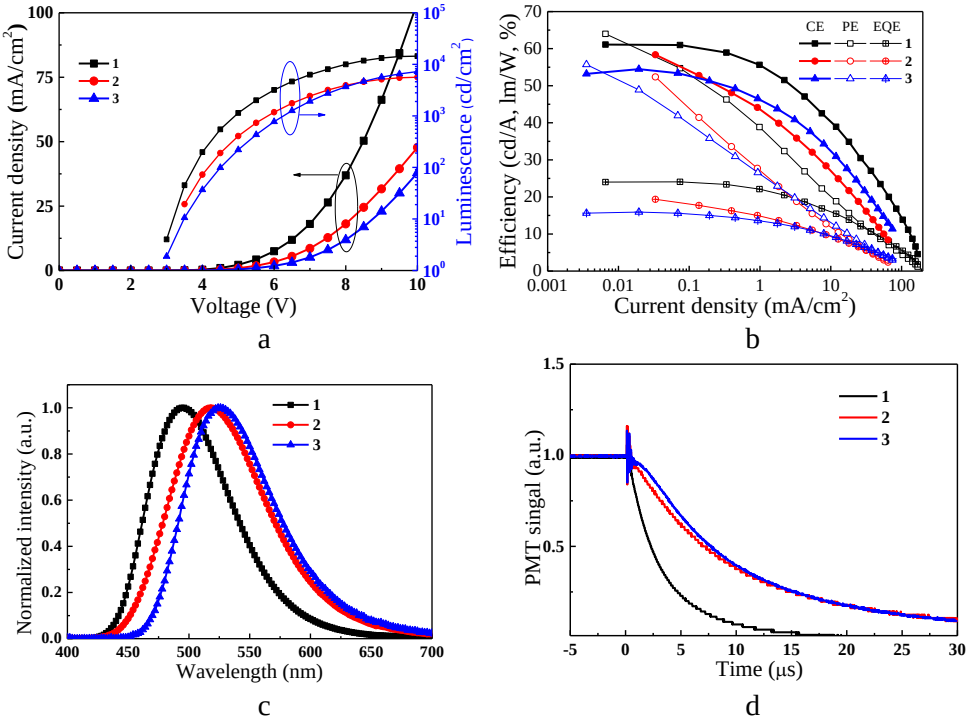

Fig. 4.22 (a) JLV curves, (b) CE, PE and EQE versus J curves, (c) emission spectra at 3.5 V, and (d) transient EL signals of devices 1–3 with compounds **3.1-3.3** as TADF emitters, respectively

Their emission spectra recorded at a driving voltage of 3.5 V are shown in Fig. 4.22c. Their peak wavelengths are located at 495, 518 and 525 nm with a full width at half maximum (FWHM) of 81, 93 and 86 nm, respectively, corresponding to the CIE coordinates of (0.18, 0.41), (0.26, 0.51), and (0.31, 0.58). The *tert*-Butyl substitution of donor moieties of an emitter led to the efficiency enhancement of the corresponding OLEDs. Device 1 outperformed any OLED with DMAC-DPS as an emitter known to date.[195]

The transient EL measurements were performed for these three devices as shown in Fig. 4.22d. The devices showed long emission lifetimes of more than 15 μs, which is delayed fluorescence caused RISC. The device with compound **3.1** shows a much shorter emission lifetime. It can be deduced that compound **3.1**

possesses an efficient RISC energy transfer from T_1 to S_1, which stems from the smaller ΔE_{ST} (Fig. 4.20c).

4.4. Derivatives of triphenyltriazine substituted by *tert*-butylcarbazolyl moieties as TADF emitters

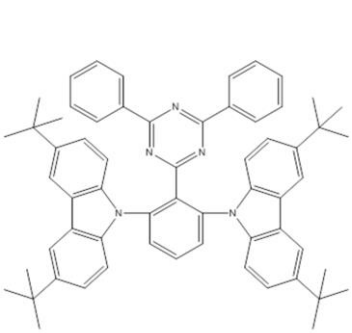

4.1

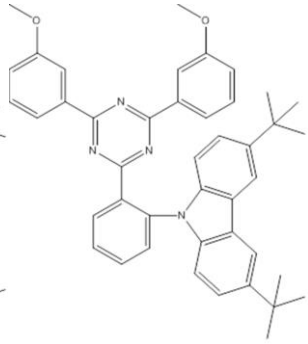

4.2

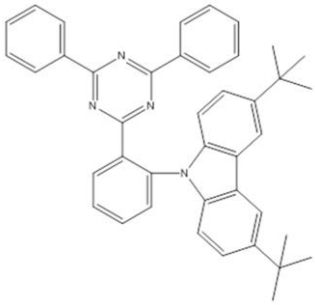

4.3

Fig. 4.23 Chemical structures of *tert*-butylcarbazolyl-substituted triphenyltriazines

Quantum chemical calculations of **4.1**, **4.2** and **4.3** derivatives were conducted *via* the density functional theory (DFT).

As shown in Fig. 4.24, the HOMOs are located on the *tret*-butyl-carbazole moiety and are extended to the neighboring phenyl rings in all the compounds, while the LUMOs are localized over the triphenyltriazine core and the neighboring phenyl rings with small overlaps between the acceptor and donor moieties. Such separated distributions of the frontier molecular orbitals endowed molecules with small ΔE_{ST} values from 0.05 to 0.07 eV thus showing that the reverse intersystem crossing process of $T_1 \rightarrow S_1$ is activated by the thermal energy of the surroundings.

The appropriate HOMO-LUMO distribution, the oscillator strength (*f*) and the singlet-triplet energies were calculated by using TD-DFT calculations with the optimized structures at the B3LYP/6-31G (d, p) level. Besides, the oscillator strength (*f*) of all the derivatives was determined to be 0.0130, 0.0122 and 0.0125 for **4.1**, **4.2** and **4.3**, respectively. In addition, the relatively small dihedral angle between the donor moieties and the adjacent phenyl rings allowed *tret*-butyl-

carbazole based derivatives to have more planar structures with dihedral angles of 62.5–69.2°.

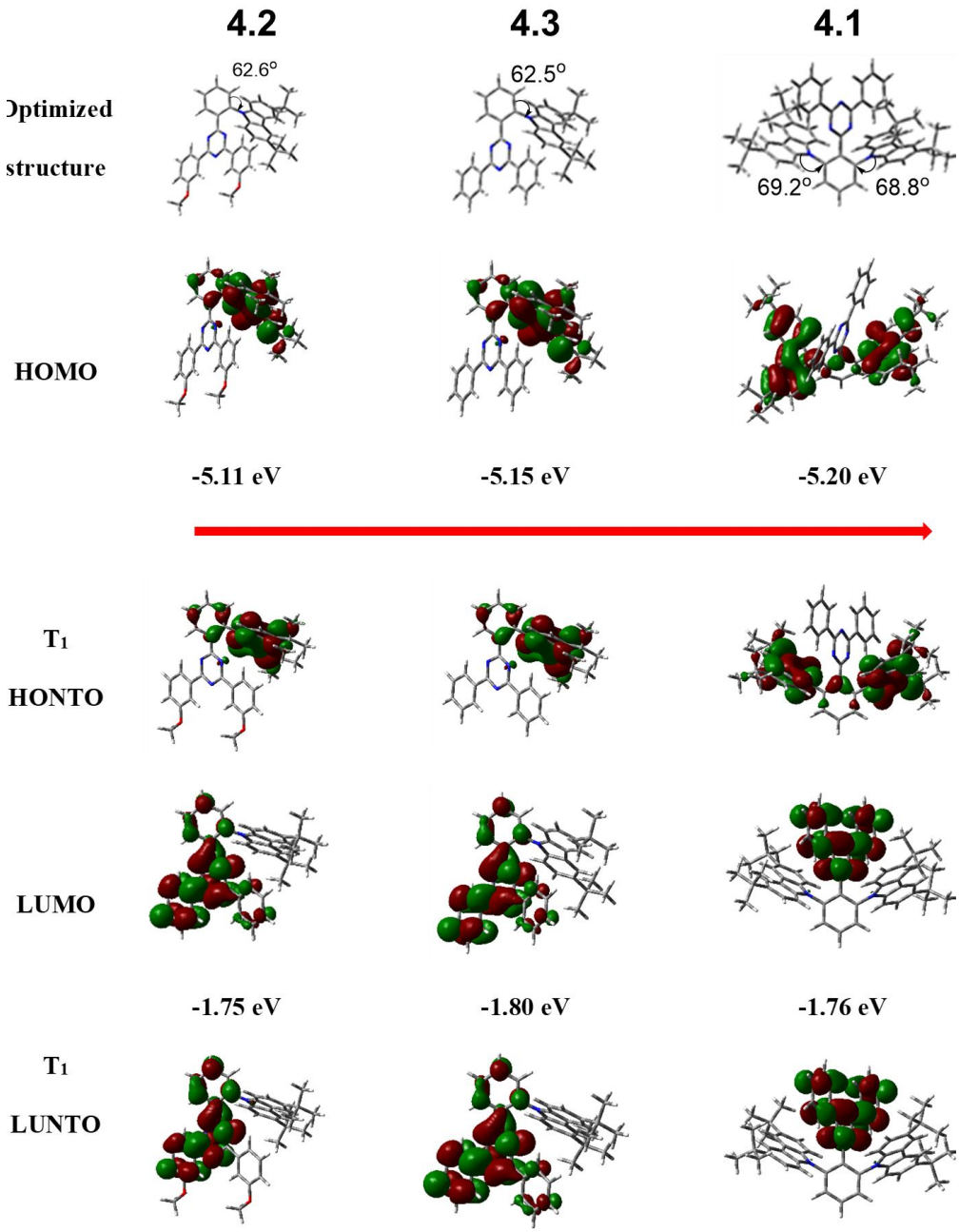

Fig. 4.24 Optimized geometries and molecular orbital plots (B3LYP/6-31G (d, p)) of **4.1–4.3** in gas phase

The HONTO and LUNTO triplet excited states of **4.1–4.3** were controlled and mainly located on the *tret*-butyl-carbazolyl moiety as well as the phenyl ring,

whereas the LUNTO was delocalized on the diphenyltriazine core. The partial separation of the HONTO and LUNTO triplet excited states between the electron accepting and donating moieties for **4.1**–**4.3** denotes a smaller ΔE_{ST}. The triplet energies were theoretically calculated based on the molecule ground state geometry with triplet energies of 2.85, 2.69, 2.69 eV for **4.1**, **4.2** and **4.3**, respectively.

4.4.1. Photophysical properties

The key photophysical data of the dilute toluene and THF solutions, thin neat films and films of 10 wt% solid solutions of the studied compounds in mCP is presented in Fig. 4.25 and Table 4.9. The absorption spectra of both the solid state and liquid samples indicate contributions of many electronic transitions. All the derivatives perform a low-energy absorption band at ~320 nm in dilute solutions and neat films. Low energy band (LEB) peaks totally correspond to the transitions from the ground state to various vibrational levels of the first excited singlet state of carbazole.[196] Similarly, the absorption bands near 295 nm originate from the transitions to the second excited singlet state. The absorbance of samples represents a clearly spectral behavior of the donor moiety. At the same time, the PL spectra of the dilute solutions of compounds revealed a single broad peak whose position depends on the solvent polarity. As it can be seen from Fig. 4.25, the substitution of toluene by polar THF leads to a bathochromic shift of the PL peak from ~490 to ~520 nm for all the compounds. Such a spectral character is evidence of CT state emission. The PL spectral band of films is hypsocromically shifted into the blue spectral diapason due to the enhanced intermolecular interactions in the solid state.

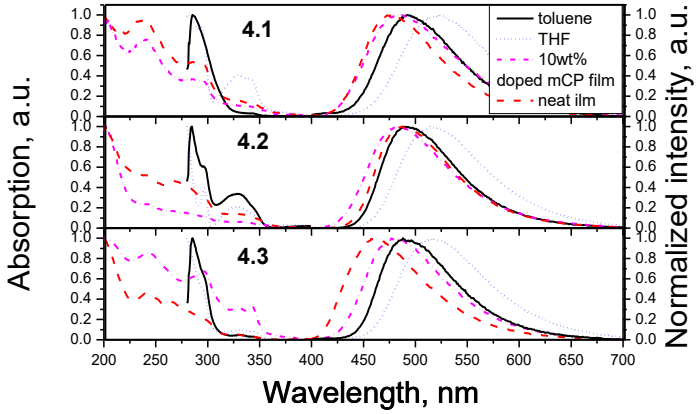

Fig. 4.25 Absorption and PL spectra of dilute toluene, THF solutions and of thin neat and doped in mCP (10 wt%) films of compounds

The presence of CT in these molecules is a reason to investigate derivatives in the guest:host systems in order to examine the TADF capabilities of the emitters. The absorption peaks of all mCP-based doped films at 329 and 342 nm relate to the typical absorption of the host.[197] The LEB of doped films is similar to those of solutions and neat films considering that mCP possesses two carbazole moieties.[198] The PL of doped films corresponds to the dopant emission. It postulates a great

electronic excitation energy transfer from mCP to the guest molecules. The effect caused by the polarity of host molecules is the most probable reason of the red shift of the peak of the emission spectra of the doped films in comparison to the corresponding neat films of **4.1** and **4.3**. Nevertheless, the electronegativity of oxygen atoms in **4.2** successfully opposes the impact of mCP as it is shown in the PL spectra of the films based on this emitter.

Optical band gaps E_g^{opt} were estimated from the onsets of the absorption spectra of neat films. The Φ of the neat film and solutions of **4.2** are the biggest of all the materials of the series. However, the **4.3**:mCP film performed a Φ of 0.64, which is bigger than any other Φ for the series. This is due to a better charge balance provided by a smaller difference of the energy levels of the frontier orbitals for **4.3** and mCP than for two other guest:host systems (Fig. 4.27).

The Φ values for deoxygenated dilute toluene solutions are nearly two times bigger than for the air equilibrated solutions. It points to the contribution of triplet excitons into emission in the absence of molecular interactions with oxygen.

In order to prove TADF appearance, the films of compounds doped in mCP were additionally investigated. It can be shown from the time resolved PL spectra of the samples (Fig. 4.26) that only the delayed fluorescence component of the PL intensity remains with delays bigger than a microsecond. The value of the decrease of emission intensity corresponds to the PF intensity. As a result, it can be concluded that the yield of DF of samples is bigger than the yield of the prompt fluorescence.

The indications of TADF in the guest:host systems were investigated by spectroscopic methods at various temperatures. The singlet-triplet energy splitting ΔE_{ST} is smaller than 0.1 eV for all the samples (Table 4.9), which correlates well with the previous analysis of the molecules. Such a division of the first excited states is great for the stimulation of the reverse intersystem crossing initiating TADF.

Table 4.9 Photophysical parameters of carbazolyl-substituted triphenyltriazines

Compound	E_g^{opt}, eV[1]	Φ_{PL} film[2]	Φ_{PL} mCP[3]	Φ_{PL} tol[4]	Φ_{PL} THF[5]	E_{S1}, eV[6]	E_{T1}, eV[6]	ΔE_{ST}, eV[6]	HOMO, eV[7]	LUMO, eV[8]
4.1	3.38	0.09	0.32	0.11/0.21	0.18	2.86	2.84	0.02	-5.95	-2.57
4.2	3.41	0.29	0.44	0.24/0.51	0.19	2.82	2.75	0.07	-5.98	-2.57
4.3	3.5	0.13	0.64	0.21/0.38	0.18	2.9	2.84	0.06	-6	-2.5

[1]Optical band gaps estimated from onset of absorption spectra of neat films. [2]Φ of neat films of compounds. [3]Φ of films of compounds doped in mCP (10 wt%). [4]Φ of dilute air equilibrated/deoxygenated toluene solutions of compounds. [5]Φ of dilute air equilibrated THF solutions of compounds. [6] Estimated from emission spectra of films of compounds doped in mCP (10 wt%) at 77K. [7]Taken from IP values. [8]Estimated by subtracting E_{gopt} from IP values

The PL decay curves of the doped films were detected as shown in Fig. 4.26b. The phosphorescent component of the decay curve vanishes with the increase of temperature. TADF occurs after heating and becomes more intensive with the lifetime values in the microsecond range as it can be estimated from the data. As it is shown in the normalized PL spectra of the films recorded at different temperatures (Fig. 4.26b), a decrease of the slight shoulder related to phosphorescence after

heating is observed at ~450 nm, which corresponds with the estimated values of E_{T1}. Besides that, the spectral character of emission is relatively the same as the temperature grows. It postulates the identical way of radiative deactivation of both triplet and singlet excitons in the samples. A slight bathochromic shift is caused by the intramolecular charge transfer undergoing vibrational relaxations under heating. All these results point to a strong TADF character of the emission.

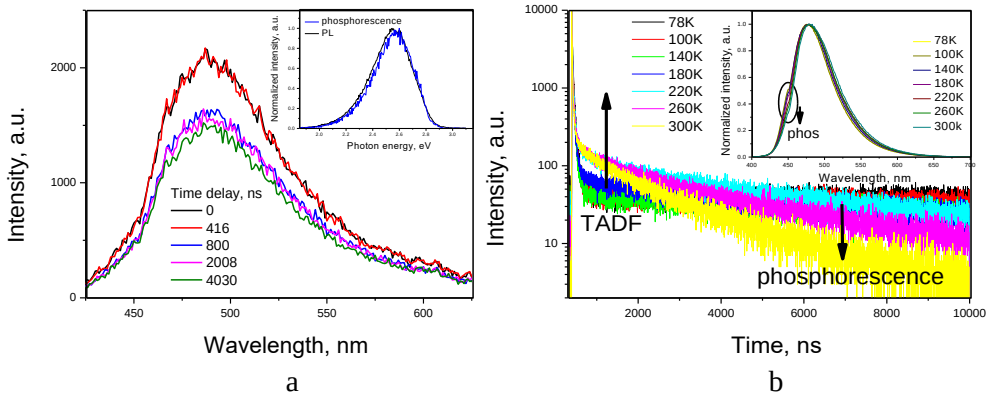

Fig. 4.26 The film of 10 wt% solid solutions of **4.1** in mCP. a) Time resolved PL spectra recorded at room temperature. Inset: Normalized PL and phosphorescence spectra (0.1 ms of delay) recorded at 78K. b) PL decay curves recorded at various temperatures. Inset: Normalized PL spectra recorded at various temperatures

4.4.2. Device fabrication and characterization

Guest:mCP systems were employed as the emitting layers (EML) of OLEDs to test the TADF capabilities of the emitters. The structures of A–C devices in the energetic domain as a representation of the HOMO/LUMO levels of the respective organic layers are showed in Fig. 4.27.

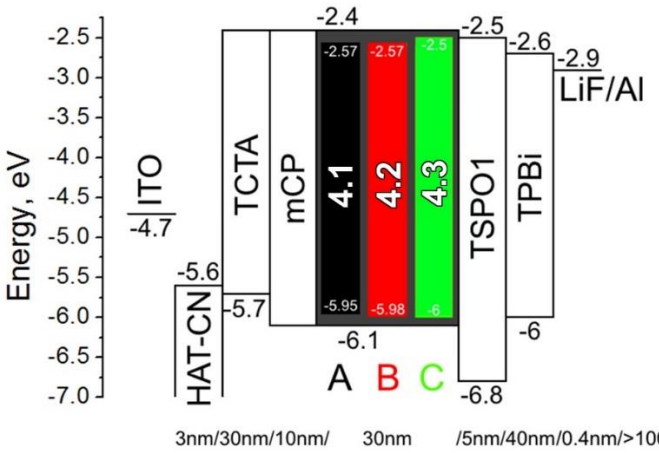

Fig. 4.27 Energy diagram of carbazolyl-substituted triphenyltriazine-based devices

The key characteristics of A–C are presented in Table 4.10 and Fig. 4.28. HAT-CN and LiF were used as the HIL and EIL, respectively. TCTA was chosen for HTL. mCP served not just as the host but also as the EBL. Layers of TSPO1 were used for hole blocking. TPBi was used as the electron transport material. The weight concentration of the materials in EML of A-C is 10 wt%.

Table 4.10 Parameters of carbazolyl-substituted triphenyltriazine-based OLEDs

Device	Compound [a]	λ, nm [b]	L_{max}, 10^3 cd/m^2 [c]	V_{on}, V [d]	η_c, cd/A [e]	η_p, lm/W [f]	EQE, % [g]	CIE [h]
A	**4.1**	474	17.3	3.5	14.9	9.9	7.7	(0.15, 0.23)
B	**4.2**	479	10.1	3.6	9.6	4.8	4.6	(0.15, 0.27)
C	**4.3**	481	13.9	4	11.1	4.5	5.1	(0.155, 0.2)

[a] Guest in EML. [b] EL peak wavelength. [c] Maximum luminance. [d] Turn-on voltage (voltage at 1 cd·m^{-2}). [e] Maximum current efficiency. [f] Maximum power efficiency. [g] Maximum external quantum efficiency. [h] Coordinates for CIE 1931 chromaticity diagram of EL spectra recorded at 7V

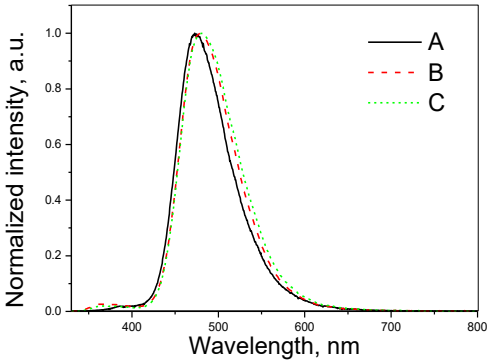

a

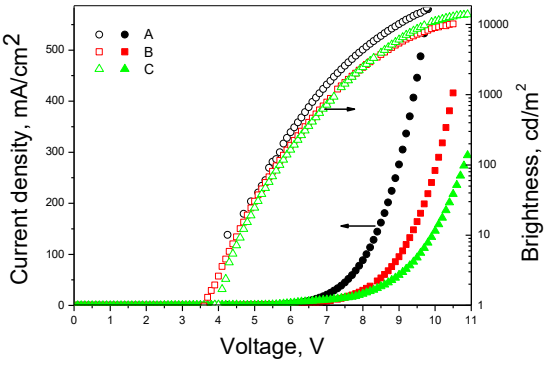

b

Fig. 4.28 A-C OLEDs: (a) Electroluminescence spectra recorded at 7V; (b) Luminance and current density curves

A single narrow peak for all the EL spectra (Fig. 4.28a) represents the dopant emission and correlates well to a great extent with the PL spectra of the respective doped films with the same weight concentration. The ultraviolet spectral shoulder attributes to the emission of mCP. Incomplete energy transfer from the host to the guest concluded from the EL spectra of A-C is the cause of the lower EQE values than the ones which could be obtained due to the use of triplet excitons. Nevertheless, the EQEs of OLEDs are big enough to be supporting evidence of the TADF nature of the emission. Low turn-on voltages of 3.6–4.1 V prove excellent charge transfer from electrodes to the recombination zones and the consequent appropriate selection of the organic layers as well as their thickness. The maximum EQE (Table 4.10) values of A-C range from 4.6 to 7.7%. Despite the lowest Φ values in various samples, **4.1** achieved the biggest efficiency values and a brightness of up to 17.3 thousand cd/m^2. The emitting guest:host layer in the OLED sandwich of vacuum-deposited organic layers under electrical power is a unique physical medium determining the TADF efficiency and the properties of the device. Apparently, the smallest E_g^{opt} and the corresponding HOMO-LUMO gap for **4.1** out of all the compounds plays a more significant role in the EL processes enhancing the emissive processes.

In order to vindicate the role of **4.1** in such high efficiency values of the devices, two additional series of OLEDs were made to compare the emitter with OMTR-tCz which exhibited the highest Φs of neat films and dilute solutions. D and E OLEDs have the following structures: ITO / HAT-CN (3 nm) / NPB (35 nm) / TCTA (10 nm) / mCP (5 nm) / EML / TSPO1 (5 nm) / TPBi (45 nm) / LiF (0.8 nm) / Al with **4.1** or **4.2** doped into mCP (20 wt%, 30 nm) as EML, respectively. For an additional series of devices, NPB was employed to enhance hole transport. *D* and *E* showed the same spectral behavior as *A* and *B*. However, the EQE dropped from 4.6% to 4.1% for **4.2** and significantly decreased from 7.1% to 3.8% for **4.1**. Such an impact of the introduction of NPB is implausible. So, the origin of this inefficiency is in the increase of the doping concentration to 20 wt%. *E* performed better than *D*, but their performances are close. *F* and *G* of the second additional series of OLEDs have the same structures as *A* and *B*, respectively, but with TCz1 as the host instead of mCP. The EL spectra of these devices have the same issue of modest host contribution into the emission. *F* with the values of brightness of up to 23.5 thousand cd/m^2 and an EQE maximum of 6.2% almost reached the results of *A*.

At the same time, the EQE maximum for **4.2**-based devices fell from 4.6% to 3.8% after the employment of TCz1 instead of mCP. In the series of devices based on TCz1 as the host, **4.1** performed better than **4.2**. TCz1 has a HOMO energy of -5.8 eV and -2.6 eV for LUMO. **4.1** has the highest HOMO and the lowest LUMO levels of all the compounds of the presented series of derivatives. Smaller energetic barriers in the guest:TCz1 systems make **4.1** the most suitable candidate for doping into the considered host matrix.

4.5. Methoxycarbazolyl-disubstituted dibenzofuranes as hole- and electron-transporting hosts for phosphorescent and TADF-based OLEDs

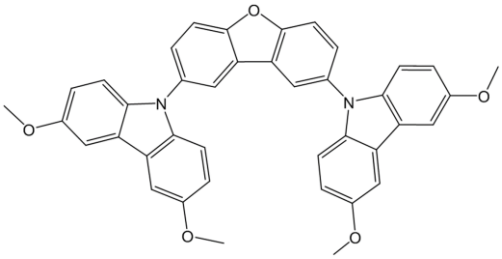

5.1

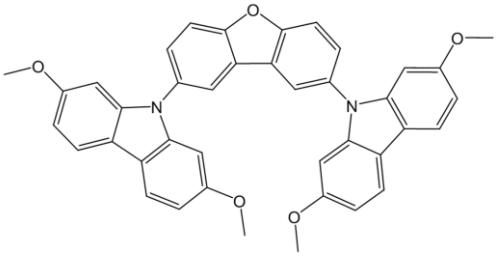

5.2

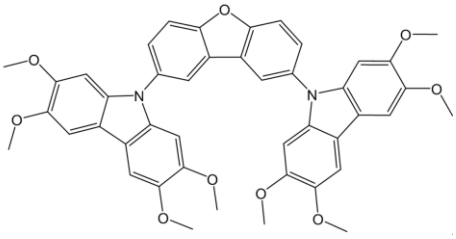

5.3

Fig. 4.29 Chemical structures of methoxycarbazolyl-substituted dibenzofurans[172]

4.5.1. Electrochemical and photoelectrical properties

The HOMO energy levels of **5.1, 5.2** and **5.3** derivatives were calculated to be equal to -5.22, -5.29, -5.06 eV, respectively. The DFT-calculated (B3LYP/6-31G (d, p)) HOMO energy levels are in good agreement with the experimentally estimated values (Table 4.11, Fig. 4.30). In comparison with dimethoxycarbazole-based derivatives (**5.1, 5.2**), tetramethoxycarbazole containing compound **5.3** showed a higher HOMO energy value by 0.20–0.30 eV thus proving a HOMO energy increase due to the methoxy group.[199] The IP^{PE} values of solid films **5.1–5.3** were measured by the photoelectron emission technique in air (Fig. 4.30). The IP^{PE} values of the layers of the synthesized compounds ranged from 5.35 to 5.53 eV.

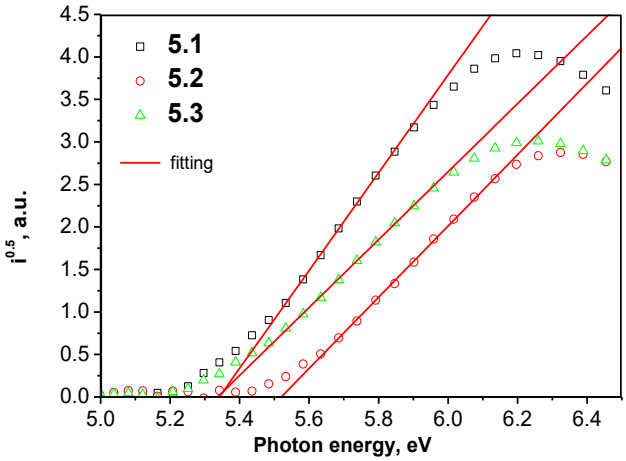

Fig. 4.30 Photoelectron emission spectra of layers of **5.1–5.3**

The effect of the substitution pattern of carbazole moieties of the studied compounds on their semiconducting properties was investigated by conducting TOF measurements. The values of charge drift mobilities for the tested films of compounds were calculated by taking t_{tr} at the cross point of the tangent lines at various slopes of the transient curves in the log-log scales as it is shown in Fig. 4.31b. Such cross points were related to the transit times since their shifts to smaller times were clearly observed with the increase of the applied voltages. The films of **5.1** were characterized by a relatively low dispersive hole transport. Much more dispersive hole transport was detected for the films of **5.2** and **5.3**.

Table 4.11 Ionization energies of methoxycarbazolyl-substituted dibenzofurans

Compound	E_{onset}, V	$E_{ox,pa}$ V[a]	$E_{ox,pc}$ V[a]	$E_{1/2}$, V	$HOMO_{ox}$ /$HOMO_{DFT}$ [d], eV	$LUMO_{DFT}$, eV[d]	IP^{PE}, eV[c]
5.1	0.44	0.55	0.45	0.50	-5.22/-4.91	-1.34	5.35
5.2	0.49	0.64	0.38	0.51	-5.29/-4.97	-1.33	5.52
5.3	0.33	0.41	0.34	0.37	-5.06/-4.80	-1.27	5.35

In addition, a strongly dispersive electron transport was observed for the tested films. Relatively high errors of the determined values of the transit times led to errors in the calculated electron mobilities (Fig. 4.31b).

Apparently, because of the strongly dispersive electron transport, it was not possible to find the transit times for films **5.1**, and its electron mobilities were not estimated. Nevertheless, the values of hole mobility of compound **5.1** exceeded 10^{-4} $cm^2V^{-1}s^{-1}$ at high electric fields (>$3.6 \cdot 10^5$ Vcm^{-1}). The values of the hole mobility of compounds **5.2** and **5.3** were several times lower at the same electric fields. Apparently, these differences are related to the differently substituted

methoxycarbazole units of the compounds, different intermolecular interactions and/or molecular packing.

Electron mobilities of **5.2** and **5.3** were found in the similar range to each other because of the same accepting moiety used in their molecular structures. Taking into account the bipolar charge-transport, the studied compounds could be of interest as the host materials for further testing in OLEDs where hole and electron transport is needed.

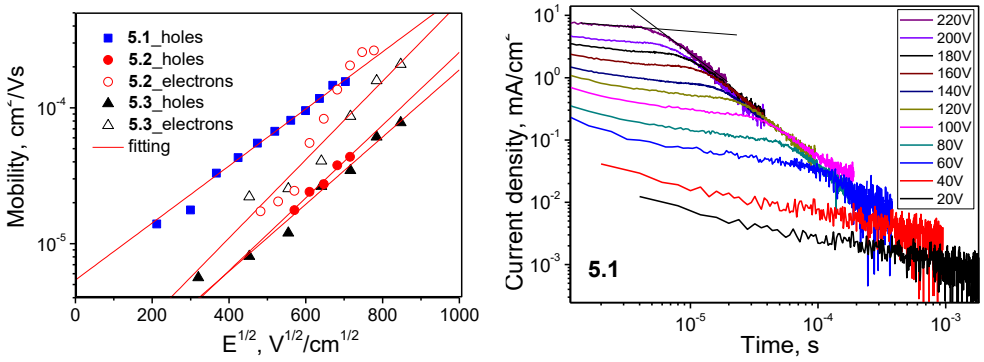

a b

Fig. 4.31 Hole and electron mobilities versus electric field (a) and time-of-flight signals for holes for film of **5.1** at different voltages (b)

4.5.2. Photophysical properties

To study the effect of various substitutions on the photophysical properties of the designed compounds, the absorption and PL spectra were recorded of their toluene and THF solutions as well as of the films (Fig. 4.32a). The key photophysical characteristics are listed in Table 4.12. A well-structured LEB was observed for the solutions of **5.1**. The LEBs of the solutions of **5.2** and **5.3** were less-structured but still observable.

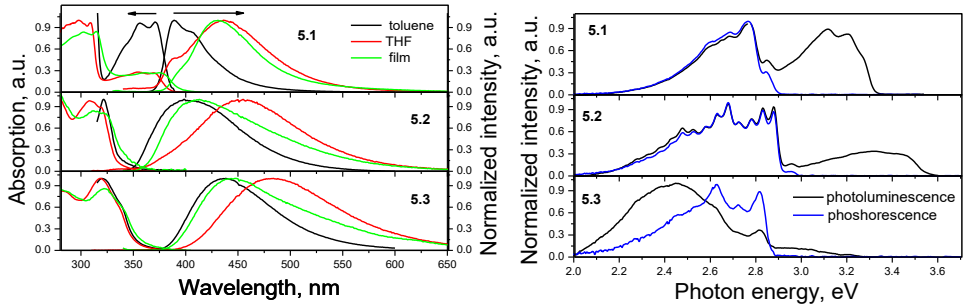

a b

Fig. 4.32 (a) Absorption and PL spectra of dilute THF, toluene solutions and neat films of **5.1–5.3**. (b) PL and phosphorescence spectra of dilute THF solutions recorded at 77 K

Despite the donor-acceptor-donor structure of the compounds, their LEBs are very similar to the LEBs of the corresponding methoxy-substituted carbazoles. They mostly relate to the local carbazole transitions as it was previously observed.[148] The presence of an electron-accepting (Fig. 4.33) dibenzofuran unit in the molecular structures of derivatives may result in the formation of low-energy absorption bands of the CT character. However, they are practically not detectable in the absorption spectra of the solutions due to the insignificant interfragment π-conjugation (Fig. 4.32a).

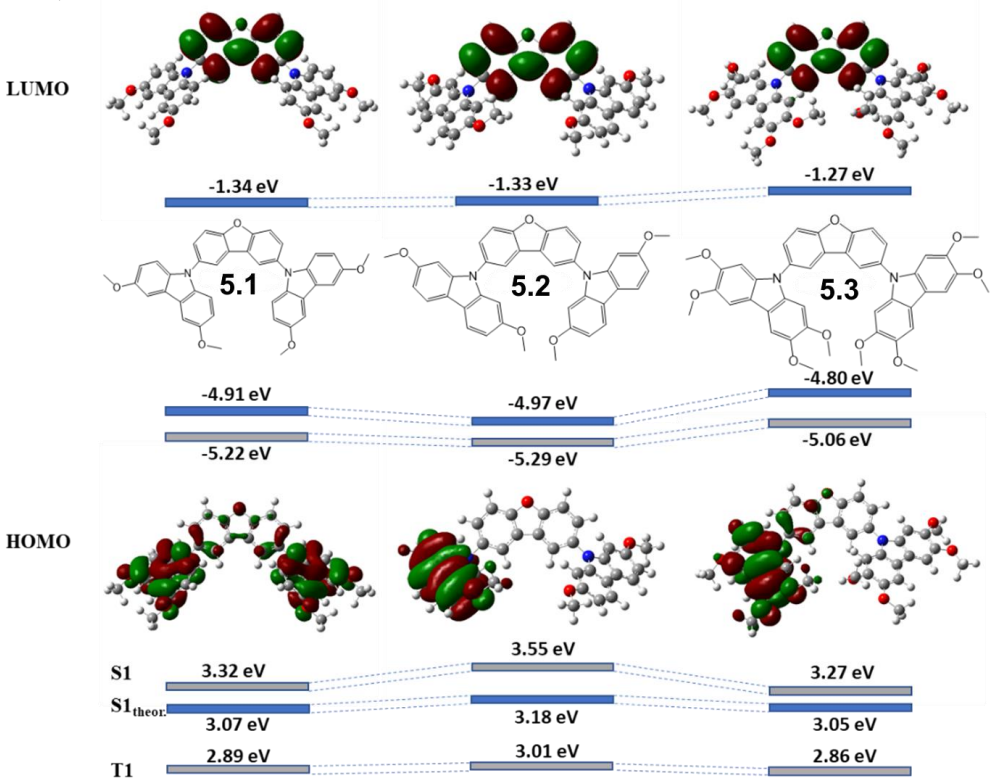

Fig. 4.33 Experimental (grey) and theoretical (blue) HOMO/LUMO levels and orbitals, S_1 and T_1 energies of **5.1–5.3**

The red shifts of the absorption spectra of the films of the studied compounds are apparently related to the formation of CT states between methoxycarbazoles and dibenzofurane units since interfragment interaction may be induced in solid films. The values of the optical band gap were estimated from the onset wavelengths of LEB of neat films and presented in Table 4.12.

The solution of **5.1** in toluene demonstrated a double-peaked emission spectrum in contrast to those of the other studied derivatives (Fig. 4.32a). The HOMO and LUMO distribution of **5.1** shows that the dibenzofuran and donor moieties are not completely separated electronically (Fig. 4.33). The PL band of the toluene solution of **5.1** can be mainly attributed to the radiative deactivation of the LE state of methoxycarbazole chromophores because of its similarity to those of

methoxycarbazoles.[148] In addition, the solution of **5.1** in toluene exhibited emission of the intramolecular CT nature. Intramolecular CT is manifested by the positive solvatochromic effect of dilute solutions. The emission peaks of the THF solution of the compound is bathochromically shifted in comparison to that of the solution in less polar toluene by *ca.* 50 nm, while the change in the position of the corresponding absorption peaks is negligible. Such an emission behavior of **5.1** may be related to the relatively weak donating ability of methoxycarbazole units attached at C-3 and C-6 positions of the carbazole moiety, which determines the weak CT emission of the solutions of **5.1** with the solvents of low polarity. In contract, the emission of toluene solutions of **5.2** and **5.3** is characterized by broader spectra with a single maximum (Fig. 4.32a). The CT character of **5.2** and **5.3** emission is evident by the red shifts of emissions of the solutions in THF in comparison to those of the solutions in toluene. Thus, the emission of the solutions of **5.2** and **5.3** is related to the transition from the LUMO of the dibenzofuran moiety to the HOMO of di(tetra)methoxycarbazole.

Table 4.12 Photophysical parameters of methoxycarbazolyl-substituted dibenzofurans

Compound	λ_{PL}, nm [a]	E_g, eV	Φ_{THF} [b]	Φ_{film}	E_{T1} [c]/ E_{T1} (theor) [d] eV	E_{S1} [c]/ E_{S1} (theor) [d] eV	ΔE_{ST} [c] / ΔE_{ST} (theor.), eV [d]
5.1	393, 431/389, 404/389, 437	3.13	0.17	0.10	2.89 / 2.89	3.32 / 3.07	0.43 / 0.16
5.2	410/398/452	3.58	0.06	0.06	3.01 / 2.96	3.55 / 3.18	0.54 / 0.19
5.3	444/436/483	3.47	0.11	0.11	2.86 / 2.86	3.27 / 3.05	0.41 / 0.17

[a] Wavelength of emission peak of neat thin film/dilute toluene solution/dilute THF solution. [b] Φ value of deoxygenated dilute THF solution. [c] Estimated from emission spectra of dilute THF solutions recorded at 77K. [d] Calculated values by DFT B3LYP/6-31(d, p) method

This explanation is supported by the spatial separation of HOMO and LUMO of **5.2** and **5.3**. The most efficient charge transport is expected for the layers of **5.2** due to the larger HOMO/LUMO distribution compared to that of **5.1** and **5.3**. Such consideration is in agreement with the largest Stokes shift observed for THF solution of **5.2** (Fig. 4.32a).

The different character of the radiative processes of derivatives can be explained by different donating abilities of di(tetra)methoxycarbazoles resulting in different distributions of the frontier molecular orbitals between these di(tetra)methoxycarbazole and dibenzofuran moieties (Fig. 4.32).

The fluorescence of the neat thin film of **5.1** is very similar to the intramolecular CT emission of the dilute THF solution of the compound (Fig. 4.32a). In addition, a high-energy shoulder is observed in the PL spectrum of the film of **5.1**. This shoulder is similar to the emission of the toluene solution of the compound which peaked at 398 nm. The solid-state emission of **5.1** similarly to the PL of the solutions stems from the recombination of the hybridized local and charge transfer (HLCT) state (mixed localized electronic (π–π*) and charge-transfer states).[200] In contrast, the fluorescence resulting from the deactivation of only CT states was detected for the films of **5.2** and **5.3** (Fig. 4.32a). In the cases of either

HLCT or CT states, the triplet excitons of compounds may exhibit radiative decay processes as it was previously reported.[201] The increase of the fluorescence intensity of both solid samples and dilute solutions was observed after deoxygenation. The maxima of the PL spectra of the films of **5.2** and **5.3** are observed close to the PL maxima of the corresponding toluene solutions indicating a low polarity of **5.2** and **5.3**.[202]

The Φ values of the deoxygenated THF solutions and neat thin films of compounds are found to be identical for **5.2** and **5.3** (Table 4.12). In the case of **5.1**, Φs of 0.17 and 0.10 for the THF solution and the solid sample, respectively, are obtained. The low Φ values of the solutions can apparently be explained by malleable flexible linkages between the donor and acceptor units. As a result, the free vibrations of methoxycarbazoles in solutions lead to emission quenching. Although these free vibrations are blocked in solid films, methoxy groups induce intermolecular interactions (e.g., h-bonding[203]) leading to ACQ.

The host materials of OLEDs have to be characterized by higher triplet levels than the energy levels of radiative states of the used emitter. In order to examine the triplet levels of derivatives, their phosphorescence and PL spectra of dilute THF solutions at 77 K were recorded (Fig. 4.32b). The shapes of the phosphorescent spectra as well as the values of the first triplet excited energy level of the compounds are in good agreement with those of the previously published compounds based only on methoxycarbazoles.[201] Thus, the phosphorescence of THF solutions was completely related to the recombination of triplet LE states of methoxycarbazoles. The influence of dibenzofuran in the role of the acceptor for these compounds on the phosphorescence spectra was not detectible.

The values of the first excited singlet and triplet state energy levels, E_{S1} and E_{T1}, were estimated from the onset of the photon energies of the PL and phosphorescence bands, respectively (Table 4.12). The theoretically predicted E_{S1} and E_{T1} values of the compounds are in good agreement with the experimental ones (Table 4.12, Fig. 4.32b). Due to the high triplet levels of 2.86–2.96 eV, the investigated compounds can be recognized as promising host materials for OLEDs.

To demonstrate the energy transfer from hosts **5.1–5.3** to the emitters, the host-guest layers were fabricated by using green TADF emitters DAcIPN[127] and DACT-II[112] as the guest at 10 wt% doping concentration. The PL spectra of these host-guest layers demonstrated single bands related to the emission of the guest, and no bands/shoulders of the hosts were recorded. The fluorescence spectra of the guest:host films are almost identical with the wavelength of the emission peaks of *ca*. 555 nm for the films containing DAcIPN, and 545 nm for the films with DACT-II. It indicates efficient host-guest interaction. The PL decay curves of the doped films recorded at room temperature contained components in the μs range which are attributed to TADF as it was proved elsewhere.[200,202] This data shows that the synthesized compounds can operate as hosts transferring the electronic excitation energy to guest emitters without suppressing TADF.

4.5.3. Device fabrication and characterization

In order to investigate the effect of the methoxy substituents of the carbazole moiety on the host efficiencies in TADF and phosphorescent OLEDs, a comparable study was performed by using two TADF emitters (DAcIPN and DACT-II) and two phosphorescent emitters $Ir(ppy)_3$ $Ir(piq)_2(acac)$. The HOMO/LUMO values of these emitters did not match well with the HOMO/LUMO values of the studied hosts (Fig. 4.34). As a result, the electroluminescent performances of the fabricated devices were lower than those of the reported OLEDs containing the same emitters.[45,204,205]

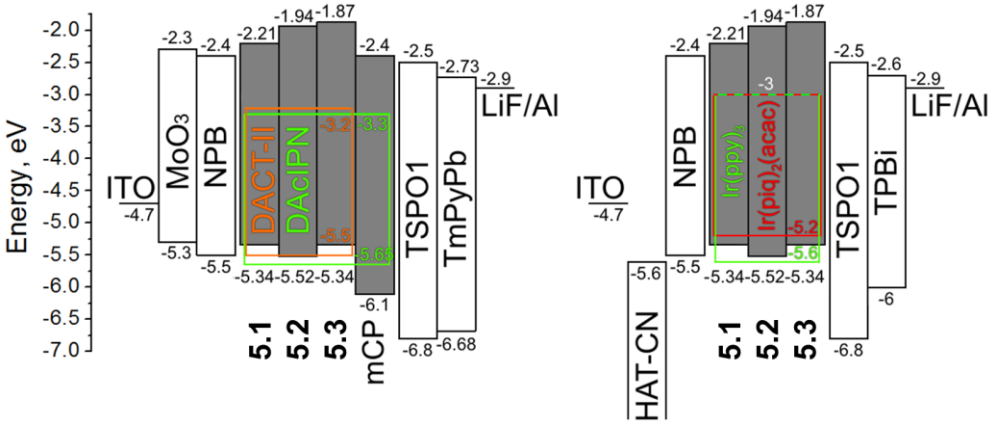

Fig. 4.34 Equilibrium energy diagram of OLEDs

Nevertheless, the comparable study provided evidence that compound **5.1** demonstrated better host efficiencies for TADF OLEDs relative to compounds **5.2** and **5.3**. In order to estimate the hosting properties of **5.1, 5.2** and **5.3**, two series of OLEDs based on DAcIPN and DACT-II as the TADF emissive species were fabricated. Additionally, the studied compounds were tested as hosts in two series of PhOLEDs using green and red emitters $Ir(ppy)_3$ and $Ir(piq)_2(acac)$. The guest:host systems were fabricated by vacuum deposition keeping 10 wt% concentration for TADF emitters and 5 wt% for the phosphorescent species. The structures of the fabricated OLEDs as well as their major electroluminescent characteristics are listed in Table 4.13. The functional layers of the fabricated devices were selected for providing good charge injection, charge transport and recombination within the light-emitting layers due to the appropriate energy levels of the materials as it is visualized in the equilibrium energy diagram (Fig. 4.34). The layer of MoO_3 or HAT-CN was used as HIL. The layer of NPB was employed as HTL. TSPO1 was used as the hole blocking material. The layers of TmPyPb and TPBi were employed as ETL. The layer of LiF was used as EIL. The anode and the cathode were made of ITO and aluminum, respectively.

The EL spectra of all the devices contain a single peak attributed to the emission of the dopant. The CIE coordinates and wavelengths of the spectral peaks correlate to a great extent with the performances of OLEDs based on other hosts reported earlier.[200,202] Good electronic excitation energy transfer from the host to the

guest is also evident from the absence of any collateral peaks in the EL spectra of OLEDs. By virtue of having small differences in their molecular structures, hosts **5.1, 5.2** and **5.3** based on the carbazolyl moiety with just a different number and substitution pattern of the methoxy groups induced essential differences in the electroluminescence characteristics of the fabricated devices.

Table 4.13 Structures and characteristics of devices A–L

Device	Host	L_{max}, 10^3 cd/m^2 [a]	η_c, cd/A [b]	η_p, lm/W [c]	EQE, % [d]	λ, nm [e]	CIE [f]
ITO / MoO_3 (1 nm) / NPB (45 nm) / DAcIPN:host (10 wt%, 30 nm) / TSPO1 (5 nm) / TmPyPb (40 nm) / LiF (0.5 nm) / Al							
A	**5.1**	38.7	28.9	9.2	8.1	533	(0.32, 0.61)
B	**5.2**	23.5	16.8	6.3	5	521	(0.27, 0.56)
C	**5.3**	12.3	11	4	3.1	538	(0.33, 0.60)
ITO / MoO_3 (1 nm) / NPB (45 nm) / DACT-II:host (10 wt%, 30 nm) / TSPO1 (5 nm) / TmPyPb(40 nm) / LiF(0.5 nm) / Al							
E	**5.1**	44.5	41.6	15.1	12.2	532	(0.31, 0.58)
F	**5.2**	35.9	21.4	7.6	6.7	521	(0.27, 0.54)
G	**5.3**	24.4	14.8	5.6	4.3	534	(0.32, 0.58)
ITO / HAT-CN (4 nm) / NPB (45 nm) / $Ir(ppy)_3$:host (5 wt%, 15 nm) / TSPO1 (5 nm) / TPBi (45 nm) / LiF (0.5 nm) / Al							
H	**5.2**	53.1	44.1	36.8	12.6	509	-
I	**5.3**	9	14	11.1	4.3	508	-
ITO / HAT-CN (4 nm) / NPB (45 nm) / $Ir(piq)_2(acac)$:host (5 wt%, 15 nm) / TSPO1 (5 nm) / TPBi (45 nm) / LiF (0.5 nm) / Al							
J	**5.1**	15.7	7.6	4.8	7.3	623	-
K	**5.2**	14.1	8.4	5.1	8.5	623	-
L	**5.3**	8.3	3.9	3.2	4.9	629	-

[a] Maximum brightness. [b] Maximum current efficiency. [c] Maximum power efficiency. [d] Maximum external quantum efficiency. [e] Wavelength of the EL spectrum peak at 6V. [f] CIE 1931 UCS coordinates at 10V

By using the TADF emitter DAcIPN in devices *A*, *B*, and *C*, the values of the maximum EQE of 8.1>5>3.1% were obtained for these devices displaying the order of host efficiency **5.1**>**5.2**>**5.3** (Table 4.13, Fig. 4.35b). The same trend of the host efficiency was obtained in the case of DACT-II-based devices *E*, *F*, and *G* according to their maximum EQEs. The difference in the efficiency of the devices is apparently related to the difference in their properties (the HOLO/LUMO values, the triplet values, the structure/morphology of the layers, etc.) of the used hosts. The obtained data put **5.2** in the middle between **5.1** and **5.3** with respect to the

efficiency of TADF OLEDs (Table 4.13). Based on the fact that in both series A-C and E-G, the same order of efficiency of the host materials remains, it can be suggested that the origin of the efficiency drop of the devices based on the TADF emitter: **5.2** layers is not in the specific guest-host interactions. The most credible explanation of the suppressing of TADF efficiency is the energy mismatch of the molecular orbitals on the interfaces of the layers where radiative recombination takes place. The LUMO level of **5.2** makes the energetic barrier of 0.56 eV for electrons to transfer from the TSPO1 layer to a recombination zone while there is no such a barrier for **5.1** and mCP (Fig. 4.35). It can be predicted that the improvement of the OLED structure including a selection of the appropriate hole blocking and/or electron transport layers may optimize the energy transfer and lead to a considerable enhancement of the efficiency of the devices based on **5.1**. One more possible reason of the best host performance of **5.1** could be its non-dispersive hole transport with a relatively high mobility level in contrast to the other studied hosts (Fig. 4.31). TADF device *A* and phosphorescent device *E* based on **5.1** as the host showed the best maximum EQE values of 8.1% and 12.2%, respectively (Fig. 4.35b).

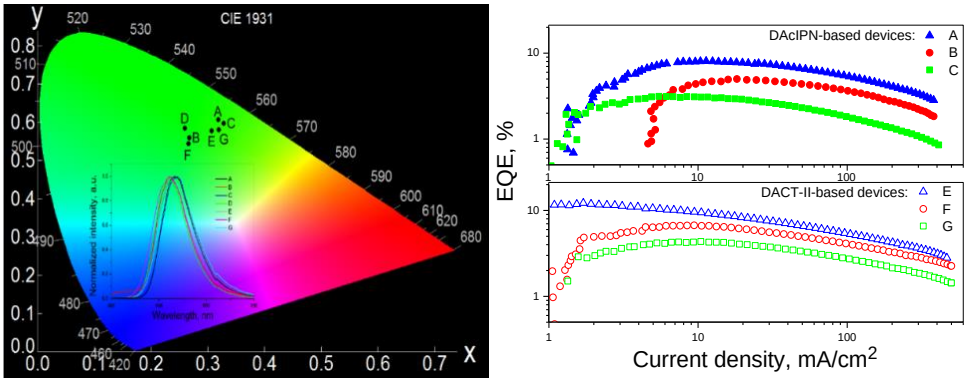

Fig. 4.35 (a) CIE 1931 UCS diagram for EL spectra recorded at 8V and EQE characteristics (b). Inset: EL spectra of TADF OLEDs recorded at 10 V

Meanwhile, **5.3** exhibited the worst performance in TADF devices *C* and *G* based on DAcIPN and DACT-II, showing 4 and 5.6 lm/W of the maximum power efficiency, 11 and 14.8 cd/A of the maximum current efficiency, respectively. Thus, it is expected that the carbazolyl moiety substituted by methoxy groups at C-3 and C-6 positions has the highest potential for the further development of bipolar host materials.

Since the first triplet excited state energy values of the studied hosts (Table 4.12) are much higher than the first triplet excited state energy levels of dopants $Ir(ppy)_3$ (2.4 eV[206]) and $Ir(piq)_2(acac)$ (1.97 eV[207]), the efficient triplet energy transfer from the host to the guest was expected. Consequently, the EL spectra of PhOLEDs are typical for an emission attributed to emitters. However, there are slight spectral bands related to the host emission of devices *H* and *I* (Fig. 4.36).

Nevertheless, the low turn-on voltages of ~3V for these PhOLEDs are manifestation of an excellent charge transport from the electrodes to the light-emitting layers.

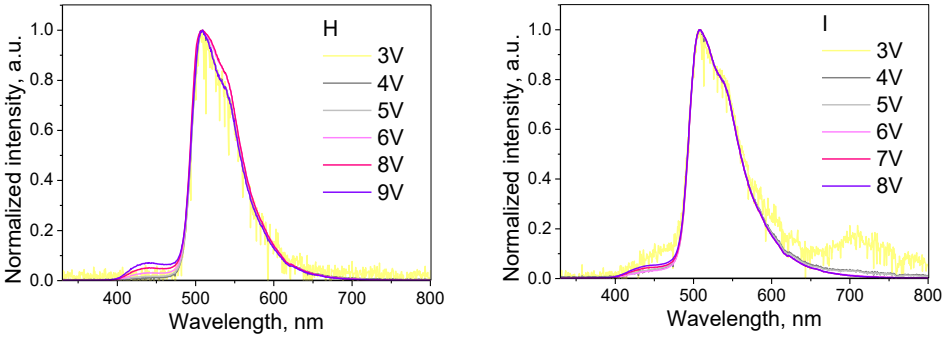

a b

Fig. 4.36 EL spectra of PhOLEDs H (a) and I (b)

Despite the similarity of the energy levels of TADF OLEDs and PhOLEDs (Fig. 4.34), the high triplet energy of **5.2** helps to employ triplet excitons more successfully in the system phosphorescent emitter: **5.2** rather than in the system TADF emitter: **5.2**. The explanation of this observation may be in the better energetic match of the frontier orbitals of **5.2** and phosphorescent emitters with a subsequent efficient energy transfer. As a result, the highest values of EQE of the fabricated PhOLEDs were observed for **5.2**-based devices (12.6% for device *H* and 8.5% for device *K*). With the EQE values of phosphorescent devices lower than 5%, **5.3** showed worse performance.

4.6. Diphenylsulfone-based donor-acceptor-donor hosts for TADF OLEDs

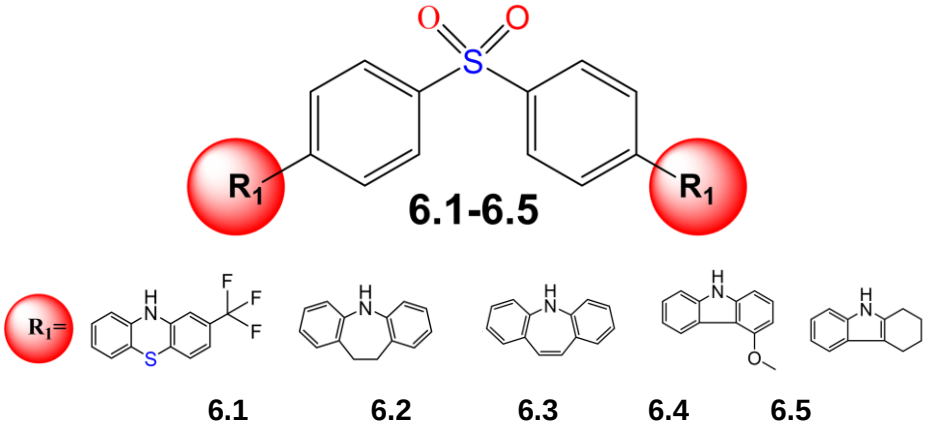

Fig. 4.37 Chemical structures of 4,4'-disubstituted diphenylsufones[173]

4.6.1. Electrochemical and photoelectrical properties

The values of IP_{CV} are given in Table 4.14. They ranged from 5.03 to 5.74 eV. Derivative **6.5** featuring a tetrahydrocarbazole moiety showed the lowest value of IP_{CV}. EA_{CV} determined from the optical band gaps (E_{onset}^{ox}) and the ionization energy values were found to range from 1.67 to 2.48 eV.

Table 4.14 Results derived from electrochemical measurements of compounds **6.1–6.5**

Compound	E_{onset}^{ox} vs Fc, V	IP^{CV}[a], HOMO, eV	EA^{CV}[b], LUMO, [eV]	E_g^{opt}, eV	I_p^{PE}, eV	E_a eV
6.1	0.54	5.35/-5.41	1.85/-1.87	3.50	5.99	2.53
6.2	0.82	5.74/-5.29	2.02/-1.48	3.72	5.88	2.28
6.3	0.78	5.69/-5.29	2.06/-1.47	3.63	5.72	2.15
6.4	0.58	5.41/-5.41	2.06/-1.60	3.35	5.83	2.56
6.5	0.31	5.03/-5.35	1.78/-1.63	3.25	5.61	2.41

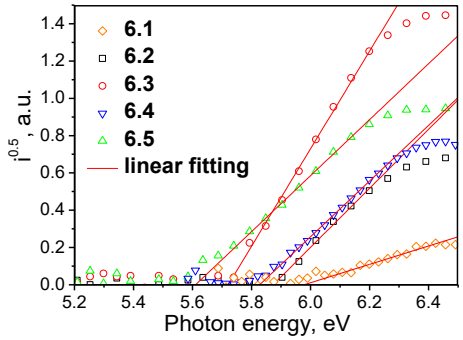

Fig. 4.38 Photoelectron emission spectra of solid samples of **6.1–6.5**

Additionally, the I_p^{PE} of compounds **6.1–6.5** in the solid state were obtained by using the method of electron photoemission spectrometry. The values of I_p^{PE} for **6.1–6.5** are listed in Table 4.14. On the grounds of the different donating abilities of 2-(trifluoromethyl)-10*H*-phenothiazine, iminodibenzyl, iminostilbene, 4-methoxy-9*H*-carbazole and 1,2,3,4-tetrahydrocarbazole moieties, the values of I_p^{PE} and E_A^{PE} for the designed diphenylsulfone derivatives were found to be in the range of 5.61–5.99 and 2.15–2.56 eV, respectively. Compounds with such I_p^{PE} and E_A^{PE} values fit for their usage as OLED hosts since both good charge-injection from the electrodes and the good exciton transfer from the host to the guest may be expected while exploiting the appropriate device structures and OLED emitters.[152,208]

4.6.2. Charge-transporting properties

In order to investigate the potential of new compounds **6.1–6.5** as OLED hosts, their charge-transporting properties were investigated by the TOF method. The electric fields of various polarity, the photocurrent transients for the holes or

electrons in the vacuum-deposited films of compounds **6.1–6.5** were recorded. For example, the transit times for both holes and electrons at different electric fields can be clearly determined from the plotted-in log-log scales corresponding to the photocurrent transients for compound **6.5** (Fig. 4.39a, b). This finding indicates the bipolar charge-transporting properties of compound **6.5**.

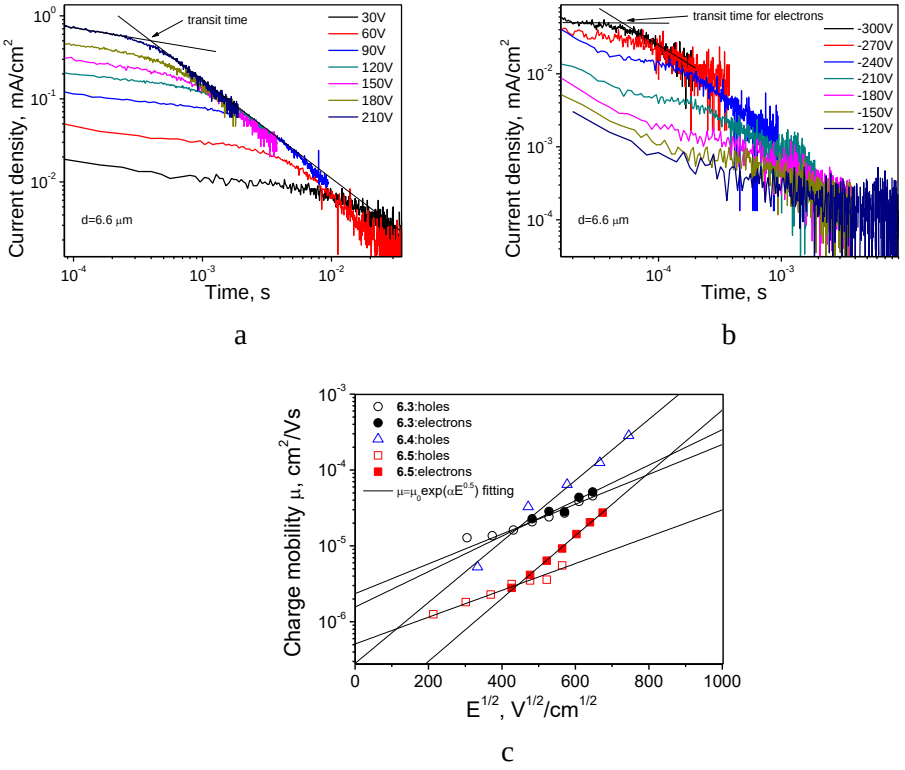

Fig. 4.39 Photocurrent transients for holes (a) and electrons (b) in vacuum-deposited film of **6.5** and electric field dependences of the charge mobilities of **6.3–6.5** (c). Fitting was performed according to Poole–Frenkel type mobility

The same properties were detected for compound **6.3**. In the case of compound **6.4**, only the hole-transporting properties were proved by the TOF technique since the transit times for electrons were not well visible. The hole and electron transport was not proved for compounds **6.1** and **6.2** since the corresponding transit times were not well detectable from the photocurrent transients. Difficulties to determine the transit times for holes/electrons in the films of compounds **6.1** and **6.2** may be explained either by strong charge-transport dispersity which is evident due to the shapes of their photocurrent transients or by higher relaxation times of the photogenerated charges than the TOF transit times.

4-methoxy-9*H*-carbazole-substituted diphenylsulfone derivative **6.4** showed the highest hole mobility achieving $2.8 \cdot 10^{-4}$ cm^2/V at an electric field of $5.6 \cdot 10^5$ V/cm (Fig. 4.39c). A lower value of the hole mobility of $4.6 \cdot 10^{-5}$ cm^2/V at an electric field of $5.6 \cdot 10^5$ V/cm was obtained for derivative **6.3** substituted by

iminostilbene in the para- position. Notably, at the same electric field, only a slightly higher value of the electron mobility of $5.1 \cdot 10^{-5}$ cm^2/V was obtained for compound **6.3** than its hole mobility showing the required charge balance for OLED hosts.[136,202] Derivative **6.5** showed hole and electron mobilities of $5.3 \cdot 10^{-6}$ and $9.1 \cdot 10^{-6}$ cm^2/V at an electric field of $3.1 \cdot 10^5$ V/cm due to the para-substitution of diphenylsulfone by the tetrahydrocarbazole moiety. In conclusion, the **6.4**>**6.3**>**6.5** dependence of the charge mobilities was obtained by showing the effect of the different donor substitutions on the charge-transporting properties. Meanwhile, the charge mobility of compounds **6.1** and **6.2** may be denoted by even lower values than these of compounds **6.3–6.5** due to the above described TOF measurements. Thus, 4-methoxy-9*H*-carbazole-based compound **6.4** demonstrated the highest hole mobility in comparison to that of compounds containing 2-(trifluoromethyl)-10*H*-phenothiazine, iminodibenzyl, iminostilbene or 1,2,3,4-tetrahydrocarbazole moieties featuring the same D-A-D chemical structure and linkage topology.

4.6.3. Photophysical properties

The absorption and the PL spectra of the neat films and dilute solutions of derivatives recorded at room and liquid nitrogen temperature are presented in Fig. 4.40. The position of the main absorption spectral peak at a low-energy wavelength strongly corresponds to the type of the donor substitution as it was for the previously investigated series of donor-acceptor-donor diphenylsulphone-based compounds.[90] At the same time, the influence of the diphenylsulfone moiety on the absorption spectra of compounds **6.1–6.5** was practically not detectible at that spectral region. The low energy peak wavelength of the absorption of films varies from 302 nm for **6.3**, 306 nm for **6.2**, 317 nm for **6.1**, 337 nm for **6.4** to 340 nm for **6.5** strongly depending on donors iminostilbene, iminodibenzyl, 2-(trifluoromethyl)-10*H*-phenothiazine, 4-methoxy-9*H*-carbazole and 1,2,3,4-tetrahydrocarbazole, respectively. The exploration of the solvatochromism of the compounds was additionally performed. The absence of a significant correlation with the solvent polarity showed no substantive CT nature of absorption.

The absorption spectra of the neat films and toluene solutions of compounds are practically identical. As expected, the absorption spectra of samples based on compounds **6.4** and **6.5** with aromatic donor moieties consist of sharp peaks with the highest oscillator strength for the $S_0 \rightarrow S_1$ excitation at ~340 nm attributed to the HOMO-LUMO transition. By contrast, the main broad absorption band of **6.1–6.2** with not aromatic donors and **6.3** with antiaromatic iminostilbenes correspond to the high energy $S_0 \rightarrow S_{3,4}$ transitions. The absorption spectra of samples based on **6.2** correspond to the absorption of the iminodibenzyl donor moiety,[209] however, with a bathochromic shift from 290 to ~305 nm. The partial LUMO localization on the donor moieties in the case of **6.2** and **6.3** points to the contribution of the LE states to various π–π^* transitions and the mentioned red shift of **6.2**. The E_g^{opt} values of 2.53, 2.36 2.39, 2.55 and 2.38 eV for **6.1–6.5**, respectively, were taken from the absorption spectra onsets of the films and used as the closest representation of the

HOMO-LUMO gap for the approximate estimation of the frontier molecular orbitals energy levels of compounds by subtraction of E_g^{opt} from IP values (Table 4.14).

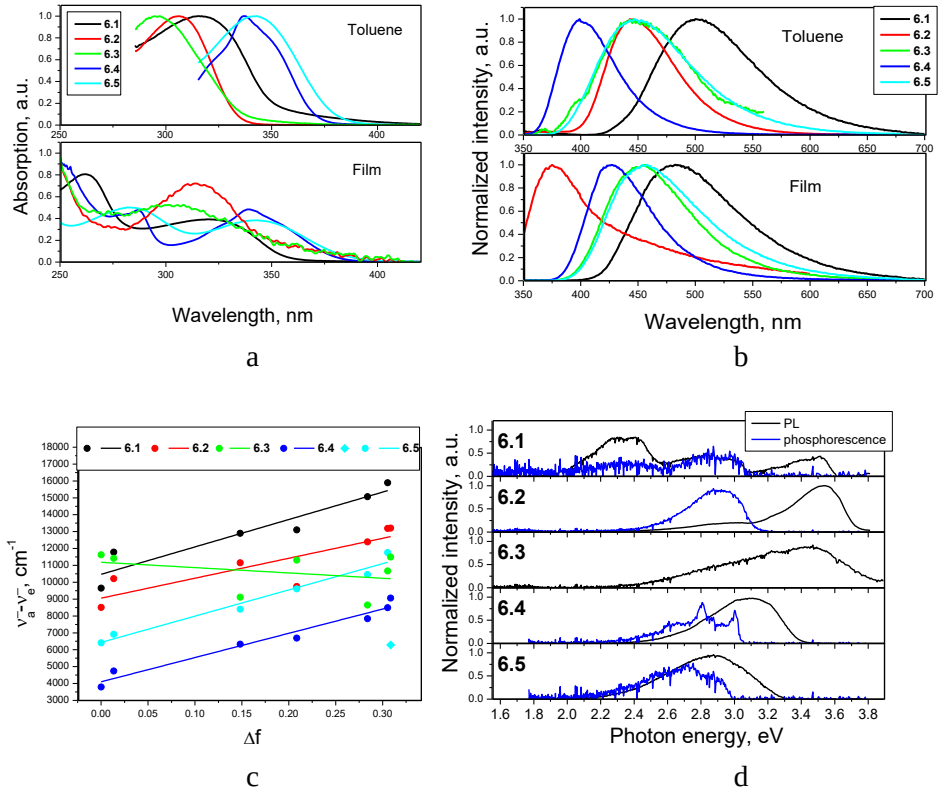

Fig. 4.40 6.1–6.5: (a) Absorption spectra of neat thin films and dilute toluene solutions; (b) PL spectra of neat thin films and dilute toluene solutions; (c) Lippert-Mataga plot showing the relation between Stokes' shift and orientation polarisability of various solvents. Data not used in estimation is marked in rhombs; (d) PL and phosphorescence spectra of dilute THF solutions recorded at 77K

The slope of the Lippert-Mataga plot for **6.3** was found to be negative and close to 0 in comparison with other plots. This is due to the fact that no strong correlation between the solvent polarity and the peak positions appeared for the derivatives. The assumptions of the Lippert-Mataga approach require linearity and a positive value of the slope.[122] It cannot be applied for the description of **6.3**. For the purpose of better fit, the polar protic methanol solution of **6.5** was excluded from the plotting. Besides these matters, the CT-character of the emission of **6.1**, **6.2**, **6.4** and **6.5** in the polar medium is evident by the monotonical bathochromic shift of the PL spectral peak with a change of the solvents to a more polar one (hexane (Δf = 0.0001) → toluene (Δf = 0.0135) → chloroform (Δf = 0.1483) → tetrahydrofuran (Δf = 0.2085) → acetone (Δf = 0.284) → acetonitrile (Δf = 0.3055) → methanol (Δf = 0.3086)). The approximated slopes for these compounds (Table 4.15) with linear relationships (R-square coefficients range from 0.69 to 0.96) correspond to

the $(\mu_e - \mu_g)^2$, thus revealing the change of the dipole moments after excitation. The obtained values correlate well with the theoretical predictions and disclose the twisted intramolecular CT nature of the emission. The high electronegativity of CF_3 and methoxy- groups indicates strong electron withdrawing as the major cause of this phenomenon in **6.1** and **6.4**. The geometry of **6.2** leads to slightly smaller differences of the dipole moments in the excited μ_e and ground μ_g states.

The PL spectra of the films of compounds correlate to a great extent to the PL spectra of dilute toluene solutions with insignificant spectral shifts. The only exclusion is the film of **6.2** which produces a major PL peak assigned to LE emission with a CT-tail in the spectral range where the peak location was expected to be. This observation is one more indication of the unsuitable for our goal donor-acceptor interactions of **6.2**. Otherwise, the films of compounds emit in the blue spectral diapason. As one of the direct results of extremely high torsion angles between the diphenylsulfone and 2-(trifluoromethyl)-10*H*-phenothiazine donor moieties and the consequent vanishing values of the oscillator strength of the $S_0 \rightarrow S_{1\text{-}2}$ excitation transitions, the Φ of **6.1** is the lowest of all the films based on any of the presented compounds in the series; it was at 2% for deoxygenated toluene and THF solutions (Table 4.15). The evidence of the phenomenon of AIE[210] is postulated from the Φ increase of **6.3** from virtually zero in dilute deoxygenated solutions to 13% in the solid state. The restriction of the intramolecular vibrational and rotational motion is the cause of AIE appearance in the solid state.

Table 4.15 Photophysical data for compounds **6.1–6.5**

Compound	Φ_{THF}[1]	Φ_{tol}[1]	Φ_{film}[2]	Φ_{4CzIPN}[3]	Lifetimes, ns[4]	Slopes, 10^3 cm^{-1}[5]	E_{S1}, eV[6]	E_{T1}, eV[6]	ΔE_{ST}, eV[6]
6.1	0.02	0.02	0.12	0.22	1.8, 4.2	16.2	3.6	3.08	0.52
6.2	0.56	0.33	0.2	0.76	0.5, 6.4	11.8	3.73	3.12	0.61
6.3	~0.0001	~0.0001	0.13	0.29	3.5, 13.7, 36.9	-3.2	3.87	-	-
6.4	0.49	0.43	0.49	0.87	4.9, 11.3	14.4	3.38	3.03	0.35
6.5	0.22	0.33	0.27	0.28	3.5, 11.5	15.5	3.29	2.99	0.3

[1] Φ values of deoxygenated dilute solutions of compounds. [2] Φ values of neat films of compounds. [3] Φ values of thin films of 4CzIPN doped in compounds (5 wt%). [4] Calculated from PL decay curves of neat films of compounds. [5] Slopes of Lippert-Mataga plots. [6] Estimated from onsets of emission spectra of dilute THF solutions recorded at 77K

The PL lifetime values derived from fitting the reconvolution of exponential functions of the PL decay curves of the neat films are attributed to the explicit prompt fluorescence character. The energy levels of the first singlet ant triplet excited states of compounds were estimated from the onsets of the PL and phosphorescence spectra, respectively, of frozen dilute THF solutions of the derivatives (Fig. 4.40d). Due to the extremely weak phosphorescence spectrum and the corresponding E_{T1}, the value for **6.3** was not obtained. The energy splitting ΔE_{ST}

between the first singlet and triplet excited states was found to be in the range of 0.3–0.6 eV.

Bipolar compounds **6.1–6.5** having triplet energy levels higher than 3 eV can be good candidates for being host materials. In order to provide a comparable study of the hosting properties of **6.1–6.5** for TADF dopants, thin host-guest films with 5 wt% doping concentration of 4CzIPN were made. A commercially available and widely studied TADF emitter 4CzIPN was selected since its triplet energy level of 2.4 eV[111] suits well for **6.1–6.5** for the triplet exciton harvesting, and also its HOMO and LUMO values suit well with these of **6.1–6.5**.[79] The absorption and PL spectra of the doped films are presented in Fig. 4.41a. The absorbance of samples of compounds corresponds to the respective absorption spectra of neat films. However, the LEB of the absorption at ~375 nm with a low intensity caused by small transition dipole moments for 4CzIPN:**6.1**, 4CzIPN:**6.2**, 4CzIPN:**6.3** films is related to $S_0 \rightarrow S_{1,2}$ transitions of the host molecules predicted by theoretical investigation. They were well spectrally resolved (Figs. 4.40a, 4.41a) due to the impact of the guest/host interactions on the positions of molecular orbitals. The broad tails starting at ~420 nm with an onset at ~590 nm are obviously ascribed to the CT processes. While the absorption of the guest:host films corresponds to the studied materials, the PL spectra represent a typical 4CzIPN emission. This observation confirms the electronic excitation energy transfer from the host to the guest. This is due to the fact that the PL spectra of most studied compounds matched with the absorption of 4CzIPN.[110]

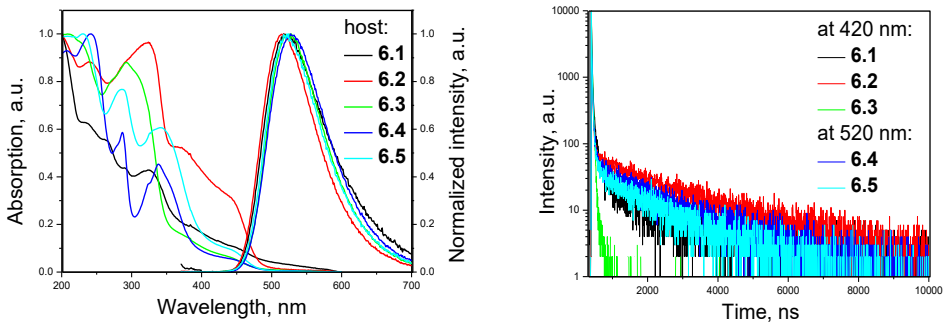

a b

Fig. 4.41 Thin films of 5 wt% solid solutions of 4CzIPN in **6.1–6.5**: (a) Absorption and PL spectra; (b) PL decay curves

The PL peak positions of the host-guest systems are slightly affected by the polarity of the host materials being in the order of **6.1**>**6.5**>**6.4**>**6.2**>**6.3** as it is for the slopes of Lippert-Mataga plots (Fig. 4.40c, Table 4.15). The PL decay curves of the molecular mixtures of the same weight concentration are shown in Fig. 4.41b. The low polarity of the host leads to the smallest DF lifetime for the system 4CzIPN:3 in the series as a result of the absence of CT. Correspondingly, the Φ of this guest:host system is as low as 29%. Due to the unfavorable HOMO distribution of **6.5**, the Φ value of the system 4CzIPN:**6.5** is almost the same. The HOMO localization on the donor units of compounds **6.2** and **6.4** facilitates CT leading to

the longest emission lifetimes (in the μs range) and the highest Φ values of 76% and 87% of the films of 4CzIPN doped in **6.2** and **6.4**, respectively. The Φ value of the film of 87% for 4CzIPN (5 wt%):**6.4** is even slightly higher than 83% observed for the film of 4CzIPN(5 wt%):CBP.[79]

4.6.4. Device fabrication and characterization

A series of A-E OLEDs with the structure of ITO / HAT-CN (4 nm) / TCTA (40 nm) / mCP (10 nm) / 4CzIPN:host (5 wt%, 30 nm) / TSPO1 (4 nm) / TPBi (45 nm) / LiF (0.6 nm) / Al with **6.1–6.5** as hosts, respectively, were fabricated and analyzed with the purpose of testing the host characteristics of compounds. The energetic diagram as a representation of the energy levels of frontier orbitals of the respective organic layers is presented in Fig. 4.42a.

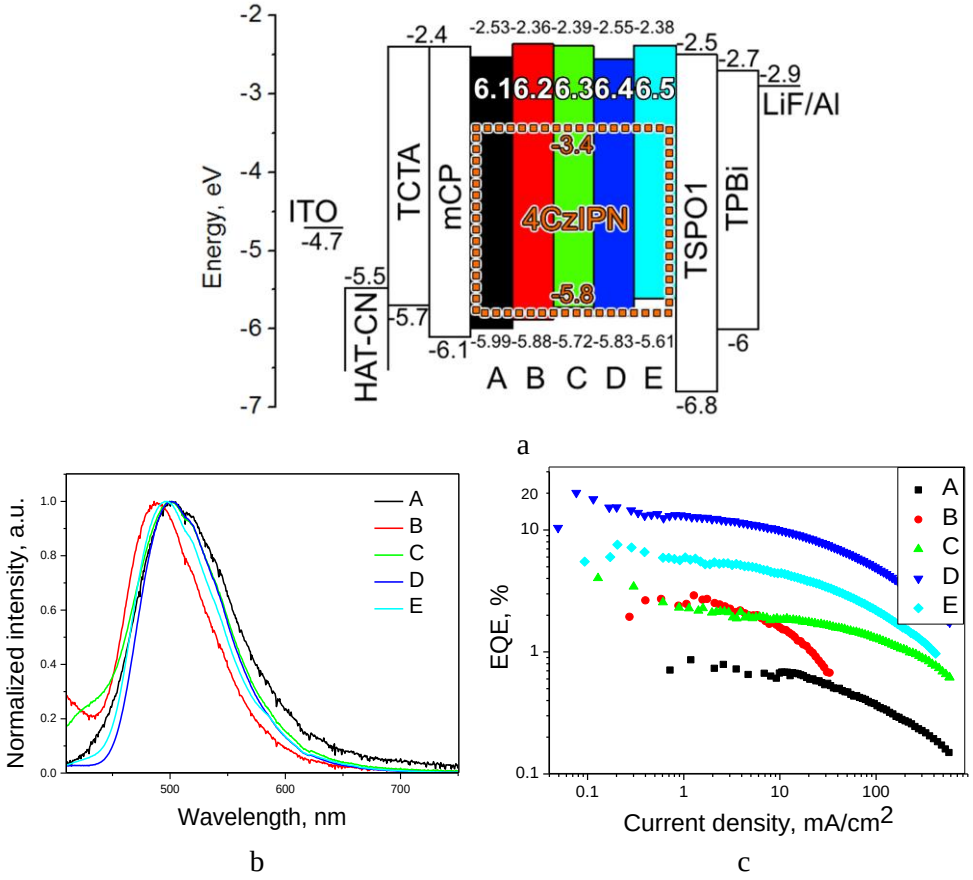

Fig. 4.42 A–E OLEDs: (a) Energy level diagram of the materials for organic layers. Estimated from the E_g^{opt} and IP values; (b) EL spectra recorded at 9V; (c) EQE-current density characteristics

The key electroluminescent data of A–E is listed in Table 4.16, Fig. 4.42b,c. HAT-CN and LiF were used for the injection of charge carriers. TCTA and TPBi were employed as HTL and ETL, respectively. mCP was taken for the fabrication of

the exciton blocking layer. The second exciton blocking layer of TSPO1 was also used for the blocking of hole penetration into TPBi. The electrodes were made of ITO (indium-tin oxide) and aluminum.

As it could be predicted from the highest Φ value of 87% of the respective guest:host films of the same weight concentration (Table 4.16), *D* based on compound **6.4** achieved the best results of the series with a maximum EQE over 20%, luminance of 28.9 thousand cd/m^2 and a CIE color index representing 4CzIPN emission the best way.[109] This result partly contributed to the highest charge mobility of compound **6.4** in comparison to that of the other compounds (Fig. 4.39c). The efficiency of device *B* with host material **6.2** was found to be much lower, apparently, due to the lower charge carrier mobilities of **6.2**.

Bluish-green electroluminescence with similar 1931 CIE chromaticity coordinates was recorded for the fabricated devices A–E (Fig. 4.42b, Table 4.16). The EL spectra of the devices are mainly attributed to the emission of the used guest 4CzIPN. Because of the differences in the dipole moments of the designed hosts **6.1**–**6.5** which are evident from the slopes of Lippert-Mataga plots decreasing in the sequence **6.1**>**6.5**>**6.4**>**6.2**>**6.3** (Fig. 4.40c, Table 4.16), all the fabricated devices showed the host contribution into the emission slightly influencing the 4CzIPN-related spectral peak position. A high-energy band peaked at 385 nm attributed to the emission of host **6.2** was observed in the EL spectra of device *B* (Fig. 4.42b). This observation indicates a weak host-guest energy transfer in the light-emitting layer of device *B*. Similarly, the high-energy shoulder (because of the emission of the host) was observed in the EL spectra of device *C* due to the weak host-guest energy transfer (Fig. 4.42b). As a result, lower maximum EQEs of 2.9% and 4% were obtained for devices *B* and *C* in comparison to that of device *D* with an efficient host-guest energy transfer in its light-emitting layer (Fig. 4.42c, Table 4.16). The TADF quenching observed from the PL decay curve (Fig. 4.42b) was apparently the cause of a relatively low EQE of 4% observed for device *C*. The emission of the host was practically not observed in the EL spectra of devices *A* and *E*. However, their corresponding maximum EQE values (0.8% and 7.6%) were also lower than that of device *D*. This result can be mainly explained by 1) the lower Φ*s* (22% and 28%) of the light-emitting layers of 4CzIPN:**6.1** and 4CzIPN:**6.5** than that (87%) of 4CzIPN:**6.4** due to the higher polarity of hosts **6.1** and **6.5** in comparison to the polarity of **6.4** (Table 4.16); and 2) the lower charge mobility at least of host **6.5** in comparison to that of host **6.2** (the charge mobility of host **6.1** was most probably also lower than that of host **6.4**, but this was not proved by TOF measurements). Meanwhile, the 'perfect' relationship between charge-transporting/-injecting properties, the appropriate[211] polarity and rigidity resulted in the high Φ value of guest 4CzIPN, and efficient host-guest energy transfer occurred in the case of host **6.4**. Therefore, the highest maximum EQE of 20.1% was obtained for device *D* in comparison to those of all other fabricated devices despite the same device structure and the same TADF emitter in use.

Table 4.16 Parameters of OLEDs based on diphenylsulfone derivatives

Device	Host	L_{max}, 10^3 cd/m^2 [1]	EQE_{max}, % [2]	$\eta_{p\ max}$, lm/W [3]	$\eta_{c\ max}$, cd/A [4]	$CIE_{x,y}$ [5]
A	**6.1**	2.2	0.8 (0.7)	0.9 (0.7)	2.1 (1.7)	(0.23, 0.43)
B	**6.2**	0.5	2.9 (2.7)	2.9 (2.6)	6 (5.7)	(0.18, 0.32)
C	**6.3**	9.1	4 (2.2)	6.8 (2.6)	10.2 (5.5)	(0.20, 0.38)
D	**6.4**	28.9	20.1 (14.9)	39.2 (25.6)	57.3 (42.4)	(0.21, 0.47)
E	**6.5**	10.8	7.6 (5.9)	13 (8.8)	20.3 (15.8)	(0.20, 0.42)

Efficiency values at 100 cd/m^2 are showed in parentheses. [1]Maximum brightness. [2]Maximum EQE. [3]Maximum power efficiency. [4]Maximum current efficiency. [5]1931 CIE chromaticity calculated from EL spectra at 9V

These findings well demonstrate the effect of different donor substitutions of diphenylsulfone-based hosts on the output characteristics of electroluminescent devices highlighting the potential of diphenylsulfone- and 4-methoxy-9*H*-carbazole-based host **6.4**.

5. CONCLUSIONS

1. Intramolecular charge transfer was observed in the derivatives of benzothiadiazole and carbazole. The reduction of molecular twisting resulted in a photoluminescence quantum yield reaching 0.60. The fluorescence of tetrahydrocarbazolyl-substituted benzothiadiazole derivative was very weak due to molecular twisting. However, this compound exhibited phosphorescence and delayed fluorescence. Di-*tert*-butylcarbazolyl-substituted benzothiadiazole showed an efficient charge transport with mobilities of $5 \cdot 10^{-5}$ $cm^2 \cdot V^{-1} \cdot cm^{-1}$ at an electric field of $5.8 \cdot 10^5$ V/cm for electrons and $1.7 \cdot 10^{-3}$ $cm^2 \cdot V^{-1} \cdot cm^{-1}$ at $5.3 \cdot 10^5$ V/cm for holes. The organic light emitting diode employing a derivative of carbazole and benzothiadiazole as the emitter demonstrated orange emission with a maximum external quantum efficiency of 1.3%.

2. The separation of the frontier molecular orbitals for the enhancement of the reverse intersystem crossing was achieved by asymmetrical substitution of the cyanobenzene moiety with electron donating fragments, which resulted in efficient thermally activated delayed fluorescence with photoluminescence quantum yields of neat solid samples of up to 42%. Organic light emitting diodes employing the layer of a benzonitrile derivative containing phenoxazine and acridine as the emissive layer showed a maximum current efficiency of 16.3 cd/A, a maximum power efficiency of 12.2 lm/W, and a maximum external quantum efficiency of 5%.

3. Nearly zero singlet-triplet energy gaps where achieved in (di-*tert*-butyl)dimethylacridin-substituted derivatives of diphenylsulfone and dibenzothiophene *S*,*S*-dioxide which resulted in effective reverse intersystem crossing and thermally activated delayed fluorescence. The organic light emitting diode with *para*-donor-substituted diphenylsulfone as the emitter showed a maximum current efficiency of 61.1 $cd \cdot A^{-1}$, a power efficiency of 64.0 $lm \cdot W^{-1}$, and an external quantum efficiency of 24.1%.

4. Thermally activated delayed fluorescence was detected for the derivatives of triphenyltriazine substituted by *tert*-butylcarbazole moieties. Organic light emitting diodes based on these derivatives doped in 1,3-bis(*N*-carbazolyl)benzene showed a maximum external quantum efficiency of up to 6.3%.

5. Derivatives of di(tetra)methoxycarbazole and dibenzofuran showed triplet energies of *ca*. 2.9 eV. The compounds were employed as host materials for green and red phosphorescent organic light emitting diodes and for devices based on thermally activated delayed fluorescence which showed a maximum external quantum efficiency exceeding 12%.

6. 4-Methoxy-9-carbazolyl-substituted derivative of diphenylsulfone demonstrated a high hole mobility reaching $3 \cdot 10^{-4}$ $cm^2 \cdot V^{-1} \cdot s^{-1}$ at an electric field of $5.3 \cdot 10^5$ V/cm. Its molecular mixture with 2,4,5,6-tetra(9-carbazolyl)isophthalonitrile showed a photoluminescence quantum yield of 87%. The organic light emitting diode based on this host and emitter exhibiting thermally activated delayed fluorescence showed green emission with a

brightness of $2.9 \cdot 10^4$ cd/m^2, and a maximum external quantum efficiency of 20.1%.

6. LIST OF REFERENCES

1. KARLICEK, R., Ch.-Ch. SUN, G. ZISSIS, and R. MA. *Handbook of advanced lighting technology*. Switzerland: Springer International Publishing AG, 2017.

2. KAFAFI, Z. H. *Organic electroluminescence (Optical engineering)*. Marcel Dekker Inc., 2005.

3. VAN DER WIELEN, Bernd. *Over One Billion Smartphones Globally Have an OLED Screen* [interactive]. 2019. [read 30-08-2019]. Access via the Internet: https://newzoo.com/insights/articles/over-one-billion-smartphones-globally-have-an-oled-screen/

4. GIEBINK, N. C., *et al*. Intrinsic luminance loss in phosphorescent small-molecule organic light emitting devices due to bimolecular annihilation reactions. *Journal of Applied Physics* [interactive]. 2008, vol. 103, 044509. Access via the Internet: <https://doi.org/10.1063/1.2884530>.

5. LEE, J., *et al*. Hot excited state management for long-lived blue phosphorescent organic light-emitting diodes. *Nature Communications* [interactive]. 2017, vol. 8, 15566. Access via the Internet: <https://doi.org/10.1038/ncomms15566>.

6. POPE, M., *et al*. Electroluminescence in organic crystals. *The Journal of Chemical Physics* [interactive]. 1963, vol. 38, 2042. Access via the Internet: <https://doi.org/10.1063/1.1733929>.

7. WILLIAMS, D. F., and SCHADT, M. A simple organic electroluminescent diode. *Proceedings of the IEEE* [interactive]. 1970, vol. 58(3), 476.

8. CHIANG, C.K., *et al*. Electrical Conductivity in Doped Polyacetylene. *Physical Review Letters* [interactive]. 1977, vol. 39(17), 1098–1110.

9. CHIANG, C.K., *et al*. Synthesis of highly conducting films of derivatives of polyacetylene, $(CH)_x$. *Journal of the American Chemical Society* [interactive]. 1978, vol. 100(3), 1013–1015. Access via the Internet: <https://doi.org/10.1021/ja00471a081>.

10. SHIRAKAWA, H., Synthesis of electrically conducting organic polymers: halogen derivatives of polyacetylene, $(CH)_x$. *Journal of the Chemical Society, Chemical Communications* [interactive]. 1977, vol. 16, 578–580. Access via the Internet: <https:// doi.org/10.1039/C39770000578>.

11. TANG, C.W. and VANSLYKE, S. A. Organic electroluminescent diodes. *Applied Physics Letters* [interactive]. 1987, vol. 51(12), 913–915. Access via the Internet: <https://doi.org/10.1063/1.98799>.

12. BURROUGHES, J.H., *et al*. Light-emitting diodes based on conjugated polymers. *Nature* [interactive]. 1990, vol. 347, 539–541. Access via the Internet: <https://doi.org/10.1038/347539a0>.

13. KOEZUKA, H., *et al*. Field-effect transistor with polythiophene thin-film. *Synthetic Metals* [interactive]. 1987, vol. 18, 699–704. Access via the Internet: <https://doi.org/10.1016/0379-6779(87)90964-7>.

14. BURROUGHES, J.H., *et al*. New semiconductor device physics in polymer diodes and transistors. *Nature* [interactive]. 1988, vol. 335, 137–141. Access via the Internet: <https://doi.org/10.1038/335137a0>.

15. HOROWITZ, G., *et al*. A field-effect transistor based on conjugated alpha-sexithienyl. *Solid State Communications* [interactive]. 1989, vol. 72 381–384. Access via the Internet: <https://doi.org/10.1016/0038-1098(89)90121-X>.

16. BURN, P. and SAMUEL, D. Light-emitting polymers – The shape of things to come? *Materials Today* [interactive]. 1998, vol. 1(4), 3-5. Access via the Internet: <https://doi.org/10.1016/S1369-7021(98)80015-1>.

17. TANG, C.W. Two-layer organic photovoltaic cell. *Applied Physics Letters* [interactive]. 1986, vol. 48, 183–185. Access via the Internet: <https://doi.org/10.1063/1.96937>.

18. WANG, Y.Z., *et al*. White luminescence of a system based on poly(9,9-di(ethylhexyl)fluorene) activated by fluorescent dyes, *Applied Physics Letters* [interactive]. 1999, vol. 74(24), 3613-3615. Access via the Internet: <https://doi.org/10.1063/1.123198>.

19. YANG, Y. Polymer electroluminescent devices. *MRS Bulletin* [interactive]. 1997, vol. 22, 31-38. Access via the Internet: <https://doi.org/10.1557/S0883769400033601>.

20. WANG, Q., *et al*. Manipulating charges and excitons within a single-host system to accomplish efficiency/CRI/color-stability trade-off for high-performance OWLEDs. *Advanced Materials* [interactive]. 2009, vol. 21, 2397. Access via the Internet: <https://doi.org/10.1002/adma.200803312>.

21. WANG, Q., and MA, D.G. Management of charges and excitons for high-performance white organic light-emitting diodes. *Chemical Society Reviews* [interactive]. 2010, vol. 39, 2387-2398. Access via the Internet: <https://doi.org/10.1039/B909057F>.

22. REINEKE, S., *et al*. White organic light-emitting diodes: Status and perspective. *Reviews of Modern Physics* [interactive]. 2013, vol. 85, 1245. Access via the Internet: <https://doi.org/10.1103/RevModPhys.85.1245>.

23. SASABE, H., and KIDO, J. Multifunctional materials in high-performance OLEDs: challenges for solid-state lighting. *Chemistry of materials* [interactive]. 2011, vol. 23(3), 621–630. Access via the Internet: <https://doi.org/10.1021/cm1024052>.

24. SCHWOERER, M., H. C. WOLF. *Organische Molekulare Festkörper*. Weinheim : Wiley-VCH, 2005.

25. BERNARD, V. *Molecular Fluorescence. Principles and Applications*. Weinheim : Wiley-VCH, 2002.

26. LAKOWICZ, Joseph R., Principles of fluorescence spectroscopy. Springer US, 2006.

27. STEPANOV, B. I. *Reports of N. A. S. Of USSR*. 1957, vol. 112, 5.

28. KENNARD, E.H. On the thermodynamics of fluorescence. *Physical Review Journal* [interactive]. 1917, vol. 11, 29. Access via the Internet: <https://doi.org/10.1103/PhysRev.11.29>.

29. MOROSHKIN, P., *et al*. Kennard-Stepanov relation connecting absorption and emission spectra in an atomic gas. *Physical Review Letters* [interactive]. 2014, vol. 11, 3 063002. Access via the Internet: <https://doi.org/10.1103/PhysRevLett.113.063002>.

30. C, X., *et al*. Electrosynthesis and characterization of a donor–acceptor type electrochromic material from poly(4,7-dicarbazol-9-yl-2,1,3-benzothiadia-zole) and its application in electrochromic devices. *Thin Solid Films* [interactive]. 2013 vol. 527, 232-238. Access via the Internet: < https://doi.org/10.1016/j.tsf.2012.12.052>.

31. MICHINOBU, T., *et al*. Band-gap tuning of carbazole-containing donor-acceptor type conjugated polymers by acceptor moieties and π-spacer groups. *Polymer (Guildf)* [interactive]. 2008, vol. 49, 192–199. Access via the Internet: < https://doi.org/10.1016/j.polymer.2007.11.022>.

32. BLOUIN, N., *et al*. A low-bandgap poly(2,7-carbazole) derivative for use in high-performance solar cells. *Advanced Materials* [interactive]. 2007, vol. 19, 2295–2300. Access via the Internet: <https://doi.org/10.1002/adma.200602496>.

33. SOCI, C., *et al*. Photoconductivity of a low-bandgap conjugated polymer. *Advanced Functional Materials* [interactive]. 2007, vol. 17, 632–636. Access via the Internet: <https://doi.org/10.1002/adfm.200600199>.

34. SHEN, M., *et al*. Electrochemistry and electrogenerated chemiluminescence of dithienylbenzothiadiazole derivative. Differential reactivity of donor and acceptor groups and simulations of radical cation-anion and dication-radical anion annihilations. *Journal of the American Chemical Society* [interactive]. 2010, vol. 132, 13453–13461. Access via the Internet: <https://doi.org/10.1021/ja105282u >.

35. KIMOTO, A., *et al*. Synthesis of asymmetrically arranged dendrimers with a carbazole dendron and a phenylazomethine dendron. *Macromolecules* [interactive]. 2004, vol. 37, 5531–5537. Access via the Internet: <https://doi.org/10.1021/ma0499674>.

36. JEON, S.O., *et al*. High-efficiency deep-blue-phosphorescent organic light-emitting diodes using a phosphine oxide and a phosphine sulfide high-triplet-energy host material with bipolar charge-transport properties. *Advanced Materials* [interactive]. 2010, vol. 22, 1872–1876. Access via the Internet: <https://doi.org/10.1002/adma.200903321>.

37. CHO, I., *et al*. Highly efficient and stable deep-blue emitting anthracene-derived molecular glass for versatile types of non-doped OLED applications. *Journal of Materials Chemistry* [interactive]. 2012, vol. 22, 123–129. Access via the Internet: <https://doi.org/10.1039/c1jm14482k >.

38. LEE, D.H., *et al*. Organic dyes incorporating low-band-gap chromophores based on π-extended benzothiadiazole for dye-sensitized solar

cells. *Dyes and Pigments* [interactive]. 2011, vol. 91, 192–198. Access via the Internet: <https://doi.org/10.1016/j.dyepig.2011.03.015>.

39. TAO, Y.M., *et al*. Synthesis and characterization of efficient luminescent materials based on 2,1,3-benzothiadiazole with carbazole moieties. *Synthetic Metals* [interactive]. 2011, vol. 161, 718–723. Access via the Internet: <https://doi.org/10.1016/j.synthmet.2011.01.020>.

40. XU, C., *et al*. Electrosynthesis and characterization of a donor-acceptor type electrochromic material from poly(4,7-dicarbazol-9-yl-2,1,3-benzothiadia-zole) and its application in electrochromic devices. *Thin Solid Films* [interactive]. 2013, vol. 527, 232–238. Access via the Internet: <https://doi.org/10.1016/j.tsf.2012.12.052>.

41. PRACHUMRAK, N., et al. Novel bis[5-(fluoren-2-yl)thiophen-2-yl]benzothiadiazole end-capped with carbazole dendrons as highly efficient solution-processed nondoped red emitters for organic light-emitting diodes. *ACS Applied Materials & Interfaces* [interactive]. 2013, vol. 5, 8694–8703. Access via the Internet: <https://doi.org/10.1021/am402349v>.

42. NI, F., *et al*. Teaching an old acceptor new tricks: rationally employing 2,1,3-benzothiadiazole as input to design a highly efficient red thermally activated delayed fluorescence emitter. *Journal of Materials Chemistry C* [interactive]. 2017, vol. 5, 1363—1368. Access via the Internet: <https://doi.org/10.1039/c7tc00025a>.

43. LIM, E. Synthesis and characterization of carbazole-benzothiadiazole-based conjugated polymers for organic photovoltaic cells with triazole in the main chain. *International Journal of Photoenergy* [interactive]. 2013, vol. 2013, 1-7. Access via the Internet: <https://doi.org/10.1155/2013/607826>.

44. TSUTSUI, T. Adachi, C. & Saito, S. Photochemical Processes in Organized Molecular Systems (ed. Honda, K.) 437–450 (Elsevier, 1991).

45. YERSHIN, H. Highly Efficient OLEDs with Phosphorescent Materials (WIiley, Weinheim, 2008).

46. TSE, S.C., C.H. CHEUNG, S.K. SO. *Organic electronics. Materials, processing, devices and applications. (Chapter 3) So Franky (Ed.), Charge transport and injection in amorphous organic semiconductors.* New York : Taylor & Francis Group, 2015.

47. KIM, K. H., *et al*. Design of heteroleptic Ir complexes with horizontal emitting dipoles for highly efficient organic light-emitting diodes with an external quantum efficiency of 38%. *Chemistry of Materials* [interactive]. 2016, vol. 28(20), 7505-7510. Access via the Internet: <https://doi.org/10.1021/acs.chemmater.6b03428>.

48. LEE, J., *et al*. Deep blue phosphorescent organic light-emitting diodes with very high brightness and efficiency. *Nature Materials* [interactive]. 2016, vol. 15(1), 92-98. Access via the Internet: <https://doi.org/10.1038/nmat4446>.

49. LI, C.-L., *et al*. Yellow and red electrophosphors based on linkage isomers of phenylisoquinolinyliridium complexes: distinct differences in photophysical and electroluminescence properties. *Advanced Functional Materials* [interactive]. 2005, vol. 15, 387-395. Access via the Internet: <https://doi.org/10.1002/adfm.200305100>.

50. FAN, C.-H., *et al*., Host and dopant materials for idealized deep-red organic electrophosphorescence devices. *Advanced Materials* [interactive]. 2011, vol. 23, 2981–2985. Access via the Internet: <https://doi.org/10.1002/adma.201100610>.

51. HOLZER, W., *et al*. Absorption and emission spectroscopic characterization of $Ir(ppy)_3$. *The Journal of Chemical Physics* [interactive]. 2005, vol. 308(1-2), 93-102. Access via the Internet: <https://doi.org/10.1016/j.chemphys.2004.07.051>.

52. HOFBECK, T., *et al*. The triplet state of fac-$Ir(ppy)_3$. *Inorganic Chemistry* [interactive]. 2010, vol. 49 (20), 9290–9299. Access via the Internet: <https://doi.org/10.1021/ic100872w>.

53. BALDO, M. A., *et al*. High-efficiency fluorescent organic light-emitting devices using a phosphorescent sensitizer. *Nature* [interactive]. 2000, vol. 403, 750-753. Access via the Internet: <https://doi.org/10.1038/35001541>.

54. CHOU, H.-H., and CHENG, C.-H. A highly efficient universal bipolar host for blue, green, and red phosphorescent OLEDs. *Advanced materials* [interactive]. 2010, vol. 22(11), 2468-2471. Access via the Internet: <https://doi.org/10.1002/adma.201000061>.

55. PANDER, P., *et al*. Room temperature phosphorescence lifetime and spectrum tuning of substituted thianthrenes. *Dyes and Pigments* [interactive]. 2017, vol. 142, 315-322. Access via the Internet: <https://doi.org/10.1016/j.dyepig.2017.03.049>.

56. MUKHERJEE, S., and THILAGAR, P. Recent advances in purely organic phosphorescent materials. *Chemical Communications* [interactive]. 2015, vol. 51, 10988-11003. Access via the Internet: <https://doi.org/10.1039/C5CC03114A>.

57. KITADE, T., *et al*. Determination of some phenothiazine derivatives by roomtemperature phosphorimetry on a poly(vinyl alcohol) substrate. *Analytical Sciences* [interactive]. 1996, vol. 12, 439-441. Access via the Internet: <https://doi.org/10.2116/analsci.12.439>.

58. GIFFORD, L.A., *et al*. Phosphorimetric analysis of phenothiazine derivatives. *Analytical Chemistry* [interactive]. 1975, vol. 47(9), 1699-1702. Access via the Internet: <https://doi.org/10.1021/ac60359a061>.

59. CANABATE DIAZ, B., *et al*. Study of the substituent groups effect on the room-temperature phosphorescent emission of fluorene derivatives in solution. *Analytica Chimica Acta* [interactive]. 2003, vol. 489, 165-171. Access via the Internet: <https://doi.org/10.1016/s0003-2670(03)00727-x>.

60. HURTUBISE, R.J., *et al*. Solid-phase room-temperature phosphorescence. *Analytical Letters* [interactive]. 2005, vol. 38, 1823-1845. Access via the Internet: <https://doi.org/10.1080/00032710500230822>.

61. BRUZZONE, L., and BADIA, R. Room-temperature phosphorescence of impure fluorene. *Analytical Letters* [interactive]. 1990, vol. 23(6), 1113-1121. Access via the Internet: <https://doi.org/10.1080/00032719008053450>.

62. PENG, Y.L., *et al*. Current state of the art in cyclodextrin-induced room temperature phosphorescence in the presence of oxygen. *Journal of Photochemistry and Photobiology A: Chemistry* [interactive]. 2005, vol. 173, 301-308. Access via the Internet: <https://doi.org/10.1016/j.jphotochem.2005.04.009>.

63. LIU, Y., *et al*. Room-temperature phosphorescence from purely organic materials. *Chinese Chemical Letters* [interactive]. Access via the Internet: <https://DOI:10.1016/j.cclet.2016.06.029>.

64. ZHANG, G., *et al*. Multi-emissive difluoroboron dibenzoylmethane polylactide exhibiting intense fluorescence and oxygen-sensitive room-temperature phosphorescence. *Journal of the American Chemical Society* [interactive]. 2007, vol. 129, 8942-8943. Access via the Internet: <https://doi.org/10.1021/ja0720255>.

65. LIU, Y., *et al*. All-organic thermally activated delayed fluorescence materials for organic light-emitting diodes. *Nature Reviews Materials* [interactive]. 2018, vol. 3,(4), 18020. Access via the Internet: <https://doi.org/10.1038/natrevmats.2018.20>.

66. CHEN, X.-K., *et al*. A new design strategy for efficient thermally activated delayed fluorescence organic emitters. *Advanced materials* [interactive]. 2017, 29(46), 1702767. Access via the Internet: <https://doi.org/10.1002/adma.201702767>.

67. BOLTON, O., *et al*. Activating efficient phosphorescence from purely organic materials by crystal design. *Nature Chemistry* [interactive]. 2011, vol. 3, 205–210. Access via the Internet: <https://doi.org/10.1038/nchem.984>.

68. EL-SAYED, M. A. Spin-orbit coupling and the radiationless processes in nitrogen heterocyclics. *The Journal of Chemical Physics* [interactive]. 1963, vol. 38, 2834–2838. Access via the Internet: <https://doi.org/10.1063/1.1733610>.

69. PANDER, P., *et al*. Synthesis and characterization of chalcogenophene-based monomers with pyridine acceptor unit. *Electrochimica Acta* [interactive]. 2016, vol. 210, 773–782. Access via the Internet: <https://doi.org/10.1016/j.electacta.2016.05.185>.

70. PANDER, P., *et al*. Electrochromic properties of novel selenophene and tellurophene derivatives based on carbazole and triphenylamine core. *The Journal of Physical Chemistry C* [interactive]. 2017,

vol. 121(21), 11027-11036. Access via the Internet: <https://doi.org/10.1021/acs.jpcc.7b00216>.

71. XUE, P., *et al*. Bright persistent luminescence from pure organic molecules through a moderate intermolecular heavy atom effect. *Chemical Science* [interactive]. 2017, vol. 8, 6060–6065. Access via the Internet: <https://doi.org/10.1039/C5SC03739E>.

72. HAYDUK, M., *et al*. Phosphorescence through hindered motion of pure organic emitters. *Chemistry - A European Journal* [interactive]. 2018, vol. 24, 12221–12230. Access via the Internet: <https://doi.org/10.1002/chem.201800521>.

73. CLINE LOVE L. J., M. SKRILEC. *Solution behaviour of surfactants. (K. L. Mittal and B. Lindman, eds.)*. New York: Springer US, 1982.

74. WARD, J. S., *et al*. The interplay of thermally activated delayed fluorescence (TADF) and room temperature organic phosphorescence in sterically-constrained donor–acceptor charge-transfer molecules. *Chemical Communications* [interactive]. 2016, vol. 52, 3–6. Access via the Internet: <https://doi.org/10.1039/C5CC09645F>.

75. KABE, R., and ADACHI, C. Organic long persistent luminescence. *Nature* [interactive]. 2017, vol. 550, 384–387. Access via the Internet: <https://doi.org/10.1038/nature24010>.

76. HIRATA, S., *et al*. Efficient persistent room temperature phosphorescence in organic amorphous materials under ambient conditions. *Advanced Functional Materials* [interactive]. 2013, vol. 23, 3386–3397. Access via the Internet: <https://doi.org/10.1002/adfm.201203706>.

77. TAO, Y.K., *et al*. Thermally activated delayed fluorescence materials towards the breakthrough of organoelectronics. *Advanced Materials* [interactive]. 2014, vol. 26(47), 7931-7958. Access via the Internet: <https://doi.org/10.1002/adma.201402532>.

78. ZHANG, Q., *et al*. Highly efficient green phosphorescent organic light-emitting diodes based on Cu^{I} complexes. *Advanced Materials* [interactive]. 2004, vol. 16, 432. Access via the Internet: <https://doi.org/10.1002/adma.200306414>.

79. UOYAMA, H., *et al*. Highly efficient organic light-emitting diodes from delayed fluorescence. *Nature* [interactive]. 2012, vol. 492, 234-238. Access via the Internet: <https://doi.org/10.1038/nature11687>.

80. ADACHI, C. Third-generation organic electroluminescence materials. *Japanese Journal of Applied Physics* [interactive]. 2014, vol. 53, 060101. Access via the Internet: <https://doi.org/10.7567/JJAP.53.060101>.

81. LIN, T. A., *et al*. Sky-blue organic light emitting diode with 37% external quantum efficiency using thermally activated delayed fluorescence from spiroacridine-triazine hybrid. *Advanced Materials* [interactive]. 2016, vol. 2 8(32), 6976–6983. Access via the Internet: <https://doi.org/10.1002/adma.201601675>.

82. OGIWARA, T., *et al*. Mechanism of intersystem crossing of thermally activated delayed fluorescence molecules. *The Journal of Physical Chemistry A* [interactive]. 2015, vol. 119(14), 3415-3418. Access via the Internet: <https://doi.org/10.1021/acs.jpca.5b02253>.

83. HU, D., *et al*. Reverse intersystem crossingfrom upper triplet levels toexcited singlet: a 'hot excition' path for organic light-emittingdiodes. *Philosophical Transactions A* [interactive]. 2014, 373, 20140318. Access via the Internet: <http://dx.doi.org/10.1098/rsta.2014.0318>.

84. YANG, Z., *et al*. Recent advances in organic thermally activated delayed fluorescence materials. *Chemical Society Reviews* [interactive]. 2017, vol. 46, 915-1016. Access via the Internet: https://doi.org/10.1039/c6cs00368k.

85. WONG, M. Y., and ZYSMAN-VOLMAN, E. Purely organic thermally activated delayed fluorescence (TADF) materials for organic light-emitting diodes (OLEDs). *Advanced Materials*. 2017, vol. 160, 5444. Access via the Internet: < https://doi.org/10.1002/adma.201605444>.

86. DIAS, F.B., *et al*. Photophysics of thermally activated delayed fluorescence molecules. *Methods and Applications in Fluorescence* [interactive]. 2017, vol. 5(1), 012001. Access via the Internet: < https://doi.org/10.1088/2050-6120/aa537e>.

87. DIAS, F.B., *et al*. Triplet harvesting with 100% efficiency by way of thermally activated delayed fluorescence in charge transfer OLED emitters. *Advanced Materials* [interactive]. 2013, vol. 25, 3707–3714. Access via the Internet: <https://doi.org/10.1002/adma.201300>.

88. ENDO, A., *et al*. Efficient up-conversion of triplet excitons into a singlet state and its application for organic light emitting diodes. *Applied Physics Letters* [interactive]. 2011, vol. 98, 083302. Access via the Internet: <https://doi.org/10.1063/1.3558906>.

89. HOSOKAI, T., *et al*. Evidence and mechanism of efficient thermally activated delayed fluorescence promoted by delocalized excited states. *Science Advances* [interactive]. 2017, vol. 3, e1603282. Access via the Internet: <https://doi.org/10.1126/sciadv.1603282>.

90. BEZVIKONNYI, O., *et al*. Effect of donor substituents on thermally activated delayed fluorescence of diphenylsulfone derivatives. *Journal of Luminescence* [interactive]. 2019, vol. 206, 250-259. Access via the Internet: <https://doi.org/10.1016/j.jlumin.2018.10.018>.

91. DIAS, F.B., *et al*. Intramolecular charge transfer assisted by conformational changes in the excited state of fluorene-dibenzothiophene-S,S-dioxide co-oligomers. *The Journal of Physical Chemistry B* [interactive]. 2006, vol. 110(39), 19329-19339. Access via the Internet: <https://doi.org/10.1021/jp0643653>.

92. MOSS, K. C., *et al*. Tuning the intramolecular charge transfer emission from deep blue to green in ambipolar systems based on dibenzothiophene S,S-dioxide by manipulation of conjugation and strength of the electron donor units. *The Journal of Organic Chemistry* [interactive]. 2010,

vol. 75, 6771–6781. Access via the Internet: <https://doi.org/10.1021/jo100898a>.

93. SANTOS, P. L., *et al*. Engineering the singlet–triplet energy splitting in a TADF molecule. *Journal of Materials Chemistry C* [interactive]. 2016, vol. 4, 3815—3824. Access via the Internet: <https://doi.org/10.1039/C5TC03849A>.

94. DIAS, F.B., *et al*. The role of local triplet excited states and D-A relative orientation in thermally activated delayed fluorescence: photophysics and devices. *Advanced Science* [interactive]. 2016, 18;3(12):1600080. Access via the Internet: <https://doi.org/ 10.1002/advs.201600080>.

95. ZHANG, Q.-S., *et al*. Efficient blue organic light-emitting diodes employing thermally activated delayed fluorescence. *Nature Photonics*. 2014, vol. 8, 326-332. Access via the Internet: <https://doi.org/10.1038/nphoton.2014.12>.

96. TANAKA. H., *et al*. Efficient green thermally activated delayed fluorescence (TADF) from a phenoxazine–triphenyltriazine (PXZ–TRZ) derivative. *Chemical Communications* [interactive]. 2012, vol. 48, 11392-11394. Access via the Internet: <https://doi.org/10.1039/C2CC36237F>.

97. LIU, W., *et al*. Novel carbazol-pyridine-carbonitrile derivative as excellent blue thermally activated delayed fluorescence emitter for highly efficient organic light-emitting devices. *ACS Applied Materials & Interfaces* [interactive]. 2015, vol. 7, 18930-18936. Access via the Internet: <https://doi.org/10.1021/acsami.5b05648>.

98. ZHANG, D., *et al*. Extremely low driving voltage electrophosphorescent green organic light–emitting diodes based on a host material with small singlet–triplet exchange energy without p– or n–doping layer. *Organic Electronics* [interactive]. 2013, vol. 1, 260-266. Access via the Internet: <https://doi.org/10.1016/j.orgel.2012.11.003>.

99. SATO, K., *et al*. Organic luminescent molecule with energetically equivalent singlet and triplet excited states for organic light–emitting diodes. *Physical Review Letters* [interactive]. 2013, vol. 110, 247401-247405. Access via the Internet: <https://journals.aps.org/prl/pdf/10.1103/PhysRevLett.110.247401>.

100. ZHANG, Q., *et al*. Design of efficient thermally activated delayed fluorescence materials for pure blue organic light emitting diodes. *Journal of the American Chemical Society* [interactive]. 2012, vol. 134, 14706-14709. Access via the Internet: <https://doi.org/10.1021/ja306538w>.

101. LEE, S. Y., *et al*. Luminous butterflies: efficient exciton harvesting by benzophenone derivatives for full–color delayed fluorescence OLEDs. *Angewandte Chemie International Edition* [interactive]. 2014, vol, 53, 6402-6406. Access via the Internet: <https://doi.org/10.1002/anie.201402992>.

102. ZHANG, Y., *et al*. Towards highly efficient red thermally activated delayed fluorescence materials by the control of intra-molecular π–π stacking interactions. *Nanotechnology* [interactive]. 2016, vol. 27, 094001.

Access via the Internet: <https://iopscience.iop.org/article/10.1088/0957-4484/27/9/094001/pdf>.

103. TOMKEVICIENE, A., *et al*. Thianthrene and acridan-substituted benzophenone or diphenylsulfone: Effect of triplet harvesting via TADF and phosphorescence on efficiency of all-organic OLEDS. *Organic Electronics* [interactive]. 2019, vol. 70, 227. Access via the Internet: <https://reader.elsevier.com/reader/sd/pii/S1566119919301909?token=F96271ACA7396CBC88B3454F5EA8C560DECC36A86AE873561F34A419FA53D05EE266591F2EB69A94400FC407D37926BD>.

104. WANG, Z., *et al*. Structure–performance investigation of thioxanthone derivatives for developing color tunable highly efficient thermally activated delayed fluorescence emitters. *ACS Applied Materials & Interfaces* [interactive]. 2016, vol. 8, 8627−8636. Access via the Internet: <https://doi.org/10.1021/acsami.5b12559>.

105. CAO, X., *et al*. CN-containing donor–acceptor-type small-molecule materials for thermally activated delayed fluorescence OLEDs. *Journal of Materials Chemistry C* [interactive]. 2017, vol. 5, 7699—7714. Access via the Internet: <https://doi.org/10.1039/C7TC02481A>.

106. CHEN, D. Y., *et al*. Isomeric thermally activated delayed fluorescence emitters for color purity-improved emission in organic light-emitting devices. *ACS Applied Materials & Interfaces* [interactive]. 2016, vol. 8 (26), 16791-16798. Access via the Internet: <https://doi.org/10.1021/acsami.6b03954>.

107. TANAKA, H., *et al*. Twisted intramolecular charge transfer state for long-wavelength thermally activated delayed fluorescence. *Chemistry of Materials* [interactive]. 2013, 25, 3766-3771. Access via the Internet: <https://doi.org/10.1021/cm402428a>.

108. PAN, K.-C., Efficient and tunable thermally activated delayed fluorescence emitters having orientation-adjustable CN-substituted pyridine and pyrimidine acceptor units. *Advanced Functional Materials* [interactive]. 2016, 26, 7560-7571. Access via the Internet: <https://onlinelibrary.wiley.com/doi/epdf/10.1002/adfm.201602501>.

109. IM, Y., and LEE, J. Y. Recent progress of green thermally activated delayed fluorescent emitters. *Journal of Information Display* [interactive]. 2017, vol. 18 (3), 101-117. Access via the Internet: <https://doi.org/10.1080/15980316.2017.1333046>.

110. LEE, D.R., *et al*. Above 30% external quantum efficiency in green delayed fluorescent organic light-emitting diodes. *ACS Applied Materials & Interfaces* [interactive]. 2015, vol. 7, 9625-9629. Access via the Internet: <https://doi.org/10.1021/acsami.5b01220>.

111. NAKANOTANI, H., *et al*. Promising operational stability of high-efficiency organic light-emitting diodes based on thermally activated delayed fluorescence. *Scientific Reports - Nature* [interactive]. 2013, vol. 3, 2127. Access via the Internet: <https://doi.org/10.1038/srep02127>.

112. KAJI, H., *et al*. Purely organic electroluminescent material realizing 100% conversion from electricity to light. *Nature Communications* [interactive]. 2015, vol. 6, 8476. Access via the Internet: <https://doi.org/10.1038/ncomms9476>.

113. ZHANG D., *et al*. Versatile indolocarbazole-isomer derivatives as highly emissive emitters and ideal hosts for thermally activated delayed fluorescent OLEDs with alleviated efficiency roll-off. *Advanced Materials* [interactive]. 2018, vol. 30, 1705250. Access via the Internet: <https://doi.org/10.1002/adma.201705406>.

114. LI, C., *et al*. Secondary acceptor optimization for full-exciton radiation: toward sky-blue thermally activated delayed fluorescence diodes with external quantum efficiency of ≈30. *Advanced Materials* [interactive]. 2018, vol. 30, 1804228. Access via the Internet: <https://doi.org/10.1002/adma.201804228>.

115. CHAN, C.-Y., *et al*. Rational molecular design for deep-blue thermally activated delayed fluorescence emitters. *Advanced Functional Materials* [interactive]. 2018, vol. 28, 1706023. Access via the Internet: <https://doi.org/10.1002/adfm.201706023>.

116. GRYBAUSKAITE-KAMINSKIENE, G., *et al*. Aggregation-enhanced emission and thermally activated delayed fluorescence of derivatives of 9-phenyl-9*H*-carbazole: Effects of methoxy and *tert*-butyl substituents. *Chemistry – A European Journal* [interactive]. 2018, vol. 24, 9581-9591. Access via the Internet: <https://doi.org/10.1002/chem.201800822>.

117. CHO, Y. J., *et al*. High efficiency in a solution-processed thermally activated delayed-fluorescence device using a delayed-fluorescence emitting material with improved solubility. *Advanced Materials* [interactive]. 2014, 26, 6642–6646. Access via the Internet: <https://doi.org/10.1002/adma.201402188>.

118. ONSAGER, L. Electric moments of molecules in liquids. *Journal of the American Chemical Society* [interactive]. 1936, vol. 58, 1486-1493. Access via the Internet: <https://doi.org/10.1021/ja01299a050>.

119. MATAGA, N., *et al*. Solvent effects upon fluorescence spectra and the dipolemoments of excited molecules. *Bulletin of the Chemical Society of Japan* [interactive]. 1956, vol. 29 (4), 465-470. Access via the Internet: <https://doi.org/10.1246/bcsj.29.465>.

120. SUMALEKSHMY. S., and GOPIDAS, K. R. Photoinduced intramolecular charge transfer in donor−acceptor substituted tetrahydropyrenes. *The Journal of Physical Chemistry B* [interactive]. 2004, vol. 108, 3705–3712. Access via the Internet: <https://doi.org/10.1021/jp022549l>.

121. LIPPERT, E. Dipolmoment und elektronenstruktur von angereten molekülen. *Zeitschrift für Naturforschung A. A Journal of Physical Sciences*

[interactive]. 1955, vol. 10, 541−545. Access via the Internet: <http://zfn.mpdl.mpg.de/data/Reihe_A/10/ZNA-1955-10a-0541.pdf>.

122. COPP, S. M., *et al*. Heterogeneous solvatochromism of fluorescent DNA-stabilized Silver clusters precludes use of simple Onsager-based Stokes shift models. *The Journal of Physical Chemistry Letters* [interactive]. 2016, vol. 7, 698-703. Access via the Internet: <https://doi.org/10.1021/acs.jpclett.5b02777>.

123. DIAS, F.B. Kinetics of thermal-assisteddelayed fluorescence in blueorganic emitters with largesinglet–triplet energy gap. *Philosophical Transactions* [interactive]. 2014, vol. 373, 0447. Access via the Internet: <https://royalsocietypublishing.org/doi/pdf/10.1098/rsta.2014.0447>.

124. LUO, J., *et al*. Aggregation-induced emission of 1-methyl-1,2,3,4,5-pentaphenylsilole. *Chemical Communications* [interactive]. 2001, vol. 18, 1740-1741. Access via the Internet: <https://doi.org/10.1039/B105159H>.

125. CHEN, Y., et al. Aggregation-induced emission: fundamental understanding and future developments. *Materials Horizons* [interactive]. 2019, vol. 6, 428-433. Access via the Internet: <https://doi.org/10.1039/c8mh01331d>.

126. GUO, J. Purely organic materials with aggregation-induced delayed fluorescence for efficient nondoped OLEDs. *Advanced Optical Materials* [interactive]. 2018, vol. 6 (15), 1800264. Access via the Internet: <https://doi.org/10.1002/adom.201800264>.

127. SKUODIS, E., *et al*. Aggregation, thermal annealing, and hosting effects on performances of an acridan-based TADF emitter. *Organic Electronics* [interactive]. 2018, vol. 63, 29–40. Access via the Internet: < https://reader.elsevier.com/reader/sd/pii/S1566119918304610?token=99C0C9B78643DDA6FE683CC54C4931E3EB5388718852C0A95F2DE12EBF7F87E498D8F41658EF5CCEE0A7167AE3B55FA2>.

128. RIZZO, F., and CUCINOTTA, F. Recent developments in AIEgens for non-doped and TADF OLEDs. *Israel Journal Chemistry* [interactive]. 2018, vol. 58, 1 – 16. Access via the Internet: <https://doi.org/10.1002/ijch.201800049>.

129. Access via the Internet: https://www.nobelprize.org/prizes/chemistry/

130. ANDREW, P., and BARNES, W. L. Förster energy transfer in an optical microcavity. *Science* [interactive]. 2000, 290 (5492), 785-788. Access via the Internet: <https://doi.org/10.1126/science.290.5492.785>.

131. FÖRSTER, T. 10th Spiers Memorial Lecture. Transfer mechanics of electronic excitation. *Discussions of the Faraday Society* [interactive]. 1959, vol. 27, 7–17. Access via the Internet: <https://doi.org/10.1039/df9592700007>.

132. DEXTER, D. L. A theory of sensitized luminescence in solids. *The Journal of Chemical Physics* [interactive]. 1953, vol. 21, 836–850. Access via the Internet: <https://doi.org/10.1063/1.1699044>.

133. TAO, Y., *et al*. Organic host materials for phosphorescent organic light-emitting diodes. *Chemical Society Reviews* [interactive]. 2011, vol. 40 (5), 2943-2970. Access via the Internet: <https://doi.org/10.1039/C0CS00160K>.

134. KIRLIKOVALI, K. O., and SPOKOYNY, A. M. The long-lasting blues: A new record for phosphorescent organic light-emitting diodes. *Chem* [interactive]. 2017, 3 (3), 385–387. Access via the Internet: < https://doi.org/10.1016/j.chempr.2017.08.013>.

135. FUKAGAWA, H., *et al*. Highly efficient and stable organic light-emitting diodes with a greatly reduced amount of phosphorescent emitter. *Scientific Reports* [interactive]. 2015, vol. 5 (1), 9855. Access via the Internet: <https://doi.org/10.1038/srep09855>.

136. CHATTERJEE, T., and WONG, K.-T. Perspective on host materials for thermally activated delayed fluorescence organic light emitting diodes. *Advanced Optical Materials* [interactive]. 2019, vol. 7(1), 1800565. Access via the Internet: <https://onlinelibrary.wiley.com/doi/epdf/10.1002/adom.201800565>.

137. JHULKI, S., and MOORTHY, J. N. Small molecular hole-transporting materials (HTMs) in organic light-emitting diodes (OLEDs): structural diversity and classification. *Journal of Materials Chemistry C* [interactive]. 2018, vol. 6 (31), 8280–8325. Access via the Internet: <https://doi.org/10.1039/C8TC01300D>.

138. WEX, B., and KAAFFARANI, B. R. Perspective on carbazole-based organic compounds as emitters and hosts in TADF applications. *Journal of Materials Chemistry C* [interactive]. 2017, vol. 5 (34), 8622–8653. Access via the Internet: <https://doi.org/10.1039/C7TC02156A>.

139. ZHANG, S., *et al*. Tuning the optoelectronicp properties of 4,4′-N , N ′-dicarbazole-biphenyl through heteroatom linkage: new host materials for phosphorescent organic light-emitting diodes. *Organic Letters* [interactive]. 2010, vol. 12 (15), 3438–3441. Access via the Internet: <https://doi.org/10.1021/ol1008872>.

140. TOMKEVICIENE, A., *et al*. Impact of linking topology on the properties of carbazole trimers and dimers. *The Journal of Physical Chemistry C* [interactive]. 2011, vol. 115, 4887–4897. Access via the Internet: <https://dx.doi.org/10.1021/jp111333v>.

141. CHIU, T.-L., *et al*. Universal host o-DiCbzBz for high efficiency phosphorescence and thermal active delayed fluorescence organic light emitting device. *SID Symposium Digest of Technical Papers* [interactive]. 2017, vol. 48 (1), 1957-1959. Access via the Internet: <https://doi.org/10.1002/sdtp.12022>.

142. E. POLIKARPOV, and PADMAPERUMA., A.B. Materials design concepts for efficient blue OLEDs: A joint theoretical and experimental study. (N. p., United States, 2012)

143. MUKHOPADHYAY, S., *et al*. Neutral and charged excited states in polar organic films: Origin of unusual electroluminescence in tri-p-tolylamine-based hole conductors. *The Journal of Physical Chemistry A* [interactive]. 2008, vol. 112 (31), 7271-7279. Access via the Internet: <https://pubs.acs.org/doi/pdf/10.1021/jp8012078?rand=63yx725i>.

144. BUCINSKAS, A., *et al*. Structure–property relationship of isomeric diphenylethenyl-disubstituted dimethoxycarbazoles. *RSC Advances* [interactive]. 2015, vol. 5 (61), 49577–49589. Access via the Internet: <https://doi.org/10.1039/C5RA09161F>.

145. GUDEIKA, D., *et al*. Carbazolyl-substituted quinazolinones as high-triplet-energy materials for phosphorescent organic light emitting diodes. *Dyes and Pigments* [interactive]. 2017, vol. 142, 394-405. Access via the Internet:
<https://reader.elsevier.com/reader/sd/pii/S0143720817302000?token=2A4C7195906725B8878FB99D6363FB94E1A1F5C7114323FAE4C29A9F3139012A778F595906BF6C852929374FC1186821>.

146. DONG, Q., *et al*. Novel spirofluorene/indole/carbazole-based hole transport materials with high triplet energy for efficient green phosphorescent organic light-emitting diodes. *Dyes and Pigments* [interactive]. 2017, 137, 84-90. Access via the Internet: <
https://reader.elsevier.com/reader/sd/pii/S0143720816307082?token=82293D65A101E3EEA4759DEAB823D9CA3EDC99E54EFF864DD7D8732E32C3AC7B10EED6E9D61D003AD35DD84B17403DFC>.

147. DONG, Q., *et al*. Thermally stable bipolar host materials for high efficiency phosphorescent green and blue organic light-emitting diodes. *Dyes and Pigments* [interactive]. 2017, vol. 143, 470-478. Access via the Internet: <https://reader.elsevier.com/reader/sd/pii/S0143720817305727?token=6C74F29506C53536AA20AE0AB2C716EDABA233FF8F09ED7D9F90E3EA577BC6D1FCF875C8791C4260B8DE636C82D0BB08>.

148. KERUCKAS, J., *et al*. Influence of methoxy groups on the properties of 1,1-bis(4-aminophenyl)cyclohexane based arylamines: experimental and theoretical approach. *Journal of Materials Chemistry* [interactive]. 2012, vol. 22 (7), 3015-3027. Access via the Internet: <https://doi.org/10.1039/C2JM14387A>.

149. LI, W., *et al*. Universal host materials for high-efficiency phosphorescent and delayed-fluorescence OLEDs. *ACS Applied Materials &*

Interfaces [interactive]. 2015, vol. 7 (47), 26206–26216. Access via the Internet: <https://doi.org/10.1021/acsami.5b08291>.

150. PAN, J.-H., *et al*. Theoretical investigation of organic amines as hole transporting materials: correlation to the Hammett parameter of the substituent, ionization potential, and reorganization energy level. *Australian Journal of Chemistry* [interactive]. 2009, vol. 62 (5), 483-492. Access via the Internet: <https://doi.org/10.1071/CH08348>.

151. SAKALYTE, A., *et al*. Effect of methoxy substituents on the properties of the derivatives of carbazole and diphenylamine. *The Journal of Physical Chemistry C* [interactive]. 2011, vol. 115 (11), 4856–4862. Access via the Internet: <https://doi.org/10.1021/jp109643r>.

152. SALLENAVE, X., *et al*. Sensitivity of redox and optical properties of electroactive carbazole derivatives to the molecular architecture and methoxy substitutions. *The Journal of Physical Chemistry C* [interactive]. 2018, vol. 122 (18), 10138–10152. Access via the Internet: <https://doi.org/10.1021/acs.jpcc.8b02148>.

153. CHOI, H. J., *et al*. Efficient deep-blue organic light-emitting diodes with asymmetric diphenylsulfone-type materials used as TADF emitter and sensitizer. *2019 Spring meeting and exhibit. Aprl 22-26, 2019 Pheonix, Arizona* [interactive]. Access via the Internet: <https://mrsspring2019.zerista.com/poster/member/144510>.

154. NAKANOTANI, H., *et al*. High-efficiency organic light-emitting diodes with fluorescent emitters. *Nature Communications* [interactive]. 2014, vol. 5, 4016, 1–7. Access via the Internet: <https://doi.org/ Access via the Internet: <https://doi.org/10.1038/natrevmats.2018.20>.

155. D'ANDRADE B.W., *et al*. Relationship between the ionization and oxidationpotentials of molecular organic semiconductors. *Organic Electronics* [interactive]. 2005, vol. 6, 11-20. Access via the Internet: <http://shubodatta.tripod.com/Papers/UPSCV_OrgEl.pdf>.

156. GUDEIKA, D. *et al*. Effect of ethynyl linkages on the properties of the derivatives of triphenylamine and 1,8-naphthalimide. *The Journal of Physical Chemistry C* [interactive]. 2015, vol. 119 (51), 28335–28346. Access via the Internet: <https://pubs.acs.org/doi/pdf/10.1021/acs.jpcc.5b10163?rand=pogd827i>.

157. ARKHIPOV, V. I., I. I. FISHCHUK, A. KADASHCHUK, H. BASSLER. *Photophysics of Molecular Materials, ed. G. Lanzani* [interactive]. 2006. Weinheim : Access via the Internet: https://archive.org/stream/PhotophysicsOfMolecularMaterials/Photophysics%20of%20Molecular%20Materials_djvu.txt

158. M.J. Frisch, G.W. Trucks, H.B. Schlegel, G.E. Scuseria, M.A. Robb, J.R. Cheeseman, G. Scalmani, V. Barone, B. Mennucci, G.A. Petersson, H. Nakatsuji, M. Caricato, X. Li, H.P. Hratchian, A.F. Izmaylov, J. Bloino, G. Zheng, J.L. Sonnenberg, M. Hada, M. Ehara, K. Toyota, R. Fukuda, J. Hasegawa, M. Ishida, T. Nakajima, Y. Honda, O. Kitao, H. Nakai, T. Vreven,

J. Montgomery, J.E. Peralta, F. Ogliaro, M. Bearpark, J.J. Heyd, E. Brothers, K.N. Kudin, V.N. Staroverov, T. Keith, R. Kobayashi, J. Normand, K. Raghavachari, A. Rendell, J.C. Burant, S.S. Iyengar, J. Tomasi, M. Cossi, N. Rega, J.M. Millam, M. Klene, J.E. Knox, J.B. Cross, V. Bakken, C. Adamo, J. Jaramillo, R. Gomperts, R.E. Stratmann, O. Yazyev, A.J. Austin, R. Cammi, C. Pomelli, J.W. Ochterski, R.L. Martin, K. Morokuma, V.G. Zakrzewski, G.A. Voth, P. Salvador, J.J. Dannenberg, S. Dapprich, A.D. Daniels, O. Farkas, J.B. Foresman, J.V. Ortiz, J. Cioslowski, D.J. Fox, Gaussian 09, Revision B.01, Wallingford CT. Gaussian Inc.; 2009.

159. WANG, Y., *et al*. Investigation of the hole transport characterization and mechanisms in co-evaporated organic semiconductor mixtures. *RSC Advances [interactive]*. 2017, vol. 7 (45), 28494-28498. Access via the Internet: <https://doi.org/10.1021/acs.jpcc.8b02148>

160. TSNAG, D. P.-K., *et al*. Operational stability enhancement in organic light-emitting diodes with ultrathin Liq interlayers. *Scientific Reports [interactive]*. 2016, vol. 6, 22463. Access via the Internet: <https://www.nature.com/articles/srep22463.pdf>.

161. DAI, Y., *et al*. Highly efficient and stable tandem organic light-emitting devices based on HAT-CN/HAT-CN:TAPC/TAPC as a charge generation layer. *Journal of Materials Chemistry C* [interactive]. 2015, vol. 3, 6809-6814. Access via the Internet: <https://doi.org/10.1039/C4TC02875A>.

162. LIN, H., *et al*. Solution-processed hexaazatriphenylene hexacarbonitrile as a universal hole-injection layer for organic light-emitting diodes. *Organic Electronics* [interactive]. 2013, vol. 14, 1204–1210. Access via the Internet: <https://dx.doi.org/10.1016/j.orgel.2013.02.01>.

163. HOLMES, R. J., *et al*. Efficient, deep-blue organic electrophosphorescence by guest charge trapping. *Applied Physics Letters* [interactive]. 2003, vol. 83, 3818. Access via the Internet: <https://doi.org/10.1063/1.1624639>.

164. JEON, S. O., *et al*. External quantum efficiency above 20% in deep blue phosphorescent organic light-emitting diodes. *Advanced Materials* [interactive]. 2011, vol. 23, 1436–1441. Access via the Internet: <https://onlinelibrary.wiley.com/doi/pdf/10.1002/adma.201004372>.

165. XIAO, L., *et al*. Nearly 100% internal quantum efficiency in an organic blue-light electrophosphorescent device using a weak electron transporting material with a wide energy gap. *Advanced Materials* [interactive]. 2009, vol. 21, 1271–1274. Access via the Internet: <https://onlinelibrary.wiley.com/doi/epdf/10.1002/adma.200802034>.

166. GAO, Z., *et al*. Bright-blue electroluminescence from a silyl-substituted ter-(phenylene–vinylene) derivative. *Applied Physics Letters* [interactive]. 1999, vol. 74, 865. Access via the Internet: <https://doi.org/10.1063/1.123392>.

167. ADACHI, C., *et al*. Endothermic energy transfer: A mechanism for generating very efficient high-energy phosphorescent emission in organic

materials. *Applied Physics Letters* [interactive]. 2011, vol. 78, 1622. Access via the Internet: <https://doi.org/10.1063/1.1400076>.

168. THOMAS, K. R., *et al*. Light-emitting carbazole derivatives: Potential electroluminescent materials. *Journal of the American Chemical Society* [interactive]. 2001, vol. 123 (38), 9404-9411. Access via the Internet: <https://pubs.acs.org/doi/pdf/10.1021/ja010819s?rand=v7rwzwxi>.

169. GUDEIKA, D., *et al*. Differently substituted benzothiadiazoles as charge-transporting emitters for fluorescent organic light-emitting diodes. *Dyes and Pigments* [interactive]. 2019, vol. 166, 217-225. Access via the Internet: <https://doi.org/10.1016/j.dyepig.2019.03.017>.

170. GUDEIKA, D., *et al*. Differently substituted benzonitriles for non-doped OLED. *Dyes and Pigments* [interactive]. 2020, vol. 172, 107789. Access via the Internet: <https://doi.org/10.1016/j.dyepig.2019.107789>.

171. GUDEIKA, D., *et al*. Flexible diphenylsulfone versus rigid dibenzothiophene dioxide as acceptor moieties in donor-acceptor-donor TADF emitters for highly efficient OLEDs. *Organic Electronics* [interactive]. 2020 vol. 83, 105733. Access via the Internet: <https://doi.org/10.1016/j.orgel.2020.105733>, < https://www.sciencedirect.com/science/article/pii/S1566119920301191>.

172. BUCINSKAS, A., *et al*. Methoxycarbazolyl-disubstituted dibenzofuranes as holes- and electrons-transporting hosts for phosphorescent and TADF-based OLEDs. *Dyes and Pigments* [interactive]. 2020, vol. 172, 107781. Access via the Internet: <https://doi.org/10.1016/j.dyepig.2019.107781>.

173. BEZVIKONNYI, O., *et al*. Diphenylsulfone-based hosts for electroluminescent devices: Effect of donor substituents *Dyes and Pigments* [interactive]. 2020, 108104. Access via the Internet: <https://doi.org/ 10.1016/j.dyepig.2019.108104>.

174. KROTKUS, S., *et al*. Pyrenyl-functionalized fluorene and carbazole derivatives as blue light emitters. *The Journal of Physical Chemistry C* [interactive]. 2012, vol. 116, 7561–7572. Access via the Internet: <https://doi.org/10.1021/jp300161k>.

175. OELKRUG, D., *et al*. Towards highly luminescent phenylene vinylene films. *Synthetic Metals* [interactive]. 1996, vol. 83, 231–237. Access via the Internet: <https://doi.org/10.1016/S0379-6779(96)04484-0>.

176. WEN, P., *et al*. A-π-D-π-A carbazole derivatives with remarkable solvatochromism and mechanoreponsive luminescence turn-on. *Journal of Materials Chemistry C* [interactive]. 2017, vol. 5, 6136–6143. Access via the Internet: <https://doi.org/10.1039/c7tc00559h>.

177. ANANT, P., *et al*. A simple route toward the synthesis of bisbenzothiadiazole derivatives. *Organic Letters* [interactive]. 2008, vol. 10, 5533–5536. Access via the Internet: <https://doi.org/10.1021/ol8022837>.

178 WALBA, H., and BRANCH G. E. K. The absorption spectra of some N-substituted p-aminotriphenylmethyl ions. *Journal of the American*

Chemical Society [interactive]. 1951, vol. 73, 3341–3348. Access via the Internet: <https://doi.org/10.1021/ja01151a102>.

179 NI, F., *et al*. Teaching an old acceptor new tricks: rationally employing 2,1,3-benzothiadiazole as input to design a highly efficient red thermally activated delayed fluorescence emitter. *Journal of Materials Chemistry C* [interactive]. 2017, vol. 5, 1363–1368. Access via the Internet: <https://doi.org/10.1039/c7tc00025a>.

180. SWORAKOWSKI, J. How accurate are energies of HOMO and LUMO levels in small-molecule organic semiconductors determined from cyclic voltammetry or optical spectroscopy? *Synthetic Metals* [interactive]. 2018, vol. 235, 125-130. Access via the Internet: <https://reader.elsevier.com/reader/sd/pii/S0379677917303041?token=AA1D3BE063EE78306AA2312D5D281687A26A9FE82132A3AF2FEB9CBA642052CB609EDA6509A3ACC95D48FA38F4D5025D>.

181. TSUTSUI, T. Progress in electroluminescent devices using molecular thin films. MRS Bulletin [interactive]. 1997, vol. 22, 39–45. Access via the Internet: <https://doi.org/10.1557/S0883769400033613>.

182. LI, W., *et al*. A twisting donor-acceptor molecule with an intercrossed excited state for highly efficient, deep-blue electroluminescence. *Advanced Functional Materials* [interactive]. 2012, vol. 22, 2797–2803. Access via the Internet: <https://doi.org/10.1002/adfm.201200116>.

183. IM, Y., *et al*. Recent progress in high-efficiency blue-light-emitting materials for organic light-emitting diodes. *Advanced Functional Materials* [interactive]. 2017, vol. 27 (13), 1603007. 1–24. Access via the Internet: <https://doi.org/10.1002/adfm.201603007>.

184. VIGANTE, B., *et al*. Synthesis of linear and V-shaped carbazolylsubstituted pyridine-3,5-dicarbonitriles exhibiting efficient bipolar charge transport and E-type fluorescence. *Chemistry – A European Journal* [interactive]. 2019, vol. 25 (13), 3325-3336. Access via the Internet: <https://doi.org/10.1002/chem.201805323>.

185. DANYLIV, Y., *et al*. Derivatives of carbazole and chloropyridine exhibiting aggregation induced emission enhancement and deep-blue delayed fluorescence. *Dyes and Pigments* [interactive]. 2018, vol. 149, 588-596. Access via the Internet: <https://reader.elsevier.com/reader/sd/pii/S0143720817318144?token=65F406CC0BFE95470890ECFB55A38428704AA746EBD744B1A566A0835ED464AE38973E40AB174E64AF8D613735864322>.

186. KOBAYASHI, T., *et al*. Contributions of a higher triplet excited state to the emission properties of a thermally activated delayed-fluorescence emitter. *Physical Review Applied* [interactive]. 2017, vol. 7, 034002. Access via the Internet: <https://journals.aps.org/prapplied/pdf/10.1103/PhysRevApplied.7.034002>.

187. RUHSTALLER, B., *et al*. Simulating electronic and optical processes in multilayer organic light-emitting devices. *IEEE Journal of*

Selected Topics in Quantum Electronics [interactive]. 2003, vol. 9, (3), 723-731. Access via the Internet: <https://ieeexplore.ieee.org/stamp/stamp.jsp?tp=&arnumber=1250472>.

188. GOUSHI, K., *et al*. Organic light-emitting diodes employing efficient reverse intersystem crossing for triplet-to-singlet state conversion. *Nature Photonics* [interactive]. 2012, vol. 6, 253-258. Access via the Internet: <https://doi.org/10.1038/nphoton.2012.31>.

189. GRANLUND, T., *et al*. Interference phenomenon determines the color in an organic light emitting diode. *Journal of Applied Physics* [interactive]. 1997, vol. 81, 8097. Access via the Internet: <https://doi.org/10.1063/1.365418>.

190. REIG, M., *et al*. Tuning the ambipolar charge transport properties of tricyanovinyl-substituted carbazole-based materials. *Physical Chemistry Chemical Physics* [interactive]. 2017, vol. 19, 6721-6730. Access via the Internet: <https://doi.org/10.1039/C6CP08078B>.

191. CHAN, C. Y. H., *et al*. Achieving time-of-flight mobilities for amorphous organic semiconductors in a thin film transistor configuration. *Organic Electronics* [interactive]. 2013, vol. 14 (5), 1351-1358. Access via the Internet: <https://reader.elsevier.com/reader/sd/pii/S1566119913000633?token=B22322870E424E5173B1AD94C8DAF054CECBB74F3D524829779FC0F85FBD669D26AF7A6A82EDE60FCB73E8D0B3F2132B>.

192. WADA, Y., *et al*. Adamantyl substitution strategy for realizing solution-processable thermally stable deep-blue thermally activated delayed fluorescence materials. *Advanced Materials* [interactive]. 2018, vol. 30, 1705641. Access via the Internet: <https://onlinelibrary.wiley.com/doi/epdf/10.1002/adma.201705641>.

193. HUANG, J.-J., *et al*. Orthogonally substituted benzimidazole-carbazole benzene as universal hosts for phosphorescent organic light-emitting diodes. *Organic Letters* [interactive]. 2016, vol. 18, 672-675. Access via the Internet: <https://doi.org/10.1021/acs.orglett.5b03631>.

194. LEE, Y.-T., Simple molecular-engineering approach for enhancing orientation and outcoupling efficiency of thermally activated delayed fluorescent emitters without red-shifting emission. *ACS Applied Materials & Interfaces* [interactive]. 2018, vol. 10, 43842. Access via the Internet: <https://doi.org/10.1021/acsami.8b16199>.

195. MOON, J.S., *et al*. δ-Carboline-based bipolar host materials for deep blue thermally activated delayed fluorescence OLEDs with high efficiency and low roll-off characteristic, *RSC Adv.* 2018, vol. 8, 17025–17033. Access via the Internet: <https://doi:10.1039/c8ra01761a>.

196. SIRAJ N., *et al*. Enhanced S_2 emission in carbazole-based ionic liquids. *RSC Advances* [interactive]. 2015, vol. 5, 9939–9945. Access via the Internet: <https://pubs.rsc.org/en/content/articlepdf/2015/ra/c4ra12362j>.

197. LI, J., *et al*. Highly efficient exciplex organic light-emitting diodes incorporating a heptazine derivative as an electron acceptor. *Chemical Communications* [interactive]. 2014, vol. 50, 6174-6176. Access via the Internet: <https://doi.org/10.1039/c4cc01590h>.

198. WANG, Q., *et al*. Harvesting excitons via two parallel channels for efficient white organic LEDs with nearly 100% internal quantum efficiency: fabrication and emission-mechanism analysis. *Advanced Functional Materials* [interactive]. 2009, vol. 19, 84-95. Access via the Internet: <https://onlinelibrary.wiley.com/doi/epdf/10.1002/adfm.200800918>.

199. WU, F.-I., *et al*. Novel distyrylcarbazole derivatives as hole-transporting blue emitters for electroluminescent devices. *Journal of Materials Chemistry* [interactive]. 2005, vol. 15 (44), 4753-4760. Access via the Internet: <https://doi.org/10.1039/B510035F>.

200. LI, W., et al. A hybridized local and charge-transfer excited state for highly efficient fluorescent OLEDs: Molecular design, spectral character, and full exciton utilization. *Advanced Optical Materials* [interactive]. 2014, vol. 2 (9), 892–901. Access via the Internet: <https://doi.org/10.1002/adom.201400154>.

201. AMBROSE, J. F., and NELSON, R. F. Anodic oxidation pathways of carbazoles. *Journal of The Electrochemical Society* [interactive]. 1968, vol. 115, 1159-1164. Access via the Internet: <https://doi.org/10.1149/1.2410929>.

202. HLADKA, I., *et al*. W-shaped bipolar derivatives of carbazole and oxadiazole with high triplet energies for electroluminescent devices. *Dyes and Pigments* [interactive]. 2018, vol. 149, 812–821. Access via the Internet: < https://reader.elsevier.com/reader/sd/pii/S0143720817317904?token=86662C342EA05423AC6A228373FC835833867649BE95C560F4D25AF2B50038341B935962885FCEB3BB8AD63B9C0AC377>.

203. KUKHTA, N. A., *et al*. Can fluorenone-based compounds emit in the blue region? Impact of the conjugation length and the ground-state aggregation. *Chemistry of Materials* [interactive]. 2017, vol. 29 (4), 1695–1707. Access via the Internet: <https://doi.org/10.1021/acs.chemmater.6b05158>.

204. KIM, K.-H., *et al*. Highly efficient organic light-emitting diodes with phosphorescent emitters having high quantum yield and horizontal orientation of transition dipole moments. *Advanced Materials* [interactive]. 2014, vol. 26 (23), 3844–3847. Access via the Internet: <https://onlinelibrary.wiley.com/doi/epdf/10.1002/adma.201305733>.

205. SONG, J., *et al*. OLEDs with over 50% external quantum efficiency via external scattering and horizontally oriented emitters. *Nature Communications* [interactive]. 2018, vol. 9 (1), 3207. Access via the Internet: <https://doi.org/10.1038/s41467-018-05671-x>.

206. BALDO, M. A., and FORREST, S. R. Transient analysis of organic electrophosphorescence: I. Transient analysis of triplet energy transfer.

Physical Review B [interactive]. 2000, vol. 62 (16), 10958. Access via the Internet: <https://journals.aps.org/prb/pdf/10.1103/PhysRevB.62.10958>.

207. BEZVIKONNYI, O., *et al*. Pyrenyl substituted 1,8-naphthalimide as a new material for weak efficiency-roll-off red OLEDs: a theoretical and experimental study. *New Journal of Chemistry* [interactive]. 2018, 42 (15), 12492–12502. Access via the Internet: <https://pubs.rsc.org/en/content/articlepdf/2018/nj/c8nj01866a>.

208. BYEON, S. Y., *et al*. Recent progress of singlet-exciton-harvesting fluorescent organic light-emitting diodes by energy transfer processes. *Advanced Materials* [interactive]. 2019, vol. 31 (34), 1803714. Access via the Internet: <https://doi.org/10.1002/adma.201803714>.

209. SUN, C., *et al*. Twisted molecular structure on tuning ultralong organic phosphorescence. *The Journal of Physical Chemistry Letters* [interactive]. 2018, vol. 9, 335−339. Access via the Internet: <https://doi.org/10.1021/acs.jpclett.7b02953>.

210. YUNING, H., *et al*. Aggregation-induced emission. *Chemical Society Reviews* [interactive]. 2011, vol. 40 (11), 5361. Access via the Internet: <https://doi.org/10.1039/c1cs15113d>.

211. ETHERINGTON, M. K., *et al*. Revealing the spin–vibronic coupling mechanism of thermally activated delayed fluorescence. *Nature Communications* [interactive]. 2016, vol. 7, 13680. Access via the Internet: <https://doi.org/10.1038/ncomms13680>.

7. LIST OF PUBLICATIONS ON THE SUBJECT OF THE THESIS

1. **Bezvikonnyi, Oleksandr**; Gudeika, Dalius; Volyniuk, Dmytro; Rutkis, Martins; Grazulevicius, Juozas V. Diphenylsulfone-based hosts for electroluminescent devices: Effect of donor substituents // Dyes and Pigments. 2020, vol. 175 108104.
2. Gudeika, Dalius; Miasojedovas, Arunas; **Bezvikonnyi, Oleksandr**; Volyniuk, Dmytro; Gruodis, Alytis; Jursenas, Saulius; Grazulevicius, Juozas V. Differently substituted benzothiadiazoles as charge-transporting emitters for fluorescent organic light-emitting diodes // Dyes and Pigments. 2019, vol. 166, p. 217-225.
3. Gudeika, Dalius; **Bezvikonnyi, Oleksandr**; Volyniuk, Dmytro; Grazulevicius, Juozas V. Differently substituted benzonitriles for non-doped OLEDs // Dyes and Pigments. 2020, vol. 172, 107789.
4. Gudeika, Dalius; Lee, Jiun Haw; Lee, Pei-His; Chen, Chia-Hsun; Chiu, Tien-Lung; Baryshnikov, Glib V.; Minaev, Boris F.; Ågren, Hans; Volyniuk, Dmytro; **Bezvikonnyi, Oleksandr**; Grazulevicius, Juozas V. Flexible diphenylsulfone versus rigid dibenzothiophene dioxide as acceptor moieties in donor-acceptor-donor TADF emitters for highly efficient OLEDs // Organic Electronics. 2020, vol. 83, 105733.
5. Bucinskas, Audrius; **Bezvikonnyi, Oleksandr**; Gudeika, Dalius; Volyniuk, Dmytro; Grazulevicius, Juozas V. Methoxycarbazolyl-disubstituted dibenzofuranes as holes- and electrons-transporting hosts for phosphorescent and TADF-based OLEDs // Dyes and Pigments. 2020, vol. 172, 107781.

8. LIST OF PRESENTATIONS AT THE INTERNATIONAL CONFERENCES

1. Bezvikonnyi, Oleksandr; Yashchuk, Valeriy; Kosach, Vitaliy; Gražulevičius, Juozas Vidas; Lygaitis, Ramūnas. Influence of EEET on characteristics of OLED light-emitting layers // Molecular crystals and liquid crystals: the jubilee 10th international conference on electronic processes in organic and inorganic materials, ICEPOM-10, May 23- 27, 2016, Ternopil, Ukraine;
2. Bezvikonnyi, Oleksandr; Volyniuk, Dmytro; Skuodis, Eigirdas; Gudeika, Dalius; Gražulevičius, Juozas Vidas. Combination of aggregation-enhanced emission and thermally activated delayed fluorescence observed in the derivatives containing donor and acceptor moieties // Baltic polymer symposium 2016: Klaipeda, September 21-24, 2016: programme and abstracts / Kaunas University of Technology, Vilnius University, Klaipeda University. Kaunas: Kaunas University of Technology, 2016. p. 76;
3. Bezvikonnyi, Oleksandr; Gudeika, Dalius; Volyniuk, Dmytro; Gražulevičius, Juozas Vidas. Diphenylsulfone-based TADF emitters substituted by different donor unites // State of the Art in Organic-only TADF OLEDs. From Theory to Applications [elektroninis išteklius] : XXII International Krutyn Summer School 2017 Krutyń, Masurian Lake District, Poland, May 21-27, 2017 / Organizers: Institute of Physical Chemistry of the Polish Academy of Sciences, Poland, Durham University, UK, Strathclyde University, UK, and Silesian University of Technology, Poland;
4. Bezvikonnyi, Oleksandr; Gudeika, Dalius; Volyniuk, Dmytro; Gražulevičius, Juozas Vidas. Combination of aggregation enhanced emission and thermally activated delayed fluorescence exhibited by donor substituted benzonitrile derivatives // Baltic polymer symposium 2017 [e-resource] : Tallinn, Estonia, 20-22 September, 2017 / Co-organized by Tallinn University of Technology and COST action CA15107. Tallinn: TTU. 2017, p. 100;
5. Bezvikonnyi, Oleksandr; Gudeika, Dalius; Volyniuk, Dmytro; Grazulevicius, Juozas V. An electroplex-forming derivative based on 1,8-naphthalimide and perynyl as the host for red PhOLEDs // ICOM 2018: 5th international conference on the physics of optical materials and devices, Igalo, Montenegro, August 27 – August 31, 2018: book of abstracts. Beograd: Institut za nuklearne nauke “Vinča”, 2018. p. 144;
6. Bezvikonnyi, Oleksandr; Gudeika, Dalius; Volyniuk, Dmytro; Grazulevicius, Juozas Vidas. Derivatives of tri-, tetra- phenylethylene and 1.8-naphtalimide exhibiting aggregation induced emission enhancement as emitters for OLEDs // 13th international conference on optical probes of organic and hybrid optoelectronic materials and applications, 7-12 July, 2019, Vilnius, Lithuania: abstract book. Vilnius. 2019, p. 16.

9. ACKNOWLEDGMENTS

I am sincerely thankful to prof. habil. dr. Juozas Vidas Gražulevičius for the great opportunity to learn and work under his lead at Kaunas University of Technology and the guidance in doing the presented work.

I am heartily grateful for the support, useful advice and contribution to my work provided by habil. dr. Dmytro Volyniuk.

Dr. Dalius Gudeika and dr. Audrius Bučinskas are greatly thanked for the permission to study their compounds and their contribution to my investigation.

My deepest gratitude and acknowledgments to my colleagues for the work, my parents and many other people who helped me throughout all these years.

SL344. 2020-07-14, 15,25 leidyb. apsk. l. Tiražas 12 egz.

Išleido Kauno technologijos universitetas, K. Donelaičio g. 73, 44249 Kaunas

Spausdino leidyklos „Technologija“ spaustuvė, Studentų g. 54, 51424 Kaunas